Single wall carbon nanotubes based transparent conducting films for flexible electronics applications

Von der Naturwissenschaftlichen Fakultät der

Gottfried Wilhelm Leibniz Universität Hannover

zur Erlangung des Grades

Doktor der Naturwissenschaften

Dr. rer. nat.

genehmigte Dissertation

von

Bibin Thomas Anto, Master of Science

geboren am 30. Juli 1981 in Kanyakumari (India)

2014

Referent   : Prof. Dr. Peter Behrens

Korreferent   : Prof. Dr. Jürgen Caro

Tag der Promotion   : 14. 11. 2014

Declaration

I, hereby, declare that the thesis "*Single wall carbon nanotubes based transparent conducting films for flexible electronics*" was written independently. Except where otherwise indicated, this thesis is my own work. Possible assistance from others or institutions to carry out the work have been fully specified.

This thesis contains no material that has been submitted previously, in whole or as in parts, for the award of any other academic degree such as Master degree or Diploma.

Leverkusen, 03.12.2014

Master of Science. Bibin Thomas Anto

Abstract

This thesis addresses the development and characterization of transparent conducting films (TCFs) using single wall carbon nanotubes (SWNTs). This work was produced within the BMBF project "Carbofilm" and European Commission project "CONTACT", which are funded in the framework of the Inno.CNT initiative, and Marie Curie Initial Training Network, respectively. A large part of the experimental work was performed at Bayer Technology Services GmbH, Leverkusen. The last three of the four chapters in this thesis are to be submitted as original journal articles.

The introductory first chapter summarizes the general background of this work on SWNTs, including their synthesis, purification, and processing methodologies that are in practice today. On the other hand, the functional requirements (e.g. sheet resistance, optical transmittance, haze and colour neutrality) for TCFs in different applications are also described in detail. Furthermore, SWNT-based TCFs reported in the literature are abridged in this section.

The second chapter describes the effect of different purification conditions of SWNTs on the electrical and optical properties of TCFs. The motivation was to find out the optimum purification conditions (e.g. reagents, temperature and time) for SWNTs in order to fabricate TCFs with better electrical and optical properties. The effect of pH on the dispersibility of SWNTs as well as on properties of TCFs was also investigated. We found that by using SWNT dispersions of higher pH, the electrical and optical properties of TCFs can be enhanced. We attribute this enhancement to the better spatial distribution of the SWNTs and their bundles which in turn depends on the increased electrostatic repulsion forces at higher pH values. This increase is due to the enhanced dissociation of functional moieties (e.g. carboxylic acid and phenolic groups) which had been introduced during the purification process.

The third chapter describes the effect of stabilizers (surfactants) used in the process of making a SWNT dispersion on the electrical and optical properties of TCFs. We found that by using a mixture of two different stabilizers at an appropriate ratio, the properties of the TCFs can be significantly enhanced as compared to those of TCFs fabricated with single stabilizers. We have used poly(sodium 4-styrene sulphonate) in combination with polyvinylpyrrolidone and lignosodium sulphonate in combination with poly(vinyl alcohol) as stabilizers in these investigations. We try to rationalize the improved electrical and optical properties for TCFs with mixed stabilizers by ascribing these to effects in the spatial orientation of the SWNTs, which are governed by the interactions between them and the stabilizers (e.g. hydrogen bonding, ionic and π-π interactions, van der Waals forces).

The fourth chapter describes the effect of doping of SWNT-based TCFs. Following a suggestion from the scientific literature, graphene oxide (GO) is used as a dopant. The motivation was to enhance the electrical and optical properties of SWNT TCFs. Although we have successfully demonstrated that the electrical properties of SWNT films are significantly enhanced, it is observed that the sheet resistance of GO-doped TCFs does not remain stable at ambient conditions. The analysis of the effects of GO-doping on the TCFs and the possible effect of moisture on the de-doping of TCFs are described.

These new insights on the preparation of SWNT TCFs are useful for upcoming technological advancements and applications. With further development, such TCFs could be used in next generation flexible electronic devices and applications.

Keywords: transparent conducting films – single wall carbon nanotubes – SWNTs – flexible electronics – dispersibility

Kurzzusammenfassung

Diese Arbeit befasst sich mit der Entwicklung und Charakterisierung von transparenten elektrisch leitfähigen Beschichtungen (engl. *Transparent conducting films*: TCFs), die mit einwandigen Kohlenstoffnanoröhren (engl. *Single Wall Nanotubes*: SWNTs) hergestellt wurden. Die Arbeiten entstammen dem BMBF-Projekt "Carbofilm", das im Rahmen der Inno.CNT-Initiative gefördert wurde. Ein Großteil der experimentellen Arbeiten wurde bei der Bayer Technology Services in Leverkusen durchgeführt. Die letzten drei Kapitel dieser Arbeit sollen in dieser Form als eigenständige Artikel in Fachzeitschriften veröffentlicht werden.

Das einleitende erste Kapitel fasst den allgemeinen Hintergrund dieser Arbeit zusammen und befasst sich zum einen mit der Herstellung, Aufreinigung und den gängigen Verarbeitungsverfahren für einwandige Kohlenstoffnanoröhren. Zum anderen werden die Leistungsanforderungen für transparente elektrisch leitfähige Schichten (z.B. Flächenwiederstand, optische Transmission, Trübung und Farbneutralität) im Hinblick auf die unterschiedlichen Anwendungsfelder im Detail beschrieben. In diesem Abschnitt werden zudem SWNT-basierte TCFs vorgestellt, die bereits in der Fachliteratur beschrieben wurden.

Im zweiten Kapitel wird darüber berichtet, welchen Einfluss verschiedene Aufreinigungsprozesse der SWNTs auf die elektrischen und optischen Eigenschaften der TCFs haben. Das Ziel dieser Versuche war es, optimale Bedingungen (z.B. Reagenzien, Temperatur und Reaktionszeit) für die Aufreinigung von SWNTs zu finden, die anschließend zu TCFs mit besseren elektrischen und optischen Eigenschaften führen. In diesem Zusammenhang wurde auch der Einfluss des pH-Wertes auf die Dispergierbarkeit der SWNTs und auf die Eigenschaften der TCFs untersucht. Dabei konnten wir feststellen, dass bei Verwendung von SWNT-Dispersionen mit einem höheren pH-Wert die elektrischen und optischen Eigenschaften der TCFs verbessert werden können. Diese Verbesserung führen wir auf eine bessere räumliche Verteilung der SWNTs bzw. deren Bündel zurück, die dadurch entsteht, dass bei einem höheren pH-Wert stärkere repulsive Kräfte wirken. Hervorgerufen werden diese Kräfte durch die vermehrte Dissoziation funktioneller Gruppen (z.B. Carboxyl- oder Phenolgruppen), die während des Aufreinigungsprozesses erzeugt wurden. Weiterhin werden die Charakterisierung der TCFs beschrieben und Hypothesen zu pH-abhängigen Umwandlungsprozessen in SWNT-basierten TCFs diskutiert.

Im dritten Kapitel werden die Effekte von Stabilisatoren (Tensiden), die zur Herstellung der SWNT-Dispersionen verwendet wurden, auf die elektrischen und optischen Eigenschaften der TCFs beschrieben. Dabei konnte festgestellt werden, dass eine Mischung aus zwei verschiedenen Stabilisatoren in einem geeigneten Verhältnis die Eigenschaften der resultierenden TCFs deutlich verbessern kann, wenn man diese mit TCFs vergleicht, die mit nur einem Stabilisator hergestellt wurden. Bei diesen Versuchen wurden als Stabilisatoren Poly(Natrium-4-Styrolsulfonat) in Kombination mit Polyvinylpyrrolidon oder Natriumligninsulfonat in Kombination mit Polyvinylalkohol verwendet. Es werden erste Erklärungsversuche unternommen, die die verbesserten elektrischen und optischen Eigenschaften von TCFs, die unter Verwendung zweier Stabilisatoren hergestellt wurden, auf die räumliche Orientierung der SWNTs zurückführen. Diese Orientierung wird durch die Wechselwirkungen (Wasserstoffbrückenbindungen, ionische und $\pi-\pi$-Wechselwirkungen, van der Waals-Kräfte) zwischen den SWNTs und den Stabilisatoren beeinflusst.

Das vierte Kapitel beschreibt die Dotierung von SWNT-basierten TCFs. Einer Idee aus der Fachliteratur folgend, wird hier Graphenoxid (GO) als Dotand verwendet. Das Ziel war es, die elektrischen und optischen Eigenschaften der SWNT-basierten TCFs zu verbessern. Auch wenn wir erfolgreich zeigen konnten, dass die Eigenschaften der SWNT-Filme durch die Dotierung deutlich verbessert werden, konnten wir doch auch beobachten, dass der Flächenwiderstand der GO-dotierten TCFs in Umgebungsbedingungen nicht stabil blieb. Die Analyse des Effekts der GO-Dotierung auf die TCFs und die Möglichkeit einer durch Luftfeuchtigkeit verursachten Verminderung der Dotierung werden beschrieben.

Diese neuen Erkenntnisse hinsichtlich der Herstellung SWNT-basierter TCFs sind hilfreich für zukünftige technologische Fortschritte und Entwicklungen. Durch weitere Entwicklungsschritte ist es denkbar, dass diese TCFs in der flexiblen Elektronik Anwendung finden könnten.

Schlagworte: transparente leitfähige Filme – Single Wall Carbon Nanotubes – SWNTs – flexible Elektronik – Dispergierbarkeit

Acknowledgement

First and foremost, I thank God for His grace on the adverse situations in my life and helping me to complete this thesis.

I take immense pleasure to thank Prof. Dr. Peter Behrens for accepting me as his Doctoral student in the Institut für Anorganische Chemie. I am grateful to Prof. Behrens for the guidance and support he has provided throughout the thesis work.

I thank Prof. Dr. Jürgen Caro for accepting my request for being the examiner for my Doctoral thesis. I thank Prof. Dr. Franz Renz for accepting my request to be the third examiner for my Doctoral thesis.

I sincerely thank PD. Dr. rer. nat. Stefanie Eiden for the guidance and support throughout this thesis work, which was carried out at Bayer Technology Services GmbH, Leverkusen.

I thank Thomas Daun, Lars Krüger, Dirk Storch, Guido Becker, Elvira Dostert, Bernard Dunkel, Silvia Hemel, Stephan Schröder and Ralf Spiale for their support and encouragement to settle down quickly on the lab activities and work procedures. I thank Jens Sicking and Christ Grade for their special care on training me to perform the XPS measurements and data processing. I also thank Joachim Neumann and Waldemer Chrzonowiz for helping me out with the TEM measurements. I thank Klaus Ide for helping me with SEM measurements and Wolfgang Weiner for the timely support with Raman spectroscopic measurements. I thank Dr. Guilio Lolli for his useful discussions on the initial phase of the project. I also thank Dr. Martina Peters and Dr. Jens Uhlemann for their support throughout my stay in BTS.

A special thanks to Dr. Andreas Schneider and Hans-Christoph Schwarz for their encouragement and support throughout the thesis work, especially with up-and-down situations. I also thank all the members of Prof. Behrens group for their warm welcome that creates a nice atmosphere whenever I visit Hannover. Special thanks to all of them for allowing me to lunch with them in the university canteen.

And last but not least, I thank my parents, siblings, Nitha Susan Anto (my wife) and Chris Jaymin Anto (my son) for their extensive support and prayers throughout my life.

Table of Contents

1. Introduction

1.1 Background

1.1.1 Flexible Electronics

Flexible electronics has drawn more attention since the discovery of polymer based semiconductor architectures and devices. The first initiative to fabricate flexible electronics devices started with silicon on plastic substrates in mid-1960s. In 1967, solar cells were prepared by depositing a thin layer of silicon (≈ 100 µm) on a plastic substrate to offer flexibility.[1] However, flexible electronics took a different direction after the discovery of conducting polymers[2] in 1977 and electroluminescent polymers[3] in 1990. These discoveries on semiconducting polymer materials, which are outstandingly mechanically flexible compared to silicon, led to a new field of research with lot more intensity to develop flexible, bendable, and stretchable polymer electronics devices. This technological advancement offers plenty of opportunities to take electronics to many places, where silicon is unable to go, e.g. plastics, textile, paper, etc.

Flexible electronic device architectures comprise 5 major parts: 1) substrate, 2) back-plane electrode, 3) active layer, 4) front-plane electrode and 5) encapsulation. In order to make the architecture flexible, all these 5 components must comply with bendability to a desired radius or angle, without compromising on its functionality. The key qualities of the materials involved in fabrication of devices are: flexible, bendable, elastic, rollable, conformally shaped, unbreakable and solution processable. Solution processing is a cheaper and easier method of fabrication compared to conventional manufacturing methodologies for inorganic materials that requires ultrahigh vacuum and temperatures. Polycarbonates (PC), polyethylene terephthalate (PET), polyethylene naphthalate (PEN), polyimide (PI) polyethersulphone (PES) polycyclic olefin (PCO), and polyarylate (PAR) are the typical plastic materials, which can be employed as substrates in flexible electronic devices, depending upon the processing temperatures and cost.

Most of the research work has been conducted on PET, PEN and PI substrates, due to their relatively low coefficient of thermal expansion (CTE, ≈ 16 ppm/°C) and acceptable resistance to processable chemicals.[4] PET and PEN are the most preferred plastic substrates due to their very low absorption to water vapour (0.14% compared to 1.8% for PI, which is also yellow in colour). Other plastic materials such as PES, PCO and PAR are optically transparent, but their CTEs are more than 50 ppm/°C.[5] Polymer-based hybrid materials with very low water vapour transmission ratio (WVTR) and oxygen permeability are used as encapsulants in flexible electronics.[5-7] Commercially available printable nanometal inks can be used as one of the electrodes.[8] For light emitting or electroluminescent and photovoltaic applications, one of the electrodes used in the device has to be optically transparent as well as electrically conductive (transparent conducting films, TCFs). More about TCFs and the requirements they must fulfill are described in the following sections.

1.1.2   Transparent Conducting Films

Transparent conducting films are integral part of electronic devices, as they serve the purpose of allowing photons to enter and exit from the device. They also complete the functions of injecting and extracting charge carriers on the light emitting display and photovoltaic devices. Metal oxides are used as TCFs (also known as transparent conductive oxides – TCOs[9]) to meet such requirements. TCOs have the ability to reflect the thermal-infrared heat, which resulted in the use of making energy conserving windows.[10] Application of TCOs on the windows of ovens helps to maintain the outside temperature to make it safe to touch them. They can also be used to defreeze the windows in vehicles, by passing electric current through transparent conductors (transparent heaters).[11] Automatically dimming rearview mirrors for automobiles are possible by sandwiching electrochromic material between the transparent conductors.[10, 12] Cadmium oxide is the first TCO as reported by Bädeker in 1907.[13] Indium tin oxide (ITO) was reported in 1951 by Mochel, who produced it by spray pyrolysis[14] and in 1953 by Holland et al., who used

sputtering method to produce it.[15] Nowadays, sputtered ITO films are the most widely used transparent conductors in the electronic industry, because of their excellent optical transmittance coupled with excellent electrical conductivity. ITO has the lowest resistivity value reported for TCOs so far, 10^{-4} $\Omega \cdot cm$.[16] At the moment, ITO has been employed in many commercially available electronic devices such as light emitting diodes, flat panel displays, electromagnetic shielding, touch panel sensors, photovoltaic cells, etc. Other TCOs under investigation are tin oxide (SnO_2), zinc oxide (ZnO) and their derivatives. Other promising materials that are under research, which can be used in such applications are single wall carbon nanotubes (SWNTs),[17-19] conducting polymers,[20-24] conducting polymers-SWNT composites,[25-27] metal nanowires,[28] and graphene.[29, 30]

1.2 Motivation

Although ITO is the most commonly used transparent conducting material, its employability on flexible electronic devices are jeopardized due to the following reasons: 1) ITO films are not highly flexible; thus the sheet resistance of the films tend to increase with the number of bending cycles.[31] 2) ITO has a yellow haze, though it is tolerable.[32] 3) Scarcity of indium increased the price levels of ITO in the recent years and also decreased the availability.[33] 4) ITO is not a solution processable material, which increases the cost implications for next generation applications. Therefore, the search for suitable transparent conducting films has taken its direction towards alternate possibilities. One of those are the conducting polymers,[20-23] which have high degree of mechanical robustness and are solution processable. Poly(3,4-ethylenedioxy thiophene):poly(4-styrene sulphonic acid) (PEDT:PSS) is the commercially available conducting polymer material for TCF applications. The drift in sheet resistance due to moisture absorption and an intolerable blue haze hinder further developments on PEDT:PSS based TCFs.[34] TCOs are similar to ITO, they are brittle and usually require ultra-high vacuum

for film deposition. Though metal nanowires are solution processable, the expensive nature of this material jeopardized the possibility to use it in flexible TCFs applications. High reflectivity and large haze values of metal nanowires are not good for transparent conducting applications.[35] Graphene is a material that is similar to SWNTs, but arrived recently in the market. The optimization on the process to produce high-quality graphene is underway; moreover graphene is available only in small quantities that are not enough for industrial-scale applications research.[36] Single walled carbon nanotubes (SWNTs) are considered to be more suitable candidates,[37, 38] as it has higher flexibility than ITO,[31] negligible amount of reflectivity,[34] better colour neutrality than both ITO and PEDT:PSS films.[32] SWNTs have further advantages such as availability in abundance, similar work-function as ITO. SWNTs are possible to process in solutions or suspensions, to print them without using etching with corrosive chemicals, and adaptability of film fabrication at room temperatures.

1.3 Single wall carbon nanotubes

1.3.1   Historical Background

In 1952, Roger Bacon, a Russian Physicist observed carbon whiskers made of concentric nanotubes, and reported a morphology of a rolled-up graphite sheet forming a cylinder.[39] The results were published in Russian language during the Cold War and so failed to receive global attention from the scientific community. These carbon whiskers were grown by arc-discharge method under high pressure. In 1991, Iijima and coworkers scripted the historical significance, by reporting multi-walled carbon nanotubes with finite carbon structures, as a result of their investigation on fullerene formation.[40] This work laid a solid foundation for the development of this area, which is the root cause of the explosion of the research interests to use this material in many applications. On the hunt for less complex system than "multi-wall" carbon nanotubes, Iijima & Ichihasi[41] and Bethun et al.[42] have come up with single wall carbon nanotubes in 1993,

two years after the discovery of carbon nanotubes. Both Iijima and Bethune et al. worked independently. Their SWNTs were produced by the arc-discharge method in the presence of a metal catalyst, which provided small amounts of nanotubes along with copious amounts of impurities such as catalyst particles, amorphous carbon, and graphite, etc. Therefore, the scientific community extended its focus on improving the production processes for nanotubes with high yield, high quality and high structural uniformity.

1.3.2   Preparation of single wall carbon nanotubes

There are three major ways to produce single wall carbon nanotubes:

1)   arc discharge method,

2)   laser vaporization (ablation), and

3)   chemical vapour deposition.

These synthesis methods produce SWNTs with different yields, purity and structural uniformity as each method has different limitations. These methods produce mixtures of single wall carbon nanotubes which vary in length, diameter, chirality and defects. Following are brief summaries of the three different methods to produce carbon nanotubes.

1.3.2.1   Arc discharge method

The arc discharge method[43] is the most common and probably the easiest way to produce single wall carbon nanotubes. In 1993, Bethune et al.[42] and Iijima et al.[41] independently reported the production of SWNTs by arc discharge method. The tubes had diameters of 1.2 ± 0.1 nm and 0.7 – 1.6 nm, respectively. Graphite rods which are impregnated with transition metals (Fe, Co, Ni, Ni/Y etc.) as catalyst are the main component used in this method. In an enclosure filled with inert gas (helium or argon at about 100–500 Torr) the graphite rods are used as both cathode and anode and are separated only by a short distance (< 1 mm). They are heated by applying an electric voltage of ≈ 20 V. Electrons flow from anode to cathode and ionize the gas molecules between them to create a hot plasma of high temperature that vaporizes carbon.

Some of the vaporized carbon recondenses back in the form of nanotubes. The tubes produced are covered with amorphous carbon soots, metal particles and metal carbide particles. Therefore it is necessary to purify the tubes through further processing steps to remove the impurities. The yield of nanotubes produced by this method is as high as 30% by weight.[44] In 2007, Mansour et al. developed a process to increase the yield and purity of SWNTs significantly by using small grain graphite powder (≈ 1 μm) and diamond powder (≈1 μm) as anodes, instead of conventional graphite powder (≈100 μm). Both single- and multi-wall carbon nanotubes can be produced by this method. Nanotubes produced by this method have a relatively small number of structural defects, as the tubes are produced at very high temperatures, which helps to graphitize the carbon. This method can produce nanotubes of lengths as large as ≈ 50 μm, which is smaller than for nanotubes produced by other methods. Coal was used, as an alternative to graphite, to fabricate the electrodes in order to reduce the raw material cost by ten-fold.[45] However, problems with contaminations produced by non-carbon materials in the coal has made this attempt insignificant.[46] With advanced developments on the arc discharge process, the Fraunhofer IWS in Dresden offers SWNTs in kilogram quantities for commercial developments.[47]

1.3.2.2   Laser Vaporization

SWNTs were first synthesized through laser vaporization method by the Smalley group in 1995.[48] A year later, the experiments were optimized and refined to better yield and purity of the SWNTs which consist of large bundles or ropes.[49] Nd:YAG lasers have been used to vaporize a cylindrical target of graphite, doped with metal catalyst (0.5 - 1 % each of Co and Ni) in a closed furnace filled with inert gas (argon) and maintained at a temperature of 1200 °C and a pressure of 500 torr. This method was capable of producing 1 g SWNTs per day at high purity. The availability of materials in gram scale further gave an important boost to nanotube research. This method was further investigated by other research groups, although high-cost powerful

lasers are required. In 1999, Iijima and co-workers came up with a laser ablation method of producing SWNTs by irradiating the graphite target (doped with Co/Ni) with a CO_2 laser.[50] It is also reported that the production of SWNTs can be performed at room temperature to 1200 °C. Later in the early 2000s, Eklund et al. came up with an up-scaled process of producing SWNTs with a 1 kW-free electron laser, at a production rate of 1.5 g/hr.[51] Reports suggests that the laser vaporization method produces larger amounts of metallic SWNTs (≈ 70%) than other methods.[52] This would be potentially important for many applications; however, these results have not been confirmed by other researchers. The diameter and the yield of the nanotubes can be controlled by varying the furnace temperature.[46] The major advantage of this method is that the average yield of SWNTs produced is very high with ≈70%, higher than that of arc discharge method. This method is widely used to produce SWNTs, although it is the most expensive method to produce SWNTs due to the implication of lasers with high implementation and energy costs.

1.3.2.3 Chemical vapour deposition

Chemical vapour deposition (CVD) is a method that requires relatively smaller amounts of energy than the other methods. CVD-produced SWNTs were first reported by Smalley's group in 1996.[53] Catalytic decomposition of hydrocarbons or carbon containing species in the presence of metal catalyst particles and condensation of the resulting carbon vapour onto a substrate is the principal mechanism behind the CVD process. In a typical experiment, CO feedstock was passed over a catalyst containing Mo nanoparticles placed in a furnace at a temperature of 1200 °C; SWNTs of a diameter range of 1–5 nm were produced. The choice of the catalyst particles depends on the feedstock material. Fe, Co, Mo, Ni and combinations of these metals are the most commonly used catalyst metals.[46] SWNTs can be produced from a variety of hydrocarbons and other carbon containing species. Konga et al. reported the CVD production of SWNTs by decomposing CH_4 in the presence of a metal oxide catalyst, Fe_2O_3.[54]

Benzene, ethylene, ethanol and acetylene have also been used as feedstock materials to produce SWNTs.[46] Understanding the formation of SWNTs became more complicated when it was reported that SWNTs can also be produced when metals are employed which had not been known for carbon formation, like Au, Ag and Cu.[55-57] However, it was shown experimentally that Cu cannot catalyze the growth of nanotubes;[58] and theoretically it was shown that Au is not capable of catalyzing the growth of SWNTs.[59] Temperature, feedstock and type of catalyst play major roles in determining the growth of SWNTs. Catalyst particle size < 8 nm facilitate the growth of SWNTs, whereas particle size > 8 nm produce multi-wall carbon nanotubes.[46] However, there are reports showing that SWNTs can be grown even with larger catalyst particle sizes (Co/Mo, 11 nm).[60] The CVD process is economic and simple to execute; but on the other hand, the understanding of the growth mechanisms of SWNT become relatively complex. As the CVD process is easily upscaled, a large volume production of SWNTs can be executed using this method. Variations of the CVD process have also been employed to fabricate SWNTs. Plasma-enhanced CVD (PECVD) can also be used for the production of SWNTs, in addition to its common usage in producing MWNTs. Dai et al. reported a process for producing vertically grown SWNTs on an SiO_2/Si substrate, using Fe as catalyst particle.[61] A high volume production was reported by Resasco et al., where SWNTs produced by catalytic disproportionation of a CO feedstock using oxides of Mo and Co as catalysts (CoMoCAT process).[62] Another large scale synthesis of SWNTs was described by Smalley's group in 1999, where a high-pressure catalytic CO (HiPCO) disproportionation was performed in the presence of Fe clusters as catalyst.[63] As the percentage of Fe in final product of SWNTs tend to be too high (14%), purification protocols were introduced to remove the excess metal catalyst. Overall, the CVD processes give a better platform to achieve high volume synthesis of SWNTs, with typical yields of 20 – 100%. This process also helps to grow longer SWNTs, as large as 40 mm,[64] which is useful for applications in composites. A limitation of this method is that the products come with more defects.

1.3.3 Purification and processing of SWNTs

Purification is an essential step in the processing of SWNTs. SWNTs, especially those produced by arc evaporation and laser vaporization techniques tend to contain large amounts of residual catalysts and amorphous carbon and other carbonaceous materials such as graphite, small fullerenes, etc. These impurities will affect the properties of the SWNT compositions and limit their use in applications. To maximize the utilization of SWNTs on the various applications, it is inevitable to remove these unwanted impurities to obtain a homogeneous material. The amount of effort put into the processing of purifications of SWNTs in the last decade is enormous.[65-67]

1.3.3.1 Dry oxidation

Oxidative treatments at elevated temperatures (performed under air, oxygen, argon and other gases) are one of the possible ways to remove the unwanted impurities such as carbonaceous materials from the SWNTs. This purification method is performed based on the principle of selective oxidation and etching, where the carbonaceous impurities are oxidized at a faster rate than the SWNTs. After the removal of carbonaceous species, the metal particles are removed by washing with inorganic acids such as hydrochloric acid.[67] Few examples of these purification methods are as follows. SWNTs produced by the arc discharge method were subjected to high temperature oxidation in air at 350 °C; the yield of nanotubes was improved by combination with the microfiltration method.[68] Nagasawa et al. reported a purification method for SWNTs produced by laser vaporization with a combination of gas phase oxidation at elevated temperature to remove the carbonaceous materials and later by refluxing in nitric acid to remove the metal catalyst particles.[69] It was observed that SWNTs of thinner diameter ($\approx$ 1 nm) burn more quickly than those with larger diameters. Zimmerman et al. reported a method of removing carbonaceous impurities by treating the raw SWNT soot with a mixture of chlorine, water vapour and hydrogen chloride gas at a temperature of 500 °C.[70] Thereafter, the material was treated with hydrochloric acid to remove the metal catalyst particles. However, the procedure was

applicable only to SWNTs synthesized by laser vaporization but did not work for SWNTs produced by arc discharge.[70] Another method of purification was reported by Vivekchand et al. which was employed on SWNTs prepared by arc discharge, laser vaporization and CVD methods.[71] The method involves dry air oxidation, subsequent acid treatment, followed by a hydrogen treatment at elevated temperatures. Arc discharge and laser vaporization tubes were oxidized at 300 °C, washed with nitric acid, followed by hydrogen treatment at 1000 °C. High pressure carbon monoxide (HiPCO) tubes were hydrogen treated at 700 °C. However, the presence of amorphous carbon was still detected in the TEM images.[71] Therefore, the purification by air oxidation combined with a treatment with inorganic acids is effective only to some extent, and the procedures need to be optimized according to the different types of nanotubes. A disadvantage of the dry air oxidation techniques is that the SWNTs will also become oxidized. During dry air oxidation, the metal catalyst particles attached to the impurities will act as a catalyst for the oxidation, which is an advantage. However the efficiency, yield and purity of SWNTs obtained from this technique depends on several factors such metal content, oxidation time, oxidation environment, oxidizing agent, temperature, etc.

1.3.3.2   Acid treatment (Wet oxidation)

Treating SWNTs with inorganic acids to purify from its impurities is a well-known procedure from the literature. Nitric acid is the commonly used inorganic acid to remove large part of the metal catalyst particles and amorphous carbon impurities from SWNTs. While oxidizing with nitric acid under sonication or reflux conditions can introduce functional moieties such as carboxylic acid at the defect sites, open ends, and also be on the side walls. The oxidation introduced functional groups on the SWNTs helps to debundle the tubes and facilitate dispersibility in water and other polar solvents, which is useful from the applications perspective. Following are few examples of purification of SWNTs by oxidation through acid treatments. Ebbesen et al. reported the first protocols on purification of carbon nanotubes in 1994.[74] 20 minutes of sonication was performed

on a mixture of laser vaporization produced SWNTs in $H_2SO_4:HNO_3$ (3:1 v/v), followed by filtration through 0.2 µm membrane. Then the residue was further sonicated in water for 20 minutes, and washed repeatedly. The sample was "polished" by stirring it in $H_2SO_4(30\%):H_2O_2(30\%)$ (4:1 v/v)) for 30 minutes followed by filtration and washing. Later, the material was washed with 35% HCl to induce the formation of carboxylic acid groups on the defect sites and open ends. Liu et al have reported the first large scale (10 g) purification of SWNTs through acid treatment process in 1998.[72, 73] Laser vaporization produced SWNTs of longer lengths have been purified by refluxing in 2.6 M nitric acid for 45 hours. Upon cooling to room temperature, the brownish yellow supernatant was decanted and the precipitate was washed with deionized water for multiple times. The tubes were resuspended with the help of surfactants and filtered through cross-filtration technique.

It is shown that the acid treatment process on arc discharge produced SWNTs can remove the excess amount of metal catalyst particles to produce high purity SWNTs. In 2002, three step purification process to obtain high purity SWNTs was reported by Kajiura et al.[76] Arc discharge produced soot containing SWNTs was refluxed in 2.8M HNO_3 to remove metal particles by dissolution. Sample was then annealed at 500 °C in air to remove the amorphous carbon followed by treatment at elevated condition of 1600 °C / 10^{-3} Pa for 3 hours to heal the defect sites. This method has produced the highly pure SWNTs but with the yield of less than 20 %. Refined and simplified protocols on acid treatment on arc discharge produced tubes by treating with 3M HNO_3 for 12 hours or 7M HNO_3 for 6 hours were reported by Hu et al. in 2003.[75] Variations on this protocol is enormous such as temperature variation, reflux duration, mixture of inorganic acids, sonications, cross flow filtration, etc. Similarly CVD produced SWNTs can also be purified with variations of acid treatment processes. Therefore, the key parameters to obtain highly pure SWNTs with maximum possible yield depends on many factors such as, reflux

temperature, reflux duration, concentration of acid, combination of acid mixtures, annealing temperature after acid treatment, etc.

1.3.3.3   Functionalization

Chemical functionalization of SWNTs is considered to be an important step in processing of tubes. Functionalization means, introducing functional moieties such as –COOH, –COO⁻, –C=O, –C-O, –OH etc. on the defect sites, open ends or sidewalls of the tubes. Dispersing SWNTs in different solvent medium is a very important step on solution processing fabrication methodologies that saves time, energy and cost, On the other hand, conventional fabrication techniques require several hours pumping down to achieve ultra-high vacuum, high energy, and high operating cost. Dispersion of SWNTs also provides room for printability of circuit patterns that avoids corrosive etching and lithographic methodologies that are in practice today. Commonly used acids and acid mixtures for functionalization of SWNT ends and defect sites are HNO_3,[77] Mixture of $HNO_3+H_2SO_4$[78] and $H_2SO4+KMnO_4$.[79] Such processes will introduce carboxyl and other groups on the tube ends and defect sites which induce dispersibility in water and other polar solvents. However, the dispersibility of functionalized tubes can be altered by other methods such as, condensing long-chain alkylamines with carboxyl groups attached to the tubes ends of SWNTs (fig 1.1).[80] After introducing octadecylamine to the carboxyl groups, SWNTs were dispersible in chloroform, dichloromethane, carbon-di-sulphide, and other aromatic solvents such as benzene, toluene, chlorobenzene and 1,2-dichlorobenzene.
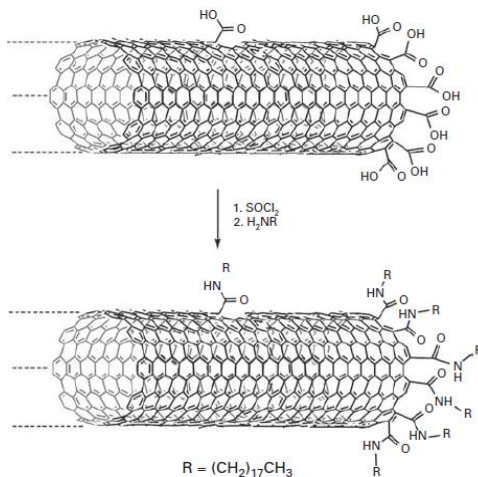
Figure 1.1. Schematic representation of defect and tube end functionalization of SWNTs with octylamine to produce dispersible tubes in various solvents.[80]

Similarly several other possibilities of attaching different functional molecules such as poly(propionylethyleneimine-co-ethylenimine),[81] poly(vinyl acetate-co-vinyl alcohol),[81] carbenes,[82] nitrenes,[83] azomethine ylides,[84] to attach to SWNTs were experimented and established. Other functionalization routes such as solution-phase ozonolysis,[85] radical addition,[86] silylation,[87] fluorination,[88] electrochemical reactions[89, 90] and attachment of polymers[91, 92] were also reported.

Non-covalent functionalization by surfactants was performed in the following ways. Sodium dodecyl sulphate (SDS) was first used to demonstrate this principle, where the ionic surfactant molecule transfers its charges to nanotube surface.[93] The tubes are then dispersed by electrostatic force, which is supported by strong dependence on the dispersion behavior with respect to pH. However, large amount (1% SDS in water) of surfactant is required to debundle the tubes; and the power and time required for ultrasonication is very high for this method. Sodium dodecyl benzene sulphonate (SDBS) was used as a surfactant to disperse SWNTs in water, which is more effective than SDS due to the presence of benzene ring which facilitates

better π-π interactions between the surfactant and SWNTs.[94] Other non-ionic surfactants such as Triton X-100 was also reported to be an effective candidate in dispersing nanotubes in water, which operates in combination with hydrogen bonding and steric dispersion forces.[95] SWNT can be suspended in different solvents by using longer molecules (polymers such as polyvinylpyrrolidone, poly(3,4-styrene sulfonicacid)) that wrap around the nanotubes.[46]

1.3.4 Structure of single wall carbon nanotubes

Understanding the structure of SWNTs received more attention after the work by Iijima et al in 1991.[41] Knowledge on the structure of SWNTs would be useful for determining the physical and electronic properties. Several experiments have been carried out since then, mainly using high-resolution transmission electron microscopy (HRTEM) to find out the structure of tubes. Later, spectroscopic techniques such as absorption spectroscopy and Raman spectroscopy added more value to the experimental determination of structure of SWNTs.
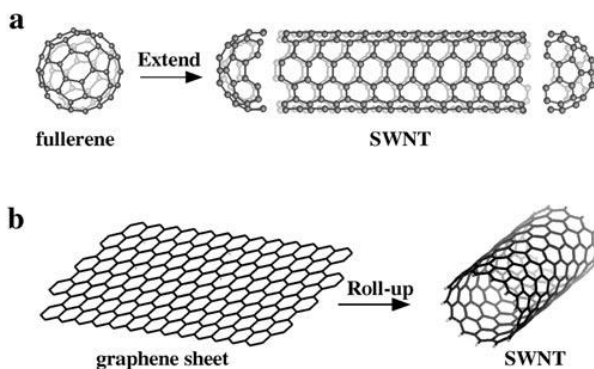
Figure 1.2. Schematic representation of SWNT: (a) extension of fullerene molecular cluster in 1D. C_{60} can be extended into nanotube of diameter 0.7 nm. (b) Graphene sheet rolled-up seamlessly in to single wall carbon nanotube. (taken from ref.[96])

Carbon nanotubes are sheets of graphite which is rolled up into a tube; SWNTs are single layer of graphite, which is called as graphene that is rolled up into a tube, or an extended C_{60}

fullerene molecular cluster (Fig 1.2). Orientation and configuration of carbon atoms present in SWNTs defines the optical and electronic properties of SWNTs. The presence of a strongly bonded network of sp^2-hybridized carbon atoms with delocalized electrons provides electrical conductivity along the graphitic planes of SWNTs. In addition, van der Waals forces, which are rather strong due to the good polarizability of the π bonding systems, keep the individual SWNTs aggregated. Due to this effect, the formation of SWNTs usually results in bundles and not in individual tubes. Some of the carbon atoms on the SWNTs are sp^3-hybridized and are viewed as defects. Heating to high temperatures can remove such defects by transforming sp^3-hybridized to sp^2-hybridized carbon atoms, a process called graphitization. Carbon nanotubes have diameters ranging from 0.7 to 10 nm, though most of the tubes have a diameter < 2 nm. SWNTs are called as one-dimensional structures because of their large length-to-diameter ratio (aspect ratio > 10^4).

1.3.4.1   Representation of the structure of carbon nanotubes

This section gives the brief summary on the theoretical representation and interpretation of different structural parameters. A SWNT is described as a graphene sheet rolled-up into a cylindrical shape.[46] The rolled up graphene sheet consists of six-membered carbon rings (hexagon) oriented in honeycomb lattice. Three different structures are possible, considering the orientation and angle of the roll-up process of a graphene sheet. The two most ordered configurations are designated as 'zigzag' and 'armchair'. A schematic representation of the structures is shown in Figure 1.3. Most of the tubes produced do not have these highly symmetric forms, but have structures where the hexagons are helically arranged around the tube axis. Such structures are known as chiral tubes (Fig. 1.3c).[97]
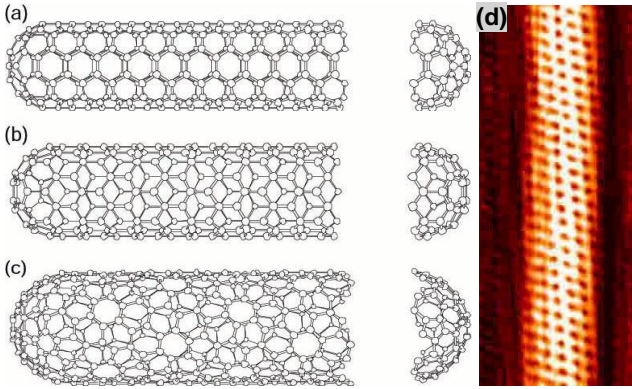
Figure 1.3. Three different structures of SWNTs: (a) armchair (b) zigzag and (c) chiral (mixture of armchair and zigzag) nanotubes (taken from ref.[97]. (d) Atomic resolution scanning tunneling microscopic image of SWNT, which is not a zigzag tube, but either a chiral tube or an armchair tube (chiral angle 30°) – taken from ref. [98]

Chiral vector $\vec{C}$, which joins the two equivalent points on the graphene lattice, is one of the key parameters with which the structure of an individual tube is specified. $\vec{C}$ is perpendicular to the tube axis, which is parallel to translational vector $\vec{T}$. The crystallographic representation of the following discussion is given in figure 1.4. The chiral vector can be represented in terms of unit cell parameters as follows:[97]

$$\vec{C} = na_1 + ma_2 \equiv (n,m) \tag{1.1}$$

where, a_1 and a_2 are the unit vectors and the length of the unit vector is calculated to be 0.246 nm ($a = \sqrt{3}a_{c-c}$; $a_{c-c} = 0.142\ nm$). The term (n,m) are the integers, where n and m are integers and $0 \le |m| \le n$, identifies a certain tube structure.
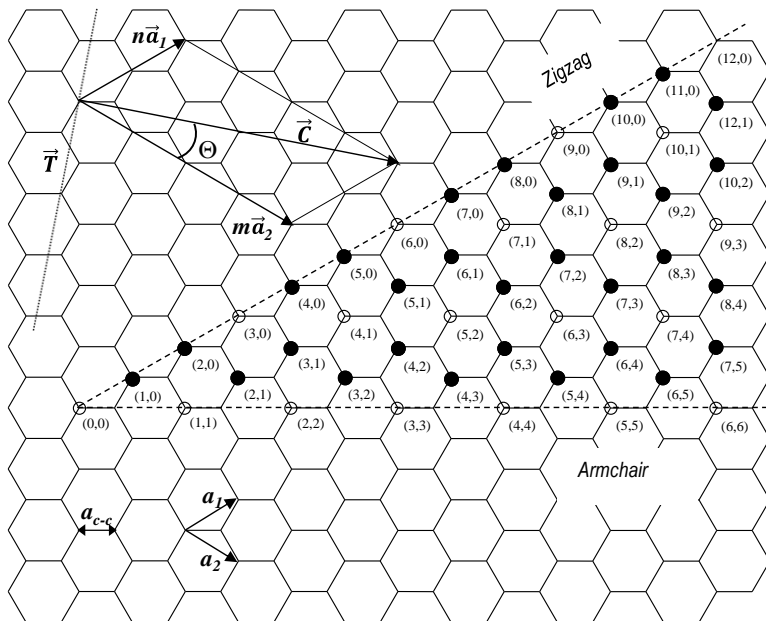
Figure 1.4. Crystallographic representation of two-dimensional graphene lattice that can be rolled into a carbon nanotube. Metallic and semiconducting SWNTs (*n, m*) are represented by the open and solid circles on the map of chiral vectors (redrawn from ref.[97])

The length of the chiral vector L, can be calculated as follows:[97]

$$L = a\sqrt{n^2 + nm + m^2} \tag{1.2}$$

$$L = 0.246\sqrt{n^2 + nm + m^2} \tag{1.3}$$

The diameter d of the tube is related to the crystallographic parameters, and this can be calculated using the following relation:[97]

$$d = \frac{L}{\pi} = \frac{0.246\sqrt{n^2 + nm + m^2}}{\pi} \tag{1.4}$$

The chiral angle Θ is given by,

$$\Theta = \sin^{-1}\frac{\sqrt{3}m}{2\sqrt{n^2 + nm + m^2}} ; \left(0 \leq |\Theta| \leq \frac{\pi}{6}\right) \tag{1.5}$$

We can see from the representation (Fig 1.4) that $m = 0$ for all the zigzag tubes, while $n = m$ for the entire set of arm chair tubes; and the remaining tubes are chiral. The following relations describe the metallic and semiconducting nature of single wall carbon nanotubes.

$$(n - m) = \begin{cases} 3p & metal \\ 3p \pm 1 & semicondutor \end{cases} \tag{1.6}$$

Particulary, arm chair tubes denoted by (n, n) are always metallic as $(n = m)$; and zigzag tubes denoted by $(n, 0)$ are metallic when n is multiple of 3. In figure 1.4, the SWNTs that are semiconducting are denoted by solid circles; metallic tubes are denoted by open circles. In theory, approximately one third of the tubes should be metallic and two thirds should be semiconducting in nature. In practice, the composition of the mixture of semiconducting and metallic tubes may differ from this. However, all the synthetic procedures produce major fractions of semiconducting and a smaller fraction of metallic tubes. Procedures for the formation of only metallic or only semiconducting tubes have yet to be discovered. Such methods would have a high potential for technological investments and developments.

1.3.5   Properties of single wall carbon nanotubes

Single wall carbon nanotubes have attracted the research community because of their combination of outstanding properties, including record-breaking mechanic resilience and variable electronic properties, ranging from metallic to semiconducting. As SWNTs are analogous to rolled-up single layers of graphite, the electronic structure of graphene sheets has been used as the basis for the theoretical representation of the electronic properties of SWNTs. It can be assumed that the graphene planes are infinite in two dimensions. The electronic properties of graphite are highly anisotropic: The electron mobility within the planes is very high, due to the delocalization of π electrons or the overlap of π orbitals among adjacent atoms. The in-plane resistivity of high quality graphite at room temperature is approximately 0.4 µΩ-m.[46]

However, the electron mobility perpendicular to the planes is low. Detailed band structure calculations for 2D graphite were performed by Wallace in 1947, ignoring interactions between planes.[99] Band structure calculations for 3D graphite were performed by Slonczewski, McClure and Weiss in the 1950s, incorporating the interactions from adjacent graphitic planes.[100, 101] This model shows that π bands overlap by $\approx$40 MeV, making graphite a semi-metal with free electrons and holes at all temperatures. This results in $\approx$10^{-4} N electrons in the conduction band and the same number of holes in the valence band at 0 K, where N is the number of atoms. The calculation also shows that the carrier density of graphite is of the order of 10^{18} cm^{-3}, which is very small. Therefore, in spite of the very high mobility of the charge carriers in the graphitic planes, the electronic conductivity of graphite is rather low compared to metals like copper, which has one free carrier per atom.

1.3.5.1 Electronic properties of single wall carbon nanotubes

In 1995, Dresselhaus and coworkers have performed a complete study on the electronic structure calculations for SWNTs.[97] Different electronic structure for different chiral structures of SWNTs were calculated using tight binding approximation.[102] Energy band gap E_g of SWNTs can be related to the diameter of tubes by the following relation:[103]

$$E_g = \frac{t a_{c-c}}{d} \qquad (1.7)$$

where, a_{c-c} is carbon-carbon bond distance in SWNT lattice (0.142 nm) and t is the tight binding overlap energy of nearest neighbor carbon-carbon bond. Three different types of band structure diagrams[102] can be discerned (Figure 1.5).
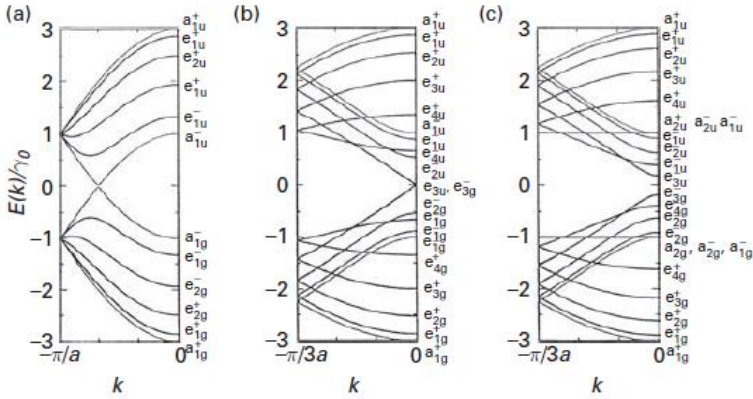
Figure 1.5. Energy dispersion relation for (a) armchair (5,5) nanotube, (b) zigzag (9,0) nanotube, and (c) zigzag (10, 0) nanotube (taken from ref.[102])

The valence bands and conduction bands crosses at the k point on the one dimensional energy dispersion relation for armchair tubes, and it takes places at the Fermi level.[102] This suggests that armchair (n,n) tubes are metallic in nature. Each curve displayed on figure 1.5 corresponds to single sub band. The energy states above the Fermi level (E = 0) are completely empty and the lower energy states are fully occupied. Figure 1.5a and 1.5b shows the electronic energy dispersion relation for armchair (5,5) and zigzag (9,0) nanotubes that are metallic. From figure 1.5c, the valence band and conduction band did not touch each other at the the Fermi level for zigzag tube (10,0). Therefore the zigzag tube (10,0) is considered as a semiconducting tube, due to its narrow band gap. Chiral tubes may also be either metallic or semiconducting, depends on the chiral angle of the tubes. Dresselhaus et al shows that metallic conduction occurs in chiral tubes, when

$$n - m = 3p \tag{1.8}$$

Where, p is an integer. Therefore, theoretically, one third of chiral tubes are metallic and two-thirds are semiconducting.

As carbon nanotubes are limited in size especially around circumference, their density of states (DOS) exhibits in sharp peaks that is known as van Hove Singularities (vHS). DOS at the Fermi level is always zero for semiconducting tubes, as there are no electronic states in the forbidden gap; DOS is non-zero for metallic tubes. This is shown in Figure 1.6 where the electronic DOS for a zigzag (9,0) metallic nanotube and a zigzag (10,0) semiconducting nanotube are depicted. The dotted line in Figure 1.6 represents the DOS for a two-dimensional graphene sheet. For both metallic and semiconducting nanotubes, the energy band gap is inversely proportional to the diameter of nanotubes (eq. 1.7)
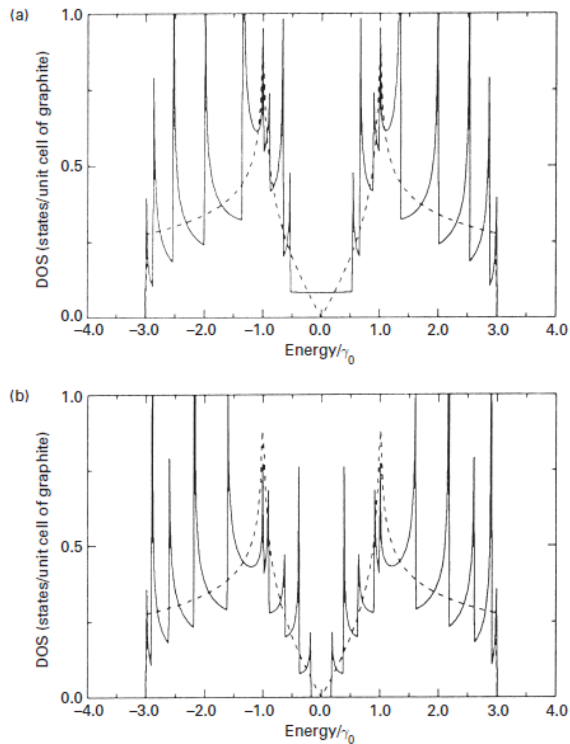
Figure 1.6. Electronic one dimensional density of states per unit cell for (a) zigzag (9,0) nanotube, and (b) zigzag (10, 0) nanotube. Dotted line represents the density of states for two-dimensional graphene sheet. (taken from ref.[104])

Electronic transitions take place between the sub-bands of conduction band and valence band, when external energy is applied. The transition of electrons from first sub-band of valence band to conductions band is represented as S_{11} for semiconducting tubes and M_{11} for metallic tubes. Similarly, the other possible electronic transitions are S_{22}, S_{33}, etc for semiconducting tubes and M_{22}, M_{33}, etc for metallic tubes. These transitions can be detected using optical absorption spectroscopy and vibrational spectroscopies, which are useful in characterizing carbon nanotubes.

1.3.5.2 Optical properties of single wall carbon nanotubes
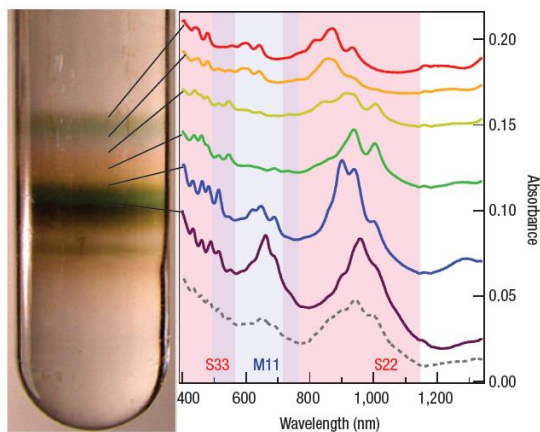
Figure 1.7. Optical absorption spectra of sodium cholate stabilized SWNTs, sorted by electronic type using density gradient ultracentrifugation. On the left hand side, SWNT dispersion in centrifuge tube, shows the separation of SWNTs by electronic type (taken from ref. [107])

Different optical properties for SWNTs are observed due to their difference in electronic structures. These differences in optical properties can be used to distinguish the nature of the tubes (e.g. semiconducting or metallic). van Hove singularities of SWNTs are formed when the two-dimensional energy bands of a graphene layer into one-dimensional band.[105] When the

energy of incident light radiation coincides with the energy level of a van Hove singularity, an optical transition of an electron from the valence band to the conduction band occurs, leading to a resonant enhancement in the corresponding photo-physical process.[106] A simple UV-Vis-NIR spectrum of SWNTs can provide this information in detail. An example of a UV-Vis spectrum of CoMoCAT-grown SWNTs dispersed in water with the help of sodium cholate as surfactant is shown in figure 1.7.[107]
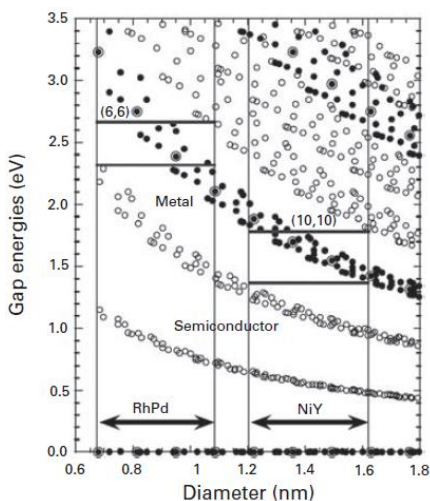
Figure 1.8. Kataura plot, shows the inter-band transition gap energies between quantized sub-bands of valence band and conduction bands. Solid circles represent the metallic tubes, open circles represent semiconducting tubes and double circles represent arm chair tubes. Arrows indicates the diameter distribution of tubes produced by arc-evaporation and laser vaporization methods using Rh-Pd and Ni-Y catalysts (taken from ref. [107])

The distinct van Hove singularities observed from the spectra are marked as S_{33}, M_{11} and S_{22} in the range of 400 to 1200 nm. M_{11} represents the first optical inter-band transition of metallic tubes. Similarly S_{22} and S_{33} represent the second and third optical inter-band transitions of semiconducting tubes, respectively. The dotted line in Fig. 1.7 represents the optical absorption

spectrum of SWNTs before their separation. The separation shown in Fig. 1.7, achieved by density gradient ultracentrifugation, was a remarkable achievement in SWNT research, as it scripted an avenue to the possible separation of tubes by the type of their electronic structure.

Optical absorption spectroscopy contains a wealth of information about SWNT structure, electronic type and band gap, etc. Kataura et al,[106] demonstrated for the first time that the van Hove singularities (inter-band transitions) of SWNTs can be decoded using optical absorption spectra. Inter-band transition gap energies with respect to diameter of nanotubes are theoretically predicted and confirmed experimentally (Fig 1.8).[106]

The transition gap energies decrease with increasing nanotube diameter. The Kataura plot also shows that simple absorption spectra are of limited use in predicting the nanotube structure, as the absorption features of nanotubes with different structures overlap with each other. Also, the absorption features of SWNTs can be influenced by molecular environments such as the dispersion medium, surfactants, pH value of the dispersions as well as on the functionalization of the tubes. However, the discovery of fluorescence in SWNTs opened up new possibilities in determining the structure of SWNTs.[108, 109]

1.3.5.3   Vibrational properties of SWNTs

Raman spectroscopy is one of the powerful tools for the analysis of SWNTs. Analysis of the samples can be done at ambient conditions. However, the same tool is not as effective for multi wall carbon nanotubes. A sample spectrum of SWNTs is shown below in figure 1.9.

The following features of SWNTs can be observed in their Raman spectra:

1. Low frequency peak (< 200 cm^{-1}), assigned to the radial breathing mode (RBM); this peak mainly depends on the diameter of the tube and corresponds to a vibration during which the diameter of the tube shrinks and increases.

2. A strong feature at about 1340 cm^{-1}, the *D*–band, which is assigned to disordered parts of graphitic structures, due to sp^3-hybridized carbon.

3. Peaks around 1550 to 1600 cm⁻¹ labelled as G–band, which stem from graphitic structures.

4. Peak at about 2600 cm⁻¹ labelled as G' band, which is a second order harmonic of the D– band.

5. Some weak second order modes between 1700 and 1800 cm⁻¹, which are not very useful for the characterization of nanotubes.
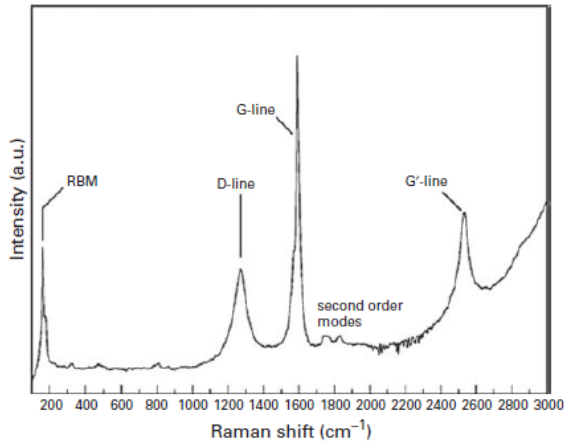
Figure 1.9. Raman spectrum of SWNT sample (taken from ref. [110])

RBM is a mode where all carbon-carbon bonds stretch and shrink, leading to a coherent motion of all carbon atoms in radial direction (see Fig. 1.10). The RBM mode frequencies (ω_{RBM}) are related to the diameter of the tube by the following relation:[111]

$$\omega_{RBM} = \frac{234}{d} + \Gamma \qquad\qquad (1.9)$$

where, Γ is a factor that is related to tube-tube interactions and the nature of sample and d is the diameter of the tube. RBM modes also give information on whether the tubes are metallic or semiconducting in nature, by offering a possibility to calculate the chiral indices from the

diameter of the tube. For tubes of diameter larger than 2 nm, the character of the electronic states becomes independent of the tube diameter, and hence approximates that of a graphene sheet.[46] The tube indices (*n,m*) can be calculated from the ω_{RBM}. [46,112]
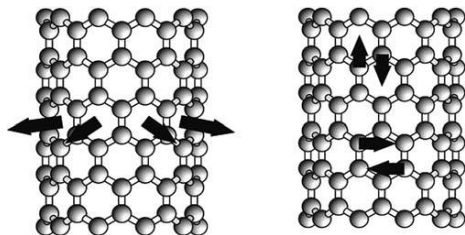
Figure 1.10. Schematic representation of atomic displacements that are associated with RBM and G-band vibrations (taken from ref.[113])

The graphitic mode *G* is the contribution from the tangential vibrations of C−C bonds along the nanotube axis, which appears at about 1585 cm⁻¹, depending on the nature of the tube. This band is composed of two main features that can be termed as G^+ and G^- bands. The split in the *G* band is probably due to the curvature of carbon nanotubes, as it does not appear normally in graphene sheets. The G^+ band appears due to the vibrations that are parallel to the tube axis which will have Lorentzian line shape. The G^- band appears due to the vibrations that are perpendicular to the tube axis, which will normally have Breit-Wagner-Fano (BWF) line shape. Lorentzian shapes are predominant in semiconducting nanotubes whereas BWF line shape is typical of metallic tubes.[102] It is also reported that the spectral features are subject to changes with respect to different excitation wavelengths and power density of the laser that is used in Raman spectroscopy.[114] The *G*−band also gives information about the state of 'doping' in SWNTs. The *G*−band is upshifted (to higher wavenumbers) for *p*-doped tubes and downshifted (to lower wavenumbers) for *n*-doped tubes with respect to *G*−band of undoped SWNTs.[115]

1.4 SWNT thin films: Transparent conductors - Overview

Using appropriate methods, SWNTs can be processed to form nanoscale network films that can be useful in many applications such as large display panels, touch-panels, light emitting diodes, sensors, transistors and electromagnetic interference shielding, etc. The wide range of potential of SWNTs in different applications are due to their excellent electron mobility (on the order of $1x10^5$ cm^{2}V^{-1}s^{-1}) and electrical conductivity (up to $4x10^5$ Scm^{-1}) due to the strong carbon-carbon bonding between the atoms in the tube.[116] The band gap of semiconducting tubes, which is inversely proportional to the diameter, is on the order of 0.7 eV for tubes of a diameter of 1 nm.[102] The work function – i.e. the amount of energy required to remove an electron from a nanotube − is a crucial parameter in optoelectronic device applications; for SWNTs, it is on the order of 4.7 to 5.2 eV and thus similar to that of ITO.[117]

1.4.1 SWNT nanoscale network

Although many interesting devices have been constructed with individual SWNTs and have shown interesting physical properties, the production of SWNT films for devices is challenging. SWNT films consist of large number of individual SWNTs that differs in quality and type. The final properties of SWNT films are the statistical average of properties of all the individual tubes in the film. Therefore, theoretical predictions of properties of SWNT films often significantly differ from the experimental results. It is difficult to control the architecture of the SWNT film, especially on larger scales. Simple film architectures can be achieved by forming a nanoscale network of randomly oriented tubes, which consists of different compositions of metallic or semiconducting tubes. An example of a randomly oriented nanoscale network of SWNTs, above the percolation threshold is shown in Figure 1.11. The percolation threshold is the point at which a sudden increase in electrical conductivity is observed, with respect to the concentration of SWNTs in a film.
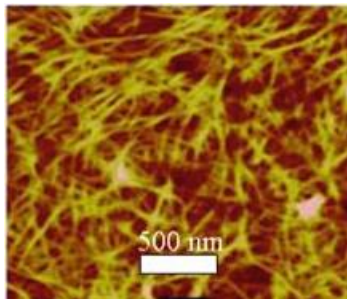
Figure 1.11. Example of atomic force microscopic image of nanoscale network comprising many SWNTs oriented randomly in order. (taken from ref. [38])

The electrical conductivity of SWNT films is limited by the inter-tube junctions, as the junction resistance is very high. The charge carrier transport through the network is not limited by the conductivity along the nanotubes, but by the resistance associated with barriers to charge propagation at the inter-tube junctions of nanotubes. Therefore the electrical conductivity of nanotube films is always lower than the electrical conductivity of an individual nanotube. The highest reported value for electrical conductivity of nanotube films is 6×10^3 Scm^{-1}, which is about 3 orders of magnitude lower than the electrical conductivity of a single nanotube.[116]

With regard to optical transmittance, SWNT films are capable of exhibiting > 95% transmittance for very thin films. However, the optical transmittance of the film will be compromised when the nanotube density or the film thickness are increased to achieve high electrical conductivity. Correspondingly, the optical transmittance and the electrical conductivity of SWNT films always play against each other. Nanotube films are well known for their flexibility compared to counterparts like ITO, which suffer a loss of electrical conductivity when subjected to bending cycle tests.[118] This feature of SWNT films provides venues for their application in several next generation flexible electronic devices.

1.4.2   Electrical and optical properties of SWNT films

Electrical properties of SWNT films depend mainly on the concentration of nanotubes present in the film, i.e. the nanotube density as projected onto the film area. At a critical nanotube density (which is also known as percolation threshold) there is a sufficient number of conducting pathways available for efficient charge transport. The available number of pathways strongly depends on the nanotube density.[119] However, the individual character of each nanotube with its structure, diameter and chirality, as well as the variability in inter-tube junctions, barrier heights, and charge propagation through inter-tube junctions brings complexities to the final electrical properties of the film.[120] Hence, the charge transport in nanotube films has to be treated differently from transport in band like in metals.

1.4.2.1   Concentration dependent electrical properties of SWNT films

One of the important parameter that affects the electrical properties of SWNT films is percolation. Percolation defines how the conducting pathways form across a SWNT film as the nanotube density of the film increases. There are established reports on theoretical and experimental studies that narrate about how the electrical properties of SWNT films scale with nanotube density.[119,121,122] Theoretical studies of percolation in nanotube films were conducted based on the assumption that the network conductance is proportional to the number of conducting path ways in the film. There are three different types which occur in randomly oriented nanotube films as seen in Figure 1.12. At low density regimes (Fig. 1.12.a), continuous path across the surface cannot be achieved; hence the conductivity (σ) at this regime is zero. At the regime of moderate nanotube density (Fig 1.12b), which is slightly above percolation threshold, continuous conduction path across the surface is achieved; therefore, the electrical conductivity is comparatively very high. At the regime of higher nanotube density (Fig 1.12c), the continuous path across the surface is slightly improved from moderate tube density regime; hence the slightly better electrical conductivity (σ) is achieved.
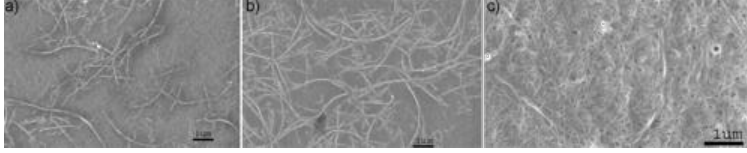
Figure 1.12. SEM images of SWNT network film on alumina substrates. Films with nanotube density (a) near percolation threshold (b) slightly above percolation threshold and (c) well above the percolation threshold. (taken from ref. [119])

As the critical nanotube density (N_c) increases, a nanotube film reaches its percolation threshold when the conducting pathways are sufficient to form a continuous path across the film. At this critical nanotube density, the conductivity of percolating networks varies as:[119]

$$\sigma \sim (N - N_c)^{\alpha} \tag{1.10}$$

where σ is the conductivity, N is the nanotube density, and N_c is the critical nanotube density corresponding the percolation threshold; α is the critical exponent, which depends on the dimensionality of the space; for a film in two dimensions, $\alpha = 1.33$ whereas for a film in three dimensions, it is 1.94 (Fig 1.13).[123]
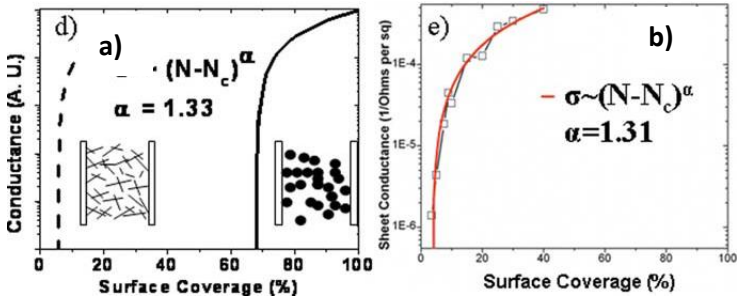
Figure 1.13. (a) Theoretical plot of the conductance versus area coverage for a 2-D surface covered with sticks (dashed, left) and discs (solid, right). Critical density for sticks (aspect ratio = 100) is ~5%, while that of discs is ~67%. (b) Experimentally measured sheet conductance versus surface coverage for nanotube films. It follows the expected power law with a critical exponent of 1.31 (taken from ref. [16])

For the random distribution of nanotubes in a conductive stick model,[124] the critical density is given by:[119]

$$N_c = \frac{5.7}{l^2} \qquad (1.11)$$

Here, l is the length of the conductive stick, which is a nanotube in our case. Equation 1.11 suggests that using longer nanotubes will decrease the critical density to achieve the percolation threshold, which will enhance the optical transmittance of the film. The critical exponent α depends only on the space of percolation, i.e. whether it is two- or three-dimensional. For densities greater than N_c, the critical exponent α become density-dependent and approaches 1 for films with $N \gg N_c$.

1.4.2.2   Geometrical factors affecting SWNT films

The resistance of SWNT networks has a strong dependence on the length of the nanotubes. Whereas long nanotubes are of advantage to surmount the percolation threshold, the resistance of an individual nanotube increases with its length when it is longer than the carrier mean free path (Fig 1.14).[125-128] Length independent resistance values are observed for tubes of length smaller than the carrier mean free path.
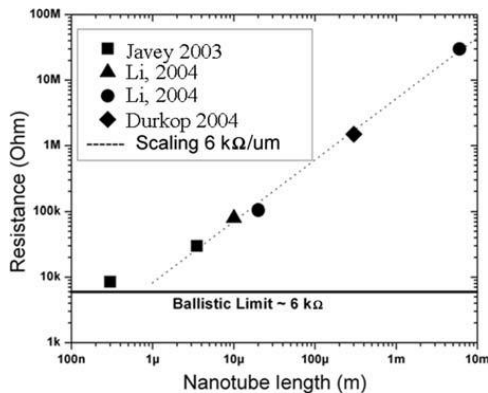
Figure 1.14. Resistance values for SWNTs of varying length. (taken from ref.[16])

The limiting resistance of 6 kΩ observed in figure 1.14 corresponds to the quantum resistance of a wire with ballistic transport. These results conclude that the mean free path of charge carriers in nanotubes are possibly in the range of 1 μm.[129]

Inter-tube junction resistance between SWNTs were measured to be in the range of 200-400 kΩ for metal-metal tube junctions, 1MΩ for semiconducting-semiconducting tube junctions and 100 MΩ for metal-semiconducting tube junction, at low bias voltages in the range of mV.[120] The effect of length of nanotubes on the electrical conductivity of network films has been studied experimentally.[130] Nanotubes were subjected to high-powered sonication to debundle them to create tubes of controllable length, and later deposited to form a SWNT network film. It was established experimentally that the electrical conductivity of the film scales with the length of thenanotubes as follows:[130]

$$\sigma = l^{1.46} \tag{1.12}$$

where, l is the average length of SWNTs or bundles present in the nanoscale network film. The average bundle size of SWNTs will also play a role in final electrical conductivity of the films, as it has been reported that smaller bundles have higher conductivity.[131] This effect is likely due to the fact that most of the current flows through the surface of the nanotube bundles, creating non-conducting parts at the center of the bundles. However, the length of the non-conducting parts in the center of the nanotube bundles decreases with respect of decreasing average bundle length, which results in higher conductivity.

1.4.2.3   Temperature effects on SWNT films

The effect of temperature on the electrical conductivity of SWNT films has been investigated in experiments with films of various nanotube densities.[132-134] At nanotube densities above the percolation threshold, the electrical conductivity of the films is not significantly influenced by the temperature. However, for films with lower nanotube density or a density close to the percolation threshold, a strong dependence of the electrical conductivity on temperature was observed. At

lower nanotube densities, the conducting networks are expected to contain some semiconducting SWNTs which leads to temperature-enhanced charge transport processes. At higher nanotube densities, all-metallic SWNT conduction pathways are feasible that nullify the effect of temperature on charge transport processes. From the point of view of applications, the temperature-dependent behavior is of interest in some cases where SWNT films serve as semiconducting channels in transistor devices. For other applications aiming at high conductivities (which require high nanotubes densities), the effect of temperature on the electrical conductivity of the films is not important.

1.4.3 Doping of SWNT films

Chemical doping of SWNT thin films enhances the electrical conductivity of the films by increasing the number of charge carriers. Doping in SWNTs can be employed in various ways, such as intercalation of electron donors or acceptors, molecular adsorption, covalent functionalization, non-covalent functionalization, substitutional doping, etc.[135-137] *p*-type doping can enhance the electrical conductivity of SWNT network films dramatically. Commonly used *p*-dopants are inorganic acids such as HNO_3, H_2SO_4, and gases like NO_2, Br_2, molecules like Tetrafluorotetracyano-*p*-quinodimethane (F_4TCNQ) and polymers, etc.[19] Dopant molecules increases the number of charge carriers present in SWNT networks, which results in relatively higher electrical conductivity of SWNT films. Such type of doping is very common and useful for SWNT thin films, especially in applications as transparent conductors. The process of doping SWNT transparent conducting films are very simple, as it can be performed by simply immersing or dipping the films into a dopant solution for a specified duration. Figure 1.15 shows the dramatic decrease in sheet resistance of SWNT transparent films after *p*-doping by immersion in 65% HNO_3 and $SOCl_2$ for 30 minutes.
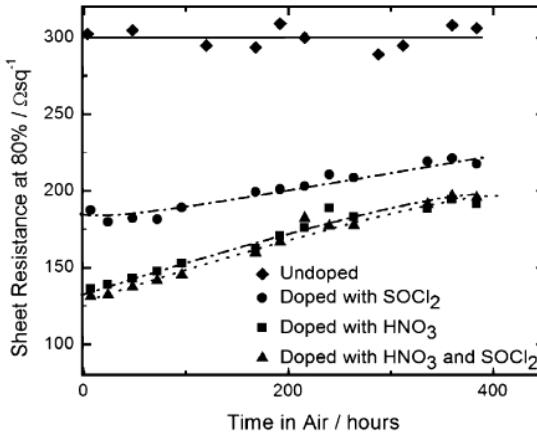
Figure 1.15. Effect of *p*-doping on the sheet resistance of SWNT conductive films. (taken from ref. [138])

Sheet resistance of as-prepared films has decreased after *p*-doping with HNO_3 to 187 $\Omega/\square$ from the initial sheet resistance of 300 $\Omega/\square$. The optical transmittance of the films evaluated in Figure 1.15 was kept at 80%. As seen from Figure 1.15, the doping effect is not stable when the films were kept in ambient conditions. The stability of doping can be improved further by encapsulation or top-coating with another layer of material. For example, PEDT:PSS was used as such a material.[138]

The effect of doping can further be evidenced by differences in the optical properties of the films. Disappearance or weakening of van Hove singularities of SWNT films in optical absorption spectra is due to the effect of *p*-doping. The *p*-doping creates states below the conduction band of semiconducting SWNTs, which reduces the total band gap between the van Hove singularities or the inter-band transitions. Figure 1.16 shows the typical example of the effect of doping on the optical properties of SWNT films in UV-Vis-NIR region.
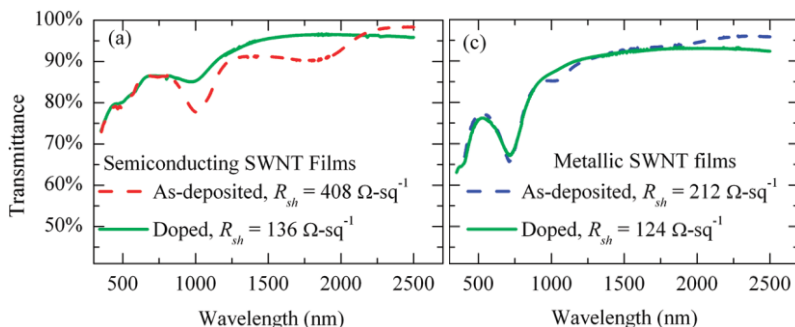
Figure 1.16. Effect of *p*-doping on the optical properties of SWNT films. (taken from ref. [139])

The bleaching or weakening of inter-band transitions due to *p*-doping is typical for SWNT films prepared from semiconducting tubes. However, SWNT films prepared from metallic tubes do not exhibit a similar effect on optical properties upon *p*-doping. Although the effective charge transfer due to *p*-doping is evidenced for metallic tubes from the reduction in sheet resistance of the films (Fig 1.16), the possible Fermi level shift due to the doping does not exceed the energy of the first metallic van Hove singularity. This results in substantially fewer holes injected into metallic SWNTs when compared to semiconducting SWNTs.[139]

Raman spectroscopy is also an effective tool to characterize of effect of doping on the SWNTs films. The G-band frequency is used to monitor the effect of doping, as it is sensitive charge transfer. The G-band upshifts for electron acceptors (*p*-doping) and downshifts for electron donors (*n*-doping), as in graphite intercalation compounds.[115]

1.4.4 Overview of SWNT transparent conductive films

SWNTs can be processed to thin films of thickness ≈ 10 – 100 nm, which will have high electrical conductivity at reasonably high optical transmittance, due to the sparse structure of the nanoscale network. The optical transmittance and sheet resistance decrease with increasing film thickness. There are several processing methods available for the fabrication of SWNT

transparent conducting films. Spraying,[140] slot coating,[38] (Meyer rod) bar coating,[38] spin coating,[141] filtration & stamping,[142] and dip coating are the methods for fabrication of SWNT TCFs, of which spraying and filtration methods are widely used in literature at the laboratory scale.

1.4.4.1   Electrical and optical properties of SWNT TCFs

As it was observed that the SWNTs are not reflective in nature (negligible amount of reflection[34]), the optical transmittance of the films is determined mainly by their absorption behavior.[143] Optical transmittance of the film is inversely proportional to the nanotube network density, but is not affected by inter-tube resistance, length of the tube, diameter of the tube and doping. As the diameter of the tube is much less than the incident wavelength of light ($d \ll \frac{\lambda}{10}$) forward scattering will be a predominant process, which does affect the optical transmittance of the film significantly.
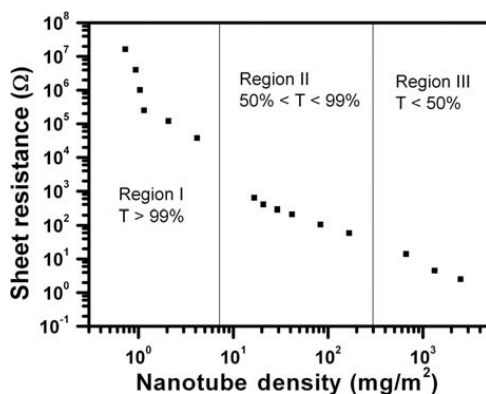
Figure 1.17. Dependence of sheet resistance of SWNT films on nanotube network density. (taken from ref.[38])

The electrical conductivity ($\sigma_{d.c.}$) of a film can be calculated as the reciprocal of the product of the sheet resistance (R_s) and the thickness of the film (t). The sheet resistance of the film decreases with increasing nanotube density (Fig 1.17). The optical transmittance varies

between 50 to 99% for a nanotube density range of 7 mg•m^{-2} to 300 mg•m^{-2}; in this regime, the

sheet resistance varies between 100 $\Omega/\square$ to 1000 $\Omega/\square$.[38] This working range is suitable for

transparent conducting films. Since the thicknesses of the films are on the order of < 50 nm for

transparent conducting films, and as the measurement of such small thicknesses using

conventional equipment are limited, the properties of the films are always described in optical

transmittance vs. sheet resistance. For this purpose, the ratio of electrical conductivity to optical

conductivity ($\frac{\sigma_{d.c.}}{\sigma_{o.c.}}$) is defined. For SWNT TCFs, the optical transmittance at a wavelength of 550

nm, T_{550}, can be deduced from the following theoretical expression, which is widely used as

figure of merit (it is found that the average value of the transmittance between 400 to 700 nm is

practically the same as the transmittance at 550 nm):[119, 144]

$$T_{550} = \left(1 + \frac{1}{2R_s}\sqrt{\frac{\mu_0}{\varepsilon_0}}\frac{\sigma_{o.c.}}{\sigma_{d.c.}}\right)^{-2} \tag{1.13}$$

where R_s is the sheet resistance of the film and μ_0 and ε_0 are the permittivity and permeability

of free space, respectively. $\frac{\sigma_{d.c.}}{\sigma_{o.c.}}$ is the ratio of electrical and optical conductivity and can be

obtained by curve fitting the experimental values of R_s vs. T_{550}. The higher $\frac{\sigma_{d.c.}}{\sigma_{o.c.}}$, the better will

be the performance of transparent conducting films. The critical values for R_s and T_{550} for

touch screen applications will be described in the following section.

1.4.4.2   Requirement for TCFs in different applications

As transparent conducting films are used in many applications such as LEDs, touch panels, flat

panel displays, solar cells, EMI shielding, etc., the requirements demanded from them also vary

from case to case. This section represents a bird eye's view on the requirement for transparent

conductors in different applications. The customer or the device producer might always want the

best, typically 100% optical transmittance, 0% haze and 0% reflection. However, the functional

requirements for specific devices are usually less demanding. The commonly used transparent

conductor, ITO, also has 90% transmittance, < 1% haze and reflection losses close to 10 % and in some cases the reflection loss exceeds 10%, and, for example, the optical transmittance required for touch screen sensors is 90% or more.[35] whereas the sheet resistance required ranges from 50 to 300 $\Omega/\square$.[35]

Most of the loss in optical transmission which occurs in current device systems is due to contributions from reflections, scatterings and additional absorptions. SWNTs exhibit very low reflection losses,[34] as compared to ITO (Fig 1.18) or silver nanowires, another alternative for the generation of conducting films. Therefore, the focus in the fabrication of SWNT TCFs lies on improving their optical transmittance by generating appropriate nanoscale networks.
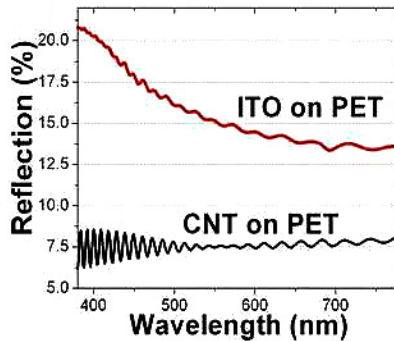
Figure 1.18. Reflection spectra of ITO and SWNTs films on plastic substrate. (taken from ref.[35])

For solar cells and LEDs, the requirements are stricter: The optical transmittance should be 90% or more, the required sheet resistance should lie between 10 to 50 $\Omega/\square$.[145] On the other hand, for large flat panel displays, the optical transmittance required is 80% (or more), but sheet resistance values between 100 to 125 $\Omega/\square$ are acceptable.[146] For large touch panel applications, the optical transmittance required is ~85% at sheet resistance of 300 to 500 $\Omega/\square$.

However, the numbers given are subject to change, depending on the sensing capabilities in sensors, switching speeds in LEDs and operating frequencies of electronic devices.[35]

Color neutrality of the films is another important parameter related to optical transmittance. SWNTs have advantages here, as — corresponding to the fact that they are black in colour — they absorb the entire range of photons in visible wavelength equally. In contrast, ITO films usually have a yellow tinge, whereas conducting polymer (PEDT:PSS) films normally have a blue tinge. The color neutrality of SWNT films is shown in figure 1.19.
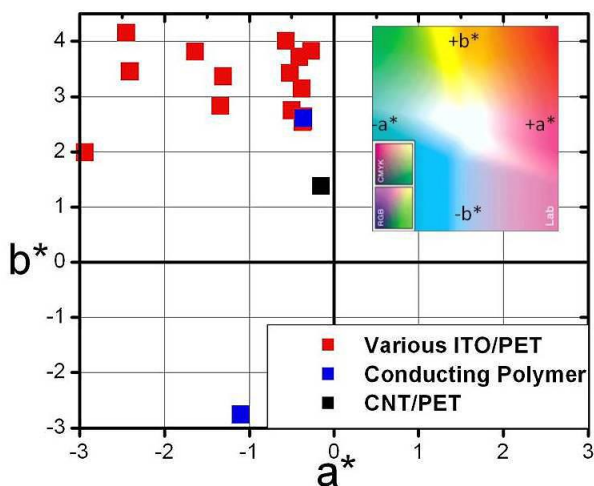
Figure 1.19. Colour coordinate values for ITO, conducting polymer and SWNT films on PET substrates. (taken from ref.[35])

Haze is another key parameter, which quantifies the amount of light scattered from the surface of films. A haze value of more than 1% is not acceptable for a transparent conductor with regard to any of the device applications mentioned above. ITO films usually have good haze values. Silver nanowires suffer from larger haze values due to the high surface roughness.[35] The haze

values for SWNT films are in the range of 0.1 to 0.3 %, which is usually controlled by appropriate processing methodologies.

1.4.4.3 SWNT TCFs – comprehensive summary of literature reports

Since the year 2004, the potential of SWNT films as transparent conductor has been realized.[116] Several reports on the development of SWNT TCFs had already surfaced before 2004. The development has included improvements in the synthesis, purification, processing and dispersion of SWNTs. On the other hand, the development and optimization of processing methodologies for film fabrication and post-film processing for the improvement of film properties have also been studied. The effect of using different types of SWNTs (CVD, laser and arc evaporation grown SWNTs) on the performance of film properties has also been studied; arc evaporation-grown SWNTs tend to give relatively better electrical and optical properties for transparent conducting films.[147] The effect of varying purification procedures of SWNTs with different types of oxidizing acids, the effect of dispersion quality and of fabrication methods (spraying, filtration, bar-coating, dip-coating, etc.), as well as the effect of post-film processes on the overall performance of SWNT TCFs have been reported.

In general, the SWNT TCFs reported in literatures can be classified into three major groups:

Group A:	TCFs prepared from SWNTs dispersed in a solvent medium
Group B:	TCFs prepared from SWNTs dispersed in a solvent medium, subsequent washing with solvents to remove any unwanted impurities from the film
Group C:	TCFs prepared from SWNTs dispersed in a solvent medium, subsequent doping of the film with dopants

SWNT TCFs of group A which have been reported in the literature are summarized in Table 1.1. The data summarized include TCFs from SWNTs which underwent a purification process and also films from SWNTs that did not undergo the purification process.

In this set of TCFs, the highest value of $\frac{\sigma_{d.c.}}{\sigma_{o.c.}}$ = 14 (R_s = 50 Ω/□ at T_{550} = 62%) was reported for TCFs which were deposited by direct growth on a substrate and then transferred to glass substrates using a "dry transfer technique".[148] The films were finally densified with ethanol. It is difficult to comment whether the densification process is only densify or also to remove the impurities. Although here the dry-transfer technique provides well-performing SWNT TCFs, other reports suggest that this technique is difficult to reproduce; the inconsistencies observed require further investigation and optimization as well as scale-up experiments.[149,150,151] TCFs prepared by conventional wet-processing techniques (dispersing the SWNTs in a solvent medium and then fabricating films through subsequent processing methods) show, for example, a value of $\frac{\sigma_{d.c.}}{\sigma_{o.c.}}$ = 5.3 (R_s = 420 Ω/□ at T_{550} = 85%) for a film prepared by spraying dispersions of SWNTs (synthesized by the CVD method) in dimethylformamide (DMF) onto glass substrates..[152] With a similar procedure, Lu et al. reported a value of $\frac{\sigma_{d.c.}}{\sigma_{o.c.}}$ = 16,[153] using dispersions of metallic SWNTs (which had been separated from the semiconducting tubes) which in addition underwent dry-air oxidation and 2.6 M HNO_3 treatments. This additional process of oxidation in dry-air and in HNO_3 significantly dopes the tubes, thereby resulting higher $\frac{\sigma_{d.c.}}{\sigma_{o.c.}}$. The majority of films prepared from SWNT-containing dispersions and measured directly without any post-processing has $\frac{\sigma_{d.c.}}{\sigma_{o.c.}}$ < 4. This suggests that a superior film can only be achieved when additional processes are performed after fabricating the films.

Table 1.1: Properties of TCFs prepared from SWNTs dispersed in a solvent medium (Group A)

S/No	Type[a]	Pre-process[b]	Additive[c]	Coating[d]	R_s[e]	T_{550}[e]	$\frac{\sigma_{d.c.}}{\sigma_{o.c.}}$ [e]	Ref
1	Arc	HNO_3	-	Spray	1000	87	2.61	154
2	-	-	PEDT	Ink-jet printing	10^4	90	0.01	155
3	-	-	PVA PSS	Layer-by-layer assembly	10^6	98	0	156
4	Arc	(purified)	-	Spray 150 °C	1200	80	1	157
5	-	-	SDS	Spray 50 °C	400	79	3.8	158
6	CVD	Refined	-	Spray	390	82	4.6	159
7	HiPCO	O_2/Air 225 °C/18 hr	In CSA	Dipping / Immersion 150 °C	471	86	5.1	160
8	APCO[161] Aerosol	-	-	Dry Transfer	80	65	9.8	162
9	Aerosol CVD	-	-	Dry Transfer	700	90	5	163
10	HiPCO	-	SDS	Spray	1100	80	1.45	164
11	HiPCO	-	SDS	Filtration	1200	85	1.85	164
12	HiPCO	-	SDS	Electrophoretic deposition	1070	75	1.24	164
13	HiPCO	-	SDS	Dip Coating	10^6	88	0	164
14	CVD	-	-	Dry Transfer	50	62	14	148
15	CAD	Oxidation/Air 225 °C/10 hr 4M HNO_3 20 °C/2 hr Drying 360 °C/3 hr	-	Spin coating 60 °C/5min	400	80	4	165
16	Arc	-	In NMP	Filtration 130 °C	925	87	2.8	166
17	Arc	-Purified-	In DCE	Dip Coating	475	82	3.8	167
18	Arc	-Purified-	In DCE	Spraying	475	72	2.2	167
19	Arc	-Purified-	In DCE	Dip Coating + Spraying	190	70	5.1	167
20	HiPCO	Dry Air 200 °C/24 hr HCl (37%) 80 °C/15 min	SDS	Filtration	320	65	2.5	122
21	HiPCO	Wet Air 225 °C/18 hr	In DMF	Filtration	800	71	1.3	168
22	HiPCO	Wet Air 225 °C/18 hr HCl + H_2O_2 60 °C/4 hr	In DMF	Filtration	1600	70	0.6	168
23	HiPCO	Wet Air 225 °C/18 hr H_2SO_4 + H_2O_2	In DMF	Filtration	1800	75	0.7	168

24	CVD	-	-	Filtration Dry Transfer	100	58	6	[169]
25	PLV	30%O_2+70%N_2 450 °C/3 hr HCl (37%)	In DMF	Spray	200	60	3.2	[170]
26	CVD	Dry air 600 °C/30 min	1,2-DCB	Spray	420	85	5.3	[152]
27	CVD	-		Dry transfer	341	80	4.7	[151]
28	CVD	Dry Air 300 °C/30min HNO_3 (2.6M) 130 °C/24 hr	In DMF (Separated Metallic)	Spray 200 °C	100	80	16	[153]
29	CVD	Directly grown	-	Dry Transfer	200	79	7.5	[150]
30	Arc	HNO_3 Purified N_2H_4 + Graphene Oxide 23 °C/7days	-	Spin Coating 115 °C	636	88	4.5	[171]
31	Arc	HNO_3 Purified N_2H_4 + Graphene Oxide 23 °C/7days	-	Spin Coating 110 °C	425	82	4.3	[172]
32	CVD	HNO_3 (7M) 130 °C/3 hr	CTAOH p-TSA	Meyer Rod 50 °C	1086	78	1.3	[173]
33	CVD	-	-	Dry Transfer	300	67	2.8	[149]
34	Arc	-Purified-	in DCE	Spray 900 °C	600	84	3.5	[174]

[a]. Type refers to the method in which the SWNT are produced. Arc – Arc evaporation method; PLV – Pulsed laser vaporization; CVD – Chemical vapor deposition; HiPCO – hi pressure carbon monoxide process.

[b]. Purification conditions performed on the SWNTs, including temperature and time.

[c]. Additive refers to the surfactant molecules added in the dispersion of SWNTs. (PEDT – poly(3,4-ethylene dioxythiophene):poly/4-styrenesulphonic acid(; PVA – polyvinyl alcohol; PSS – poly(4-styrene sulphonic acid); SDS – sodium dodecylsoulphate). Most of the dispersions mentioned above are prepared in water. Dispersion prepared in other solvents like CSA (chlorosulphonic acid) NMP (N-methyl pyrrolidone), DMF (dimethyl formamide), DCE (dichloroethane), o-DCB – orthodichlorobenzene, and 1,2-DCB (1,2-dichlorobenzene) are mentioned specifically.

[d]. Coating methods in which the film is fabricated, and annealed at a temperature.

[e]. R_s is the sheet resistance of the film in $\Omega/\square$, T_{550} is the optical transmittance of the film, and $\frac{\sigma_{d.c}}{\sigma_{o.c.}}$ is the ratio of electrical to optical conductivity calculated using equation (1.14).

The second set of SWNT TCFs (group B) reported in the literature is summarized in Table 1.2, above. This compilation summarizes preparation and properties of films prepared from SWNT dispersions which underwent a subsequent washing process with solvents to remove excessive surfactants or impurities from the film. A high $\frac{\sigma_{d.c.}}{\sigma_{o.c.}}$ value of 15.6 is reported for a film prepared by spraying a dispersion containing SWNTs (synthesized by arc evaporation) in water with sodium dodecylbenzene sulphonate as a surfactant onto glass substrates.[196] The TCF was washed with copious amounts of water to remove the SDBS surfactant molecules that are insulating by nature. Hecht et al. reported the film with the highest $\frac{\sigma_{d.c.}}{\sigma_{o.c.}}$ of 65 in this group of SWNT TCFs, which was prepared by the filtration method.[197] The SWNTs used were subjected to dry air oxidation and an acid purification process (which was not described) and then dispersed in chlorosulphonic acid (CSA). Filtered films were then washed with diethyl ether and water repeatedly. Similarly, Wu et al reported a high value of $\frac{\sigma_{d.c.}}{\sigma_{o.c.}}$ = 32 for TCFs prepared by filtration of a SWNT dispersion containing TX-100 surfactant.[116] The SWNTs used were purified by refluxing in concentrated nitric acid for 45 hours. Later the filtered films were washed repeatedly with water, acetone and methanol. These high values of $\frac{\sigma_{d.c.}}{\sigma_{o.c.}}$ reported by Wu et al. and Hecht et al. could not be reproduced by others, suggesting that some of the key parameters went unknown during the processes. The majority of the reports in group B consistently report $\frac{\sigma_{d.c.}}{\sigma_{o.c.}}$ values between 5 to 12, implying that better performance of SWNT TCFs can only be improved if additional doping processes are implemented (vide infra).

Table 1.2: Properties of TCFs prepared from SWNT dispersions, with subsequent washing (Group B)

S/No	Type[a]	Pre-process[b]	Additive[c]	Coating[d]	Washing[f]	R_s[e]	T_{550}[e]	$\frac{\sigma_{d.c.}[e]}{\sigma_{o.c.}}$	Ref
1	PLV	-	SDS	Spray 120°C	H_2O	300	90	11.6	175
2	Arc	HNO_3	SDS	Filtration	Acetone	300	80	5.3	138
3	Arc	HNO_3	PVP	Wet coating	H_2O	1250	85	1.8	176
4	Arc	-	SDBS	Spray	H_2O	90	65	8.7	177
5	-	-	DMSAPS Glycerol	Filtration	H_2O Acetone	200	82	9	178
6	Arc	O2 / Air	SDBS	Spray	H_2O	1250	70	0.8	179
7	Arc	HNO_3	SDBS	Spray	H_2O	600	83	3.2	179
8	Arc	-	Na Cholate	Filtration	H_2O	210	72	5	180
9	HiPCO	-	SDS	Spray	H_2O	600	90	5.8	164
10	Arc	Step Gradient Centrifugation	SDS	Filtration	H_2O Acetone	246	75	5	181
11	HiPCO	-	SDBS	Meyer rod	H_2O + Ethanol	210	64	3.6	182
12	Arc	-	SDS	Spray	H_2O	220	85	10.1	183
13	Arc	-	SDS	Spray 100°C	H_2O	180	80	8.9	146
14	Arc	Purified	Nafion	Spray 100°C	H_2O	430	84	4.8	184
15	CVD	-	SDS	Spray 100°C	H_2O	7000	72	0.2	147
16	HiPCO	-	SDS	Spray 100°C	H_2O	1070	83	1.8	147
17	PLV	-	SDS	Spray 100°C	H_2O	500	77	2.7	147
18	Arc	-	SDS	Spray 100°C	H_2O	202	72	5.2	147
19	Arc	-	SDBS	Spray 100°C	H_2O	274	90	12.7	185
20	Arc	-	SDBS	Spray 100°C	H_2O	200	82	9	186
21	Arc	-	SDS	Filtration	H_2O	250	82	7.2	187
22	Arc	HNO_3	SDS	Spray	H_2O	1000	80	1.6	188
23	HiPCO	Dry Air 200°C/24hr HCl (37%) 80°C/15min	SDS	Filtration	H_2O	100	70	9.7	189
24	Arc	HNO_3	TX-100	Filtration	Tris-HCl	900	82	2	190
25	Arc	HNO_3	TX-100	Filtration	Tris-HCl Acetone Methanol (50%)	250	84	8.3	190
26	HiPCO	HNO_3	TX-100	Filtration	Tris-HCl	2700	83	0.7	190
27	HiPCO	HNO_3	TX-100	Filtration	Tris-HCl Acetone Methanol	300	76	4.3	190

28	PLV	HNO$_3$	TX-100	Filtration	Tris-HCl	900	86	2.7	190
29	PLV	HNO$_3$	TX-100	Filtration	Tris-HCl Acetone Methanol	200	78	7.1	190
30	Arc	Dry Air 200°C/10hr Aminopolycarboxylic acid 110°C/18hr	in o-DCB	Filtration	Acetone H$_2$O	300	88	9.5	191
31	CVD	2.6 M HNO$_3$ 140°C/48hr	Nafion	Filtration	Acetone	600	84	3.5	192
32	CVD	2.6 M HNO$_3$ 140°C/48hr	SDS	Filtration	Acetone H$_2$O	870	81	2	192
33	Arc	Dry Air	SDS	Filtration	H$_2$O	100	60	6.5	193
34	Arc	-Purified-	SDS	Filtration	H$_2$O Acetone	100	80	16	194
35	HiPCO	Density gradient separation	SDS:SC 3:2 (v/v)	Filtration	H$_2$O Unsorted Metallic (0.9nm) Metallic (1nm)	1500 400 200	76 79 76	0.9 3.76 6.4	195
36	Arc	Dry Air	SDBS	Spray 70°C	H$_2$O	250	91	15.6	196
37	CVD	Dry Air Acid purified	In CSA	Filtration	DEE H$_2$O	60	91	65	197
38	Arc	-Purified-	SDS	Spray 80°C	H$_2$O	300	80	5.3	198
39	Arc	-	5TN-PEG In Ethanol	Spin Coating	DCM H$_2$O	3000	80	5.3	199
40	PLV	30%O$_2$+70%N$_2$ 450°C/3hr HCl (37%)	In DMF	Spray	-	200	60	3.2	170
41	HiPCO	-	SDS PEDT:PSS	Spin Coating 120°C	Methanol	350	84	5.9	26
42	Arc	Dry Air	Sodiumdeoxycholate	Layer-by-layer; 350°C	H$_2$O	1236	86.5	2	200
43	HiPCO	-Purified-	Sodiumdeoxycholate	Layer-by-layer; 350°C	H$_2$O	309	83.5	6.5	200
44	Arc	Dry Air O$_2$ 425°C/2hr HCl (37%) 23°C/12min	SDS	Spray 100°C	H$_2$O	2100	85	1.1	201
45	Arc	Dry Air O$_2$ 425°C/2hr HCl (37%) 23°C/12min HNO$_3$(65%)	SDS	Spray 100°C	H$_2$O	956	85	2.3	201

46	CVD	-	SDS PEDT:PSS	Filtration	H_2O Acetone Methanol	80	75	15.2	202
47	Arc	Dry Air O_2 400°C/30min Argon 1000°C/1hr O_2 & Ar 1000°C/1.5hr	SDS	Filtration	NaOH H_2O H_2O	540 2465 187	80 80 80	3 0.7 8.5	203
48	PLV	HNO_3 130°C/45min	TX - 100	Filtration	H_2O Acetone Methanol	30	70	32.2	116
49	CVD	HNO_3 (7M) 130°C/3hr	CTAOH p-TSA	Meyer Rod,50°C	Ethanol	1086	78	1.3	173

[a] to [e], as described in Table 1.1

More surfactant molecules abbreviated in table 2: PVP – polyvinyl pyrrolidone; SDBS – sodium dodecyl benzene sulphonate; DMSAPS – 3-(N,N-dimethylstearylammonio)-propanesulfonate; TX-100 – Triton surfactant; SC – sodium cholate; 5TN-PEG – quinquethiophene terminated poly(ethylene glycol); p-TSA – para toluene sulphonic acid, and CTAOH - cetyltrimethylammonium hydroxide.

[f]. Describes the solvent with which washing process was performed on the fabricated SWNT TCFs, in order to remove the excessive surfactant molecules & impurities.

Properties of the last set of SWNT TCFs (group C) are summarized in Table 1.3. These films were fabricated from dispersions of SWNTs that were pre-treated with strong oxidizing agents. Later the films were subjected to washing to remove unwanted insulating surfactant molecules, and finally to a doping process with dopants such as inorganic acids, graphene oxide, conducting polymers, or others. The $\frac{\sigma_{d.c.}}{\sigma_{o.c.}}$ values of the majority of films reported in this group range from 15 to 20, which can be considered as sufficient for TCFs for several different applications. Nitric acid is the most common doping agent for SWNT TCFs. Kim et al. reported a $\frac{\sigma_{d.c.}}{\sigma_{o.c.}} \approx 32$ for TCFs prepared from dispersions of SWNTs containing hydroxypropylcellulose (HPC) as surfactant.[204] Subsequently the film is washed with large amount of IPA to remove the insulating surfactant molecules and then doped with nitric acid for 30 minutes.

Table 1.3: Properties of TCFs prepared from SWNT dispersions, prepared with doping (Group C)

S/No	Type[a]	Pre-process[b]	Additive[c]	Coating[d]	Post-process[f]	R_s [e]	T_{550} [e]	$\dfrac{\sigma_{d.c.}[e]}{\sigma_{o.c.}}$	Ref
1	HiPCO	HNO_3(6M) 80°C/12hr	SDBS	Spray 120°C	H_2O 12M HNO_3/1hr	125	81	13.5	205
2	Arc	-	SDBS	Spray 110°C	H_2O 12M HNO_3/1hr	125	86	19.2	206
3	Arc	-	SDBS	Spray 110°C	H_2O 12M HNO_3+$SOCl_2$/1.7hr	105	86	22.9	206
4	Arc	HNO_3	SDS	Filtration	Acetone HNO_3/30min	140	80	11.4	138
5	Arc	HNO_3	SDS	Filtration	Acetone $SOCl_2$/30min	170	80	9.4	138
6	Arc	HNO_3	SDS	Filtration	Acetone HNO_3 + $SOCl_2$/30min	115	80	13.9	138
7	Arc	HNO_3	PVP	Wet coating	H_2O Insitu PEDT:PTS	350	85	6.4	176
8	Arc	O_2/Air 100°C/18hr	-	Spin coating	IPA/ H_2O 4M HNO_3+16M HNO_3 / 12+0.5 hr	128	90	27.2	207
9	Arc	O_2/Air 100°C/18hr	SDS	Spray 90°C	IPA/ H_2O 4M HNO_3+16M HNO_3 / 12+0.5 hr	57	65	13.7	207
10	Arc	O_2/Air 100°C/18hr	SDBS	Spray 90°C	IPA/ H_2O 4M HNO_3+16M HNO_3 / 12+0.5 hr	68	70	14.2	207
11	Arc	H_2SO_4:HNO_3 23°C/3hr	SDBS	Dipping 23°C	H_2O $AuCl_3$/30 sec	424	63	1.7	208
12	Arc	-	SDBS	Spray	H_2O;Graphene Oxide (GO)	75	65	10.4	177
13	HiPCO	-	SDBS TX100	Mayer rod	9M HNO_3/18hr	100	53	5	209
14	HiPCO	-	CMC	Mayer rod	9M HNO_3/18hr	100	59	6.2	209
15	Arc	-	CMC	Mayer rod	9M HNO_3/18hr	100	81	17	209
16	PLV	-	CMC	Spray 80°C	4M HNO_3/18hr	50	75	24.4	210

17	PLV	-	CMC	Spray 80°C	4M HNO_3 + 4M N_2H_4 / 24 hr	70	75	17.4	[210]
18	-	-	DMSAPS Glycerol	Filtration	H_2O, Acetone 5M HNO_3	115	82	15.7	[178]
19	HiPCO	-	PSSNa	Layer-by-layer	H_2O ; PEDT:PEG	10^3	81.8	1.7	[211]
20	Arc	O_2 / Air	SDBS	Spray	H_2O ; H_2SO_4	180	74	6.4	[179]
21	Arc	HNO_3	SDBS	Spray	H_2O ; H_2SO_4	155	73	7.1	[179]
22	CVD	-	SDBS	Spray	H_2O ; H_2SO_4	370	81	4.6	[179]
23	Arc	HNO_3	SDBS	Spray	H_2O ; H_2O_2:H_2SO_4[3:1]	385	90	9	[179]
24	CVD	NaOH 170°C/5min	Phenylene	Filtration	H_2O HNO_3(60%)/12 hr	380	65	2.1	[212]
25	Arc	-	Na Cholate	Filtration	H_2O ; $HAuCl_4.3H_2O$	80	78	17.8	[180]
26	CVD	Refined	-	Spray	PEDT:PSS	220	81	7.7	[159]
27	CVD	H_2SO_4:HNO_3 125°C/25hr	LB Assembly	GO	400	84	5.2	[213]
28	-	-	In Hydrazine	Spin Coating	rGO	254	58	2.4	[214]
29	CVD	H_2SO_4:HNO_3	SDBS	Dip Coating 120°C	PEDT:PSS	173	55	3.1	[215]
30	Aerosol CVD[161]	-	-	Dry Transfer	Ethanol NO_2 (Gas phase)/10min	84	90	41.5	[162]
31	Aerosol CVD	-	-	Dry Transfer	Ethanol HNO_3 (65%)/1min	110	90	31.7	[163]
32	Arc	Acid mixture 125°C/-	SDS	Spray	Conductive polymer	100	82	18.1	[216]
33	Arc	Step Gradient Centrifugation	SDS	Filtration	H_2O, Acetone 12 M HNO_3/1hr	152	75	8	[181]
34	Arc	Step Gradient Centrifugation	SDS	Filtration	H_2O, Acetone ; 1hr 12 M HNO_3 + 0.23M Triethyloxonium hexachloroantimonate	63	75	19.3	[181]
35	Arc	HNO_3	SDS	Filtration	H_2O ; HNO_3	400	60	1.6	[217]
36	Arc	HNO_3	SDS	Filtration	H_2O ; HNO_3 & $SOCl_2$/3hr	150	62	4.7	[217]
37	HiPCO	HNO_3	SDS	Filtration	H_2O ; HNO_3	200	40	1.6	[217]

38	HiPCO	HNO$_3$	SDS	Filtration	H$_2$O ; HNO$_3$ & SOCl$_2$/3hr	155	63	4.7	[217]
39	HiPCO	-	SDBS + TX100	Meyer rod	H$_2$O+Ethanol 12M HNO$_3$/Oleum-0.5hr	90	72	11.7	[182]
40	Arc	-	SDS	Spray	H$_2$O ; 12M HNO$_3$/1hr	100	85	22.3	[183]
41	Arc	-	SDS	Spray 100°C	H$_2$O ; 12M HNO$_3$/1hr	70	80	22.8	[146]
42	Arc	Purified	Nafion	Spray 100°C	H$_2$O ; 12M HNO$_3$/1hr	130	84	15.9	[184]
43	Arc	-	SDBS	Spray	H$_2$O ; TEOS sol (top coat)	208	90	16.7	[185]
44	Arc	-	SDBS	Spray 100°C	H$_2$O ; HNO$_3$/1hr	84	82	21.5	[186]
45	Arc	-	SDBS	Spray 100°C	H$_2$O ; 1hr HNO$_3$ & AuCl$_3$(spun)	50	80	31.9	[186]
46	Arc	Dry Oxidation Acid treated	-	Spin Coating 110°C	UV-O$_3$ PEDT:PSS	362	91	10.8	[218]
47	Arc	Dry Oxidation Acid treated	-	Spin Coating 110°C	UV-O$_3$ PEDT:PSS HNO$_3$ /1hr	91	92	48.6	[218]
48	CVD	HCl (37%) 100°C/48hr Oleum 120°C/96hr HNO$_3$(67%) 70°C/1hr	-	Filtration 550°C	HCl (37%)/2min HNO$_3$(67%)/30 min	133	90	26.2	[219]
49	CVD	-	-	Dry Transfer	Direct Synthesis	50	62	14	[148]
50	Arc	Oxidation/Air 360°C/10hr 4M HNO$_3$ 20°C/2hr Drying 360°C/3hr	-	Spin coating 60°C/5min	HNO$_3$ /1hr	100	80	16	[165]
51	CVD	HCl (29%) 100°C/10hr	SDS	Electrophoretic deposition	2M HNO$_3$/2hr	340	76	3.8	[220]
52	Arc	-	Unknown	Filtration	PEDT:PSS	200	85	11.1	[221]
53	Arc	-	In NMP	Filtration 130°C	HNO$_3$/10min	94	87	27.8	[166]
54	-	-	SDS	Dip coating	H$_2$O 16M	550	83	3.5	[222]

55	HiPCO	Dry Air 200°C/24hr HCl (37%) 80°C/15min	SDS	Filtration	HNO_3 (69.7%)/3hr	250	65	3.1	122
56	-	-	TX-100 PEDT:PSS	Dip Coating 110°	H_2O ; HNO_3	66	80	24.2	223
57	-	-	TX-100	Dip Coating 110°	H_2O ; HNO_3	67	58	9	223
58	HiPCO	Wet Air 225°C/18hr	In DMF	Filtration	1mM $HAuCl_3$/10min	325	71	3.1	168
59	HiPCO	Wet Air 225°C/18hr HCl + H_2O_2 60°C/4hr	In DMF	Filtration	1mM $HAuCl_3$/10min	600	70	1.6	168
60	HiPCO	Wet Air 225°C/18hr H_2SO_4 + H_2O_2 23°C/4hr	In DMF	Filtration	1mM $HAuCl_3$/10min	290	73	3.8	168
61	Arc	Dry Air	SDBS	Spray 70°C	H_2O ; GO	215	90.7	20.5	196
62	Arc	SDS-Filtration Acetone Wash	rr-P3HT In $CHCl_3$	Spin Coating 120°C	$CHCl_3$; $SOCl_2$/12hr	80 170	72 81	13.2 10	224
63	Arc	Dry Air	Porphyrin alkane in $CHCl_3$	Centrifuge Coating	$CHCl_3$;HNO_3/30min	600	90	5.8	225
64	-	-Purified-	- (Metallic)	Filtration	Acetone; HNO_3/45min	76	65	10.3	139
65	-	-Purified-	- (Semicon.)	Filtration	Acetone HNO_3/45min	60	73	18.4	139
66	Arc	-	5TN-PEG In Ethanol	Spin Coating	DCM, H_2O; HNO_3/1hr $SOCl_2$/30min HNO_3+$SOCl_2$/90min	200 150 110	81.5 80.5 80	8.8 11 14.5	199
67	CVD	Dry air 600°C/30min	1,2-DCB	Spray	F_4TCNQ	220	84	9.4	152
68	DWNT	H_2SO_4:HNO_3 3:1 v/v, 100°C	SDS Nano Silver	Meyer Rod	5M HNO_3	300	94	20	226
69	CVD	-		Dry transfer	HNO_3/1hr	210	87	12.4	151
70	CVD	-Purified-	Sodium Deoxy-cholate	Layer-by-layer, 350°C	H_2O HNO_3 (Vapor)/30min	324	82	5.6	227, 228
71	Arc	Dry Air	Sodium Deoxy-cholate	Layer-by-layer, 350°C	H_2O HNO_3 (Vapor)/30min	227	86.5	11	200
72	HiPCO	-Purified-	Sodium Deoxy-cholate	Layer-by-layer, 350°C	H_2O HNO_3 (Vapor)/30min	107	83.5	18.7	200

73	Arc	Dry Air O$_2$ 425°C/2hr HCl (37%) 23°C/12min HNO$_3$(65%) 23°C/12min HCl(37%) 23°C/12min	SDS	Spray 100°C	H$_2$O HNO$_3$ (65%)/2hr	472	85	4.7	201
74	CVD MWNT	TFA + Toluene ANI+H$_2$SO$_4$+ (NH$_4$)$_2$S$_2$O$_8$	-	Wet transfer	H$_2$O Camphorsulfonic acid (0.1M) m-Cresol	10^6 282	89 89	0 11.1	229, 230
75	Arc	Dry Air O$_2$ HNO$_3$	SDBS	Spray	H$_2$O H$_2$SO$_4$ (98%)/15min	175	73	6.3	231
76	PLV	HNO$_3$ (3M) 120°C/16hr	CMC or SDS	Spray 80°C	H$_2$O HNO$_3$ (4M)/18hr	80	81 (400-1800)	21.2	232
77	Arc	HNO$_3$ Purified N$_2$H$_4$ + Graphene Oxide 23°C/7days	-	Spin Coating 115°C	SOCl$_2$ vapor/15min	240	86	10	171
78	Arc	HNO$_3$ Purified N$_2$H$_4$ + Graphene Oxide 23°C/7hr	-	Spin Coating 110°C	SOCl$_2$ vapor/15min	103	82	17.5	172
79	CVD	HNO$_3$ (7M) 130°C/3hr	CTAOH p-TSA	Meyer Rod 50°C	Ethanol; SOCl$_2$	480	78	3	173
80	Arc	HNO$_3$	SDS	Filtration 100°C	H$_2$O; SOCl$_2$/12hr	160	87	16.3	233
81	CVD	-	-	Dry Transfer	Ethanol; HNO$_3$	90	78	15.8	149
82	Arc	-Purified-	in DCE	Spray 900°C	TFSI	40	84	51.7	174
83	CVD	-	HPC	Doctor blading 300°C	IPA HNO$_3$/30min	170	93.5	32.4	204
84	Arc	HNO$_3$	TX – 100	Dip Coating	H$_2$O HNO$_3$/1hr	130	69	7.1	234

[a] to [e], as described in Table 1.1

Abbreviations listed in table 3, other than table 1 & 2: CMC – Carboxymethyl cellulose; rr-P3HT – *region regular* Poly(3-hexylthiophene-2,5-diyl); HPC – hydroxypropylcellulose; TFA – trifluoroacetic acid; ANI – Aniline; and TCFSI - bis(trifluoromethanesulfonyl)imide.

[f]. Describes the post-process performed on the SWNT TCFs including washing, doping with different dopant molecules and doping duration.

TCFs fabricated without surfactant molecules has $\frac{\sigma_{d.c.}}{\sigma_{o.c.}} \approx 50$, reported by Kim et al.[174] The SWNTs were purified and dispersed in dichloroethane, and the dispersions were sprayed onto glass substrates. Later, bis(trifluoromethanesulfonyl)imide is deposited onto the film as dopant. The films without surfactant molecules perform better in terms of electronic properties. However, the adhesion between SWNTs and plastic substrates is facilitated by the presence of surfactant molecules, as the chemical affinity between SWNTs and plastic substrates is poor. However, when the amount of surfactant is as minimal as possible, improved adhesion properties go in hand with good film formation.

Graphene oxide (GO) is another dopant mentioned in the literature which is relatively easy to handle compared to other corrosive inorganic acid dopants. The $\frac{\sigma_{d.c.}}{\sigma_{o.c.}}$ for GO doped films are as high as ≈ 20, for TCFs prepared by spraying the SWNT dispersions containing SDBS surfactants.[196] The films were washed with copious amount of water to remove the surfactants and further doped with GO to enhance the electrical properties.

From the compilation of SWNT TCFs listed in the tables above (Table 1.1 to Table 1.3), it is clear that the performance of the films depends on the variations in process methodologies. Among them are:

- type of SWNT
- pre-treatment conditions to purify the SWNTs
- surfactant used in dispersion
- film fabrication method
- washing processes to remove the surfactants from the films
- dopant type and doping duration.

1.5 Summary

The application of SWNTs in transparent conducting films for flexible electronics applications have been studied thoroughly. The production of SWNTs using different methods and the implications of the methods on the type of SWNTs produced (including compositions of metallic and semiconducting tubes) has been established. The influence of the structural properties on the electrical and optical properties of SWNTs and nanotube network films has been studied. The functional requirements for transparent conducting films for different applications such as sensors, LEDs, displays, solar cells, etc. are known. Different processes to fabricate TCFs from SWNT dispersions containing different surfactant molecules have been reviewed. This detailed information helps us to focus more on fundamental insights on the development of SWNT dispersion systems and its implications on the electrical and optical properties of TCFs fabricated thereof.

1.6 References

1. Crabb, R. L.; Treble, F. C., Thin Silicon Solar Cells for Large Flexible Arrays. *Nature* **1967,** 213, 1223-1224.
2. Shirakawa, H.; Louis, E. J.; Macdiarmid, A. G.; Chiang, C. K.; Heeger, A. J., Synthesis of Electrically Conducting Organic Polymers: Halogen Derivatives of Polyacetylene, (CH)x. *JCS Chem. Comm.* **1977**, 578-580.
3. Burroughes, J. H.; Bradeley, D. D. C.; Brown, A. R.; Marks, R. N.; Mackay, K.; Friend, R. H.; Burns, P. L.; Holmes, A. B., Light-emitting diodes based on conjugated polymers. *Nature* **1990,** 347, 539-541.
4. MacDonald, W. A., Engineered films for display technologies. *J. Mater. Chem.* **2004,** 14, 4–10.
5. MacDonald, B. A.; Rollins, K.; MacKerron, D.; Rakos, K.; Eveson, R.; Hashimoto, K.; Rustin, B., Engineered Films for Display Technologies. In *Flexible Flat Panel Displays*, Crawford, G. P., Ed. John Wiley & Sons: Chichester, UK, 2005.
6. Fahlteich, J.; A-Schwab, S.; Weber, U.; Noller, K.; Miesbauer, O.; Boeffel, C.; Schiller, N., Ultra-High Barriers for Encapsulation of Flexible Displays and Lighting Devices. *SID Symp. Digest* **2013,** 44, 344-357.

7. Logothetidis, S., Polymeric Substrates and Encapsulation for Flexible Electronics: Bonding Structure, Surface Modification and Functional Nanolayer Growth. *Rev. Adv. Mater. Sci.* **2005,** 10, 387-397.

8. Anto, B. T.; Wong, L.-Y.; Png, R.-Q.; Sivaramakrishnan, S.; Chua, L.-L.; Ho, P. K. H., Printable Metal Nanoparticle Inks. In *Handbook of Nanophysics: Functional nanomaterials*, Sattler, K. D., Ed. CRC Press: Boca Raton, FL, 2010; Vol. 5.

9. Fortunato, E.; Ginley, D.; Hosono, H.; Paine, D. C., Transparent Conducting Oxides for Photovoltaics. *MRS Bull.* **2009,** 32, 242-247.

10. Gordon, R. G., Criteria for Choosing Transparent Conductors. *MRS Bull.* **2000,** 25, 52-57.

11. Zhang, M.; Fang, S.; Zakhidov, A. A.; Lee, S. b.; Aliev, A. E.; Williams, C. D.; Atkinson, K. R.; Baughman, R. H., Strong, Transparent, Multifunctional, Carbon Nanotube Sheets. *Science* **2005,** 309, 1215-1219.

12. Hu, L.; Gruner, G.; Li, D.; Kaner, R. B.; Cech, J., Patternable transparent carbon nanotube films for electrochromic devices. *Appl. Phys. Lett.* **2007,** 101, 016102.

13. Bädeker, K., Über die elektrische Leitfähigkeit und die thermoelektrische Kraft einiger Schwermetallverbindungen. *Ann. Phys.* **1907,** 327, 749–766.

14. Mochel, J. M. Electrically conducting coatings on glass and other ceramic bodies. 1951.

15. Holland, L.; Siddall, G., The properties of some reactively sputtered metal oxide films. *Vacuum* **1953,** 3, 375-391.

16. Wong, W. S.; Salleo, A., *Flexible Electronics: Materials and Applications*. Springer: New York, 2009; Vol. 11, p 462.

17. Cao, Q.; Rogers, J. A., Ultrathin films of single-walled carbon nanotubes for electronics and sensors: A review of fundamental and applied prospects. *Adv. Mater.* **2009,** 21, 29-53.

18. Gruner, G., Carbon nanotube films for transparent and plastic electronics. *J. Mater. Chem.* **2006,** 16, 3533-3539.

19. Hu, L.; Hecht, D. S.; Grüner, G., Carbon nanotube thin films: Fabrication, properties, and applications. *Chem. Rev.* **2010,** 110, 5790-5844.

20.   Aernouts, T.; Vanlaeke, P.; Geens, W.; Poortmans, J.; Heremans, P.; Borghs, S.; Mertens, R.; Andriessen, R.; Leenders, L., Printable anodes for flexible organic solar cell modules. *Thin Solid Films* **2004,** 451-452, 22-25.

21. Gustafsson, G.; Cao, Y.; Treacy, G. M.; Klavetter, F.; Colaneri, N.; Heeger, A. J., Flexible light-emitting diodes made from soluble conducting polymers. *Nature* **1992,** 357, 477-479.

22. Huang, J.; Wang, X.; deMello, A. J.; deMello, J. C.; Bradley, D. D. C., Efficient flexible polymer light emitting diodes with conducting polymer anodes. *J. Mater. Chem.* **2007,** 17, 3551-3554.

23. Jonas, F.; Karbach, A.; Muys, B.; van Thillo, E.; Wehrmann, R.; Elschner, A.; Dujadin, R. Conductive Coatings. EP0686662 A2, 1995.

24. Jonas, F.; Karbach, A.; Muys, B.; van Thillo, E.; Wehrmann, R.; Elschner, A.; Dujadin, R. Conductive Coatings. US 6083635, 1998.

25. Anglada, N. F.; Kaempgen, M.; Skákalová, V.; D-Weglikowska, U.; Roth, S., Synthesis and characterization of carbon nanotube-conducting polymer thin films. *Diamond Relat. Mater.* **2004,** 13, 1256-260.

26. Kymakis, E.; Klapsis, G.; Koudoumas, E.; Stratakis, E.; Kornilios, N.; Vidakis, N.; Franghiadakis, Y., Carbon nanotube/PEDOT:PSS electrodes for organic photovoltaics. *EPJ Appl. Phys.* **2007,** 36, 257-259.

27. Yoo, J. B.; Moon, J. S.; Park, J. H.; Lee, T. Y.; Kim, Y. W.; Park, C. Y.; Kim, J. M.; Jin, K. W., Transparent conductive film based on carbon nanotubes and PEDOT composites. *Diamond Relat. Mater.* **2005,** 14, 1882–1887.

28. Hu, L.; Wu, H.; Cui, Y., Metal nanogrids, nanowires, and nanofibers for transparent electrodes. *MRS Bull.* **2011,** 36, 760-765.

29. Song, J.; Kam, F.-Z.; Png, R.-Q.; Zhou, J.-M.; Lim, G.-K.; Ho, P. K. H.; Chua, L.-L., A general method for transferring graphene onto soft surfaces. *Nat. Nanotechnol.* **2013,** 8, 356-362.

30. Wassei, J. K.; Kaner, R. B., Graphene, a promising transparent conductor. *Mater. today* **2010,** 13, 52-59.

31. Saran, N.; Parikh, K.; Suh, D.-S.; Munoz, M.; Kolla, H.; Manohar, S. K., Fabrication and characterization of thin films of single-walled carbon nanotube bundles on flexible plastic substrates. *J. Am. Chem. Soc.* **2004,** 126, 4462-2263.

32. Trottier, C. M.; Glatkowski, P.; Wallis, P.; Luo, J., Properties and characterization of carbon-nanotube-based transparent conductive coating. *J. Soc. Info. Disp.* **2005,** 13, 759-763.

33. Chipman, A., A commodity no more. *Nature* **2007,** 449, 131.

34. Hecht, D. S.; Thomas, D.; Hu, L.; Ladous, C.; Lam, T.; Park, Y.; Irvin, G.; Drzaic, P., Carbon-nanotube film on plastic as transparent electrode for resistive touch screens. *J. SID* **2009,** 17, 941-946.

35. Mackey, B., Invited Paper: Trends and Materials in Touch Sensing. *SID Digest. Tech. Papers* **2011,** 42, 617-620.

36. Arthur, D.; Silvy, R. P.; Wallis, P.; Tan, Y.; Rocha, J. D. R.; Resasco, D.; Praino, R.; Hurley, W., Carbon nanomaterial commercialization: Lessons for graphene from carbon nanotubes. *MRS Bull.* **2012,** 37, 1297-1306.

37. Hecht, D. S.; Hu, L.; Irvin, G., Emerging Transparent Electrodes Based on Thin Films of Carbon Nanotubes, Graphene, and Metallic Nanostructures. *Adv. Mater.* **2011,** 23, 1482–1513.

38. Wong, W. S.; Salleo, A., *Flexible Electronics: Materials and Applications*. Springer: New York, 2009; p 462.

39. Colbert, D. T.; Smalley, R. E., Past, Present and Future of Fullerene Nanotubes: Buckytubes. In *Perspectives of Fullerene Nanotechnology*, Osawa, E., Ed. KLUWER ACADEMIC PUBLISHERS: New York, 2002; pp 3-10.

40. Iijima, S., Helical micrtubules of graphitic carbon. *Nature* **1991,** 354, 56-58.

41. Iijima, S.; Ichihashi, T., Single-shell carbon nanotubes of 1-nm diameter. *Nature* **1993,** 363, 603-605.

42. Bethune, D. S.; Kiang, C. H.; de Vries, M. S.; Gorman, G.; Savoy, R.; Vazquez, J.; Beyers, R., Cobalt-catalysed growth of carbon nanotubes with single-atomic-layer walls. *Nature* **1993,** 363, 605-607.

43. Ebbesen, T. W.; Ajayan, P. M., Large-scale synthesis of carbon nanotubes. *Nature* **1992,** 358, 220-222.

44. Collins, P. G.; Avouris, P., Nanotubes for electronics. *Scientific American* **2000**, 62-69.

45. Taylor, G. H.; Gerald, J. D. F.; Pang, L.; Wilson, M. A., Cathode deposits in fullerene formation – microstructural evidence for independent pathways of pyrolytic carbon and nanobody formation. *J. Cryst. Growth* **1994,** 135, 157-164.

46. Harris, P. F. J., *Carbon Nanotube Science: Synthesis, Properties and Applications*. Cambridge University Press: Cambridge, 2009.

47. http://www.iws.fraunhofer.de/content/dam/iws/en/documents/publications/product_sheets/500-3_swcnt_en.pdf. (*accessed on June 2014*)

48. Guo, T.; Nikolaev, P.; Thess, A.; Colbert, D. T.; Smalley, R. E., Catalytic growth of single-walled nanotubes by laser vaporization. *Chem. Phys. Lett.* **1995,** 243, 49-54.

49. Thess, A.; Lee, R.; Nikolaev, P.; Dai, H.; Petit, P.; Robert, J.; Xu, C.; Lee, Y. H.; Kim, S. G.; Rinzler, A. G.; Colbert, D. T.; Scuseria, G. E.; Tománek, D.; Fischer, J. E.; Smalley, R. E., Crystalline ropes of metallic carbon nanotubes. *Science* **1996,** 273, 483-487.

50. Kokai, F.; Takahashi, K.; Yudasaka, M.; Yamada, R.; Ichihashi, T.; Iijima, S., Growth Dynamics of Single-Wall Carbon Nanotubes Synthesized by CO2 Laser Vaporization. *J. Phys. Chem. B* **1999,** 103, 4346-4351.

51. Eklund, P. C.; Pradhan, B. K.; Kim, U. J.; Xiong, Q.; Fischer, J. E.; Friedman, A. D.; Holloway, B. C.; Jordan, K.; Smith, M. W., Large-Scale Production of Single-Walled Carbon Nanotubes Using Ultrafast Pulses from a Free Electron Laser. *Nano Lett.* **2002,** 2, 561-566.

52. Li, Y.; Mann, D.; Rolandi, M.; Kim, W.; Ural, A.; Hung, S.; Javey, A.; Cao, J.; Wang, D.; Yenilmez, E.; Wang, Q.; Gibbons, J. F.; Nishi, Y.; Dai, H., Preferential growth of semi-conducting single-walled carbon nanotubes by a plasma enhanced CVD method. *Nano Lett.* **2004,** 4, 317-321.

53. Dai, H.; Rinzler, A. G.; Nikolaev, P.; Thess, A.; Colbert, D. T.; Smalley, R. E., Single-wall nanotubes produced by metal-catalyzed disproportionation of carbon monoxide. *Chem. Phys. Lett.* **1996,** 260, 471-475.

54. Konga, J.; Cassell, A. M.; Dai, H., Chemical vapor deposition of methane for single-walled carbon nanotubes. *Chem. Phys. Lett.* **1998,** 292, 567-574.

55. Bhaviripudi, S.; Mile, E.; Steiner, S. A.; Zare, A. T.; Dresselhaus, M. S.; Belcher, A. M.; Kong, J., CVD synthesis of single-walled carbon nanotubes from gold nanoparticle catalysts. *J. Am. Chem. Soc.* **2007,** 129, 1516-1517.

56. Takagi, D.; Homma, Y.; Hibino, H.; Suzuki, S.; Kobayashi, Y., Single-walled carbon nanotube growth from highly activated metal nanoparticles. *Nano Lett.* **2006,** 6, 2642-2645.

57. Zhou, W.; Han, Z.; Wang, J.; Zhang, Y.; Jin, Z.; Sun, X.; Zhang, Y.; Yan, C.; Li, Y., Copper catalyzing growth of single-walled carbon nanotubes on substrates. *Nano Lett.* **2006,** 6, 2987-2990.

58. Deck, C. P.; Vecchio, K., Prediction of carbon nanotube growth success by the analysis of carbon–catalyst binary phase diagrams. *Carbon* **2006,** 44, 267-275.

59. Raty, J.-Y.; Gygi, F.; Galli, G., Growth of Carbon Nanotubes on Metal Nanoparticles: A Microscopic Mechanism from Ab Initio Molecular Dynamics Simulations. *Phys. Rev. Lett.* **2005,** 95, 096103.

60. Ago, H.; Ohshima, S.; Uchida, K.; Yumura, M., Gas-phase synthesis of single-wall carbon nanotubes from colloidal solution of metal nanoparticles. *J. Phys. Chem. B* **2001,** 105, 10453-10456.

61. Zhang, G.; Mann, D.; Zhang, L.; Javey, A.; Li, Y.; Yenilmez, E.; Wang, Q.; McVittie, J. P.; Nishi, Y.; Gibbons, J.; Dai, H., Ultra-high-yield growth of vertical single-walled carbon nanotubes: hidden roles of hydrogen and oxygen. *Proc. Nat. Acad. Sci. USA,* **2005,** 102, 16141-16145.

62. Resasco, D. E.; Alvarez, W. E.; Pompeo, F.; Balzano, L.; Herrera, J. E.; Kitiyanan, B.; Borgna, A., A scalable process for production of single-walled carbon nanotubes (SWNTs) by catalytic disproportionation of CO on a solid catalyst. *J. Nanopart. Res.* **2002,** 4, 131-136.

63. Nikolaev, P.; Bronikowski, M. J.; Bradley, R. K.; Rohmund, F.; Colbert, D. T.; Smith, K. A.; Smalley, R. E., Gas-phase catalytic growth of single-walled carbon nanotubes from carbon monoxide. *Chem. Phys. Lett.* **1999,** 313, 91-97.

64. Zheng, L. X.; O'Connell, M. J.; Doorn, S. K.; Liao, X. Z.; Zhao, Y. H.; Akhadov, E. A.; Hoffbauer, M. A.; Roop, B. J.; Jia, Q. X.; Dye, R. C.; Peterson, D. E.; Huang, S. M.; Liu, J.; Zhu, Y. T., Ultralong single-wall carbon nanotubes. *Nat. Mater.* **2004,** 3, 673-676.

65. Haddon, R. C.; Sippel, J.; Rinzler, A. G.; Papadimitrakopoulos, A., Purification and separation of carbon nanotubes. *MRS Bull.* **2004,** 29, 252-259.

66. Hou, P.-X.; Liu, C.; Cheng, H.-M., Purification of cabon nanotubes. *Carbon* **2008,** 46, (2003-2025).

67. Park, T.-J.; Banerjee, S.; Benny, T. H.; Wong, S. S., Purification strategies and purity visualization techniques for single-walled carbon nanotubes. *J. Mater. Chem.* **2006,** 16, 141-154.

68. Shi, Z.; Lian, Y.; Liao, F.; Zhou, X.; Gu, Z.; Zhang, Y.; Iijima, S., Purification of single-wall carbon nanotubes. *Sold State Commun.* **1999,** 112, 35-37.

69. Nagasawa, S.; Yudasaka, M.; Hirahara, K.; Ichihashi, T.; Iijima, S., Effect of oxidation on single-wall carbon nanotubes. *Chem. Phys. Lett.* **2000,** 328, 374-380.

70. Zimmerman, J. L.; Bradley, R. K.; Huffman, C. B.; Hauge, R. H.; Margrave, J. L., Gas-phase purification of single wall carbon nanotubes. *Chem. Mater.* **2000,** 12, 1361-1366.

71. Vivekchand, S. R. C.; Govindaraj, A.; Seikh, M. M.; Rao, C. N. R., New Method of Purification of Carbon Nanotubes Based on Hydrogen Treatment. *J. Phys. Chem. B* **2004,** 108, 6935-6937.

72. Liu, J.; Rinzler, A. G.; Dai, H.; Hafner, J. H.; Bradley, R. K.; Boul, P. J.; Lu, A.; Iverson, T.; Shelimov, K.; Huffman, C. B.; Rodriguez-Macias, F.; Shon, Y.-S.; Lee, T. R.; Colbert, D. T.; Smalley, R. E., Fullerene Pipes. *Science* **1998,** 280, 1253-1256.

73. Rinzler, A. G.; Liu, J.; Dai, H.; Nikolaev, P.; Huffman, C. B.; Rodriguez-Macias, F. J.; Boul, P. J.; Lu, A. H.; Heymann, D.; Colbert, D. T.; Lee, R. S.; Fischer, J. E.; Rao, A. M.; Eklund, P. C.; Smalley, R. E., Large-scale purification of single-wall carbon nanotubes: process, product, and characterization. *Appl. Phys. A* **1998,** 67, 29-37.

74. Ebbesen, T. W.; Ajayan, P. M.; Hiura, H.; Tanigaki, K., Purification of nanotubes. *Nature* **1994,** 367, 519.

75. Hu, H.; Zhao, B.; Itkis, M. E.; Haddon, R. C., Nitric Acid Purification of Single-Walled Carbon Nanotubes. *J. Phys. Chem. B* **2003,** 107, 13838-13842.

76. Kajiura, H.; Tsutsui, S.; Huang, H.; Murakami, Y., High-quality single-walled carbon nanotubes from arc-produced soot. *Chem. Phys. Lett.* **2002,** 364, 586-592.

77. Tsang, S. C.; Chen, Y. K.; Harris, P. J. F.; Green, M. L. H., A simple chemical method of opening and filling carbon nanotubes. *Nature* **1994,** 372, 159-162.

78. Dujardin, E.; Ebbesen, T. W.; Krishnan, A.; J., T. M. M., Purification of Single-Shell Nanotubes. *Adv. Mater.* **1999,** 10, 611-613.

79. Hiura, H.; Ebbesen, T. W.; Tanigaki, K., Opening and Purification of Carbon Nanotubes in High Yields. *Adv. Mater.* **1995,** 7, 275-276.

80. Chen, J.; Hamon, M. A.; Hu, H.; Chen, Y.; Rao, A. M.; Eklund, P. C.; Haddon, R. C., Solution properties of single-walled carbon nanotubes. *Science* **1998,** 282, 95-98.

81. Riggs, J. E.; Guo, Z. X.; Carroll, D. L.; Sun, Y. P., Strong luminescence of solubilized carbon nanotubes. *J. Am. Chem. Soc.* **2000,** 122, 5879-5880.

82. Chen, Y.; Haddon, R. C.; Fang, S.; Rao, A. M.; Eklund, P. C.; Lee, W. H.; Dickey, E. C.; Grulke, E. A.; Pendergrass, J. C.; Chavan, A.; Haley, B. E.; Smalley, R. E., Chemical attachment of organic functional groups to single-walled carbon nanotube material. *J. Mater. Res.* **1998,** 13, 2423-2431.

83. Holzinger, M.; Abraham, J.; Whelan, P.; Graupner, R.; Ley, L.; Hennrich, F.; M., K.; Hirsch, A., Functionalization of single-walled carbon nanotubes with (R-)oxycarbonyl nitrenes. *J. Am. Chem. Soc.* **2003,** 125, 8556-8580.

84. Georgakilas, V.; Voulgaris, D.; Vazquez, E.; Prato, M.; Guldi, D. M.; Kukovecz, A.; Kuzmany, H., Purification of HiPco carbon nanotubes via organic functionalization. *J. Am. Chem. Soc.* **2004,** 124, 14318-14319.

85. Banerjee, S.; Wong, S. S., Rational sidewall functionalization and purification of single-walled carbon nanotubes by solution-phase ozonolysis. *J. Phys. Chem. B* **2002,** 106, 12144.

86. Umek, P.; Seo, J. W.; Hernadi, H.; Mrzel, A.; Pechy, P.; Mihailovic, D. D.; Forró, L., Addition of carbon radicals generated from organic peroxides to single wall carbon nanotubes. *Chem. Mater.* **2003,** 15, 4751-4755.

87.Benny, T.-H.; Wong, S. S., Silylation of single-walled carbon nanotubes. *Chem. Mater.* **2006,** 18, 4827.

88.Mickelson, E. T.; Chiang, I. W.; Zimmerman, J. L., Solvation of fluorinated single-wall carbon nanotubes in alcohol solvents. *J. Phys. Chem. B* **1999,** 103, 4318.

89.Bahr, J. L.; Yang, J. P.; Kosynkin, D. V., Functionalization of carbon nanotubes by electrochemical reduction of aryl diazonium salts: a bucky paper electrode. *J. Am. Chem. Soc.* **2001,** 123, 6536.

90.Kooi, S. E.; Schlecht, U.; Burghard, M., Electrochemical modification of single carbon nanotubes. *Angew. Chem. Int. Ed.* **2002,** 41, 1353.

91.Viswanathan, G.; Chakrapani, N.; Yang, H., Single-step in situ synthesis of polymer-grafted single-wall nanotube composites. *J. Am. Chem. Soc.* **2003,** 125, 9258.

92.Blake, R.; Gun'ko, Y. K.; Coleman, J. N., A generic organometallic approach toward ultra-strong carbon nanotube polymer composites. *J. Am. Chem. Soc.* **2004,** 126, 10226.

93.Richard, C.; Balavoine, F.; Schultz, P.; Ebbesen, T. W.; Mioskowski, C., Supramolecular Self-Assembly of Lipid Derivatives on Carbon Nanotubes. *Science* **2003,** 300, 775-778.

94.Islam, M. F.; Rojas, E.; Bergey, D. M.; Johnson, A. T.; Yodh, A. G., High weight fraction surfactant solubilization of single-wall carbon nanotubes in water. *Nano Lett.* **2003,** 3, 269-273.

95.Kang, M.; Myung, S. J.; Jin, H.-J., Nylon 610 and carbon nanotube composite by in situ interfacial polymerization. *Polymer* **2006,** 47, 3961-3966.

96.Odom, T. W.; Huang, J.-L.; Lieber, C. M., STM studies of single-walled carbon nanotubes. *J. Phys.: Condens. Matter* **2002,** 14, R145-R167.

97.Dresselhaus, M. S.; Dresselhaus, G.; Saito, R., Physics of carbon nanotubes. *Carbon* **1995,** 33, 883-891.

98.Dekker, C.; Tans, S. J.; Devoret, M. H.; Geerlings, R. J.; Groeneveld, R. J. A.; Venema, J. W.; Wildöer, J. W. G.; Verschueren, A. R. M.; Bezryadin, A.; Thess, A.; Dai, H.; Smalley, R. E., *Molecular Nanostructures*. Springer-Verlag: New York, 1997.

99.Wallace, P. R., The band theory of graphite. *Phys. Rev.* **1947,** 71, 622.

100.Slonczewski, J. C.; Weiss, P. R., Band structure of graphite. *Phys. Rev.* **1958,** 109, 272.

101.McClure, J. C., Band structure of graphite and de Haas–van Alphen effect. *Phys. Rev.* **1957,** 108, 612.

102.Saito, R.; Dresselhaus, G.; Dresselhaus, M. S., *Physical properties of carbon nanotubes*. Imperial College Press: London, 1998.

103.Wildoer, J. W. G.; Venema, L. C.; Rinzler, A. G.; Smalley, R. E.; Dekker, C., Electronic structure of atomically resolved carbon nanotubes. *Nature* **1998,** 391, 59-62.

104.Saito, R.; Fujita, M.; Dresselhaus, G.; Dresselhaus, M. S., Electronic structure of chiral graphene tubules. *Appl. Phys. Lett.* **1992,** 60, 2204.

105.Berber, S.; Kwon, Y.-K.; Tománek, D., Unusually High Thermal Conductivity of Carbon Nanotubes. *Phys. Rev. Lett.* **2000,** 84, 4613-4616.

106. Kataura, H.; Kumazawa, Y.; Maniwa, Y.; Umezu, I.; Suzuki, S.; Ohtsuka, Y.; Achiba, Y., Optical Properties of Single-Wall Carbon Nanotubes. *Synth. Met.* **1999,** 103, 2555-2558.

107. Arnold, M. S.; Green, A. A.; Hulvat, J. F.; Stupp, S. I.; Hersam, M. C., Sorting carbon nanotubes by electronic structure using density differentiation. *Nat. Nanotechnol.* **2006,** 1, 60-65.

108. O'Connell, M. J.; Bachilo, S. M.; Huffman, C. B., Band gap fluorescence from individual single-walled carbon nanotubes. *Science* **2002,** 297, 593.

109. Bachilo, S. M.; Strano, M. S.; Kittrell, C., Structure-assigned optical spectra of single walled carbon nanotubes. *Science* **2002,** 298, 2361.

110. Belin, T.; Epron, F., Characterization methods of carbon nanotubes: a review. *Mater. Sci. Eng. B* **2005,** 119, 105.

111. Kuzmany, H.; Plank, W.; Hulman, M.; Kramberger, C.; Grüneis, A.; Pichler, T.; Peterlik, H.; Kataura, H.; Achiba, Y., Determination of SWCNT diameters from the Raman response of the radial breathing mode. *Eur. Phys. J. B* **2001,** 22, 307{320.

112. Jishi, R. A.; Venkataraman, L.; Dresselhaus, M. S., Phonon modes in carbon nanotubules. *Chem. Phys. Lett.* **1993,** 209, 77.

113. Jorio, A.; Saito, R.; Dresselhaus, G.; Dresselhaus, M. S., Determination of nanotubes properties by Raman spectroscopy. *Phil. Trans. Roy. Soc. A* **2004,** 362, 2311-2336.

114. Rao, A. M.; Richter, E.; Bandow, S.; Chase, B.; Eklund, P. C.; Williams, K. A.; Fang, S.; Subbaswamy, K. R.; Menon, M.; Thess, A.; Smalley, R. E.; Dresselhaus, G.; Dresselhaus, M. S., Diameter-Selective Raman Scattering from Vibrational Modes in Carbon Nanotubes. *Science* **1997,** 275, 187-191.

115. Dresselhaus, M. S.; Dresselhaus, G.; Saito, R.; Jorio, A., Raman spectroscopy of carbon nanotubes. *Physics Reports* **2005,** 409, 47-99.

116. Wu, Z.; Chen, Z.; Du, X.; Logan, J. M.; Sippel, J.; Nikolou, M.; Kamaras, K.; Reynolds, J. R.; Tanner, D. B.; Hebard, A. F.; Rinzler, A. G., Transparent, Conductive Carbon Nanotube Films. *Science* **2004,** 305, 1273-1276.

117. Sun, J. P.; Zhang, Z. X.; Hou, S. M.; Gu, Z. N.; Zhao, X. Y.; Liu, W. M.; Xue, Z. Q., Work function of single-walled carbon nanotubes determined by field emission microscopy. *Appl. Phys. A: Mater. Sci. Process* **2004,** 75, 479-483.

118. Chen, Y.; Cotterell, B.; Wang, W., The fracture of brittle thin films on compliant substrates in flexible displays. *Eng. Fract. Mech.* **2002,** 69, 597-603.

119. Hu, L.; Hecht, D. S.; Grüner, G., Percolation in Transparent and Conducting Carbon Nanotube Networks. *Nano Lett.* **2004,** 4, 2513–2517.

120. Fuhrer, M. S.; Nygard, J.; Shih, L.; Forero, M.; Yoon, Y.; Mazzoni, M. S. C.; Choi, H. J.; Ihm, J.; Louie, S.; Zettl, A.; McEuen, P. L., Crossed nanotube junctions. *Science* **2000,** 288, 494-497.

121. Lebovka, N. I.; Manna, S. S.; Tarafdar, S.; Teslenko, N., Percolation in Models of Thin Film Depositions. *Phys. Rev. E* **2002,** 66, 066134.

122. Unalan, H. E.; Hiralal, P.; Kuo, D.; Parekh, B.; Amaratunga, G.; Chhowalla, M., Flexible organic photovoltaics from zinc oxide nanowires grown on transparent and conducting single walled carbon nanotube thin films. *J. Mater. Chem.* **2008,** 18, 5909-5912.

123. Stauffer, G., *Introduction to Percolation Theory*. Taylor & Francis: London, 1985.

124. Pike, G. E.; Seager, C. H., Percolation and conductivity: A computer study. I. *Phys. Rev. B* **1974,** 10, 1421-1434.

125. Durkop, T.; Getty, S. A.; Cobas, E.; Fuhrer, M. S., Extraordinary mobility in semiconducting carbon nanotubes. *Nano Lett.* **2004,** 4, 55-59.

126. Javey, A.; Guo, J.; Wang, Q.; Lundstrom, M.; Dai, H. J., Ballistic carbon nanotube field-effect transistors. *Nature* **2003,** 424, 654-657.

127. Li, S.; Yu, Z.; Rutherglen, C.; Burke, P. J., Electrical properties of 0.4 cm long single-walled carbon nanotubes. *Nano Lett.* **2004,** 4, 2003-2007.

128. Li, S.; Yu, Z.; Yen, S. F.; Tang, W. C.; Burke, P. J., Carbon nanotube transistor operation at 2.6 GHz. *Nano Lett.* **2004,** 4, 753-756.

129. Wharam, D. A.; Thornton, T. J.; Newbury, R.; Pepper, M.; Ahmed, H.; Frost, J. E. F.; Hasko, D. G.; Peacock, D. C.; Ritchie, D. A.; Jones, G. A. C., One-dimensional transport and the quantization of the ballistic resistance. *J Phys. C: Solid State Phys.* **1988,** 21, L209-L214.

130. Hecht, D. S.; Hu, L.; Grüner, G., Conductivity scaling with bundle length and diameter in single walled carbon nanotube networks. *Appl. Phys. Lett.* **2006,** 89, 13312.

131. Kaempgen, M.; Duesberg, G. S., Transparent carbon nanotube coatings. *Appl. Surf. Sci.* **2005,** 252, 425-429.

132. Bekyarova, E.; Itkis, M. E.; Cabrera, N.; Zhao, B.; Yu, A.; Gao, J.; Haddon, R. C., Electronic properties of single-walled carbon nanotube networks. *J. Am. Chem. Soc.* **2004,** 127, 5990-5995.

133. Hone, J.; Llaguno, C.; Nemes, N. M.; Johnson, A. T.; Fischer, J. E.; Walters, D. A.; Casavant, M. J.; Schmidt, J.; Smalley, R. E., Electrical and thermal transport properties of magnetically aligned single wall carbon nanotube films. *Appl. Phys. Lett.* **2000,** 77, 666-668.

134. Kaiser, A. B.; Dusberg, G.; Roth, S., Heterogeneous model for conduction in carbon nanotubes. *Phys. Rev. B* **1998,** 57, 1418-1421.

135. Banerjee, S.; Hemraj-Benny, T.; Wong, S. S., Covalent surface chemistry of single-walled carbon nanotubes. *Adv. Mater.* **2005,** 17, 17-29.

136. Jhi, S. H.; Louie, S. G.; Cohen, M. L., Electronic Properties of Oxidized Carbon Nanotubes. *Phys. Rev. Lett.* **2000,** 85, 1710-1713.

137. Zhao, J. J.; Xie, R. H. J., Electronic and photonic properties of doped carbon nanotubes. *J. Nanosci. Nanotech.* **2003,** 3, 459-478.

138. Jackson, R.; Domercq, B.; Jain, R.; Kippelen, B.; Graham, S., Stability of Doped Transparent Carbon Nanotube Electrodes. *Adv. Funct. Mater.* **2008,** 18, 2548-2554.

139. Jackson, R. K.; Munro, A.; Nebesny, K.; Armstrong, N.; Graham, S., Evaluation of Transparent Carbon Nanotube Networks of Homogeneous Electronic Type. *ACS Nano* **2010,** 4, 1377-1384.

140. Hecht, D. S.; Hu, L.; Grüner, G., Electronic properties of carbon nanotube/fabric composites. *Curr. Appl. Phys.* **2007,** 7, 60-63.

141. Meitl, M.; Zhou, Y.; Gaur, A.; Jeon, S.; Usrey, M. L.; Strano, M. S.; Rogers, J. A., Solution casting and transfer printing single-walled carbon nanotube films. *Nano Lett.* **2004,** 4, 1643-1647.

142. Zhou, Y.; Hu, L.; Grüner, G., A method of printing carbon nanotube thin films. *Appl. Phys. Lett.* **2006,** 88, 123109.

143. Ruzicka, B.; Degiorgi, L.; Gaal, R.; Thien, L.; Bacsa, R.; Salvetat, J. P.; Forro, L., Optical and dc conductivity study of potassium-doped single-walled carbon nanotube films. *Phys. Rev. B* **2000,** 61, R2469.

144. Dressel, M.; Grüner, G., *Electrodynamics of Solids: Optical Properties of Electrons in Matter*. Cambridge University Press: Cambridge, 2002.

145. Blackburn, J. L.; Barnes, T. M.; Beard, M. C.; Kim, Y.-H.; Tenent, R. C.; McDonald, T. J.; To, B.; Coutts, T. J.; Heben, M. J., Transparent Conductive Single-Walled Carbon Nanotube Networks with Precisely Tunable Ratios of Semiconducting and Metallic Nanotubes. *ACS Nano* **2008,** 2, 1266-1274.

146. Geng, H.-Z.; Kim, K. K.; So, K. P.; Lee, Y. S.; Chang, Y.; Lee, Y. H., Effect of acid treatment on carbon nanotube based flexible transparent conducting films. *J. Am. Chem. Soc.* **2007,** 129, 7758-7759.

147. Geng, H.-Z.; Kim, K. K.; Lee, K.; Kim, G. L.; Choi, H. K.; Lee, D. S.; An, K. H.; Lee, Y. H., Dependence of material quality on performance of flexible transparent conducting films with single-walled carbon nanotubes. *NANO: Brief Rep. Rev.* **2007,** 2, 157-167.

148. Ma, W.; Song, L.; Yang, R.; Zhang, T.; Zhao, Y.; Sun, L.; Ren, Y.; Liu, D.; Liu, L.; Shen, J.; Zhang, Z.; Xiang, Y.; Zhou, W.; Xie, S., Directly Synthesized Strong, Highly Conducting, Transparent Single-Walled Carbon Nanotube Films. *Nano Lett.* **2007,** 7, 2307-2311.

149. Znidarsic, A.; Kaskela, A.; Laiho, P.; Gaberscek, M.; Ohno, Y.; Nasibulin, A. G.; Kauppinen, E. I.; Hassanien, A., Spatially Resolved Transport Properties of Pristine and Doped Single-Walled Carbon Nanotube Networks. *J. Phys. Chem. C* **2013,** 117, 13324-13330.

150. Niu, Z.; Zhou, W.; Chen, J.; Feng, G.; Li, H.; Hu, Y.; Ma, W.; Dong, H.; Li, J.; Xie, S., A Repeated Halving Approach to Fabricate Ultrathin Single-Walled Carbon Nanotube Films for Transparent Supercapacitors. *Small* **2013,** 9, 518-524.

151. Li, Z.; Jia, Y.; Wei, J.; Wang, K.; Shu, Q.; Gui, X.; Zhu, H.; Cao, A.; Wu, D., Large area, highly transparent carbon nanotube spiderwebs for energy harvesting. *J. Mater. Chem.* **2012,** 20, 7236-7240.

152. Kishi, N.; Miwa, I.; Okazaki, T.; Saito, T.; Mizutani, T.; Tsuchiya, H.; Soga, T.; Jimbo, T., Transparent conductive thin films of single-wall carbon nanotubes encapsulating dopant molecules. *Appl. Phys. Lett.* **2012,** 100, 063121.

153. Lu, F.; Wang, W.; Fernando, K. A. S.; Meziani, M. J.; Myers, E.; Sun, Y.-P., Metallic single-walled carbon nanotubes for transparent conductive films. *Chem. Phys. Lett.* **2010,** 497, 57-61.

154. Han, J. T.; Kim, B. G.; Yang, M.; Kim, J. S.; Jeong, H. J.; Jeong, S. Y.; Hong, S.-H.; Lee, G.-W., Titania-Assisted Dispersion of Carboxylated Single-Walled Carbon Nanotubes in a ZnO Sol for Transparent Conducting Hybrid Films. *ACS Appl. Mater. Interfaces* **2011,** 3, 2671–2676.

155. Mustonen, T.; Kordás, K.; Saukko, S.; Tóth, G.; Penttilä, J. S.; Helistö, P.; Seppä, H.; Jantunen, H., Inkjet printing of transparent and conductive patterns of single-walled carbon nanotubes and PEDOT-PSS composites. *Phys. Stat. Sol. (B)* **2007,** 244, 4336 - 4340.

156. Nakashima, T.; Zhu, J.; Qin, M.; Hoa, S.; Kotov, N. A., Polyelectrolyte and carbon nanotube multilayers made from ionic liquid solutions. *Nanoscale* **2010,** 2, 2084 - 2090.

157. Sangeeth, C. S. S.; Jaiswal, M.; Menon, R., Charge transport in transparent conductors: A comparison. *J. Appl. Phys.* **2009,** 105, 063713.

158. Sorel, S.; Khan, U.; Coleman, J. N., Flexible, transparent dielectric capacitors with nanostructured electrodes. *Appl. Phys. Lett.* **2012,** 101, 103106.

159. Zhang, B.; Li, F.; Lin, Z.; Wu, C.; Guo, T.; Liu, W.; Su, Y.; Du, J., Flexible White Organic Light-Emitting Diodes Based on Single-Walled Carbon Nanotube:Poly(3,4-ethylenedioxythiophene)/Poly(styrene sulfonate) Transparent Conducting Film. *Jap. J. Appl. Phys.* **2012,** 51, 070204.

160. Saha, A.; Ghosh, S.; Weisman, R. B.; Marti, A. A., Films of Bare Single-Walled Carbon Nanotubes from Superacids with Tailored Electronic and Photoluminescence Properties. *ACS Nano* **2012,** 6, 5727 - 5734.

161. Moisala, A.; Nasibulin, A. G.; Brown, D. P.; Jiang, H.; Khriachtchev, L.; Kauppinen, E. I., Single-walled carbon nanotube synthesis using ferrocene and iron pentacarbonyl in a laminar flowreactor. *Chem. Engg. Sci.* **2006,** 61, 4393 - 4402.

162. Nasibulin, A. G.; Kaskela, A.; Mustonen, K.; Anisimov, A. S.; Ruiz, V.; Kivistö, S.; Rackauskas, S.; Timmermans, M. Y.; Pudas, M.; Aitchison, B.; Kauppinen, M.; Brown, D. P.; Okhotnikov, O. G.; Kauppinen, E. I., Multifunctional Free-Standing Single-Walled Carbon Nanotube Films. *ACS Nano* **2011,** 5, 3214 - 3221.

163. Kaskela, A.; Nasibulin, A. G.; Timmermans, M. Y.; Aitchison, B.; Papadimitratos, A.; Tian, Y.; Zhu, Z.; Jiang, H.; Brown, D. P.; Zakhidov, A.; Kauppinen, E. I., Aerosol-Synthesized SWCNT Networks with Tunable Conductivity and Transparency by a Dry Transfer Technique. *Nano Lett.* **2010,** 10, 4349 - 4355.

164. de Andrade, M. J.; Lima, M. D.; Skákalová, V.; Bergmann, C. P.; Roth, S., Electrical properties of transparent carbon nanotube networks prepared through different techniques. *Phys. Stat. Sol. (RRL)* **2007,** 1, 178 - 180.

165. Manivannan, S.; Ryu, J. H.; Jang, J.; Park, K. C., Fabrication and effect of post treatment on flexible single-walled carbon nanotube films. *J. Mater Sci: Mater. Electron.* **2010,** 21, 595-602.

166. Shin, D.-W.; Lee, J. H.; Kim, Y.-H.; Yu, S. M.; Park, S.-Y.; Yoo, J.-B., A Role of HNO$_3$ on transparent conducting film with single-walled carbon nanotubes. *Nanotechnol.* **2009,** 20, 475703.

167. Song, Y. I.; Yang, C. M.; Kim, D. Y.; Kanoh, H.; Kaneko, K., Flexible transparent conducting single-wall carbon nanotube film with network bridging method. *J. Coll. Interf. Sci.* **2008,** 318, 365-371.

168. Yang, S. B.; Kong, B.-S.; Kim, D.-W.; Baek, Y.-K.; Jung, H.-T., Effect of Au Doping and Defects on the Conductivity of Single-Walled Carbon Nanotube Transparent Conducting Network Films. *J. Phys. Chem. C* **2010,** 114, 9296-9300.

169. Aitola, K.; Kaskela, A.; Halme, J.; Ruiz, V.; Nasibulin, A. G.; Kauppinen, E. I.; Lunda, P. D., Single-Walled Carbon Nanotube Thin-Film Counter Electrodes for Indium Tin Oxide-Free Plastic Dye Solar Cells. *J. Electrochem. Soc.* **2010,** 157, B1831-B1837.

170. Jung, H.; Quy, N. V.; Hoa, N. C.; Kim, D., Transparent Field Emission Device from a Spray Coating of Single-Wall Carbon Nanotubes. *J. Electrochem. Soc.* **2010,** 157, J371-J375.

171. Tung, V. C.; Chen, L.-M.; Allen, M. J.; Wassei, J. K.; Nelson, K.; Kaner, R. B.; Yang, Y., Low-Temperature Solution Processing of Graphene-Carbon Nanotube Hybrid Materials for High-Performance Transparent Conductors. *Nano Lett.* **2009,** 9, 1949-1955.

172. Wassei, J. K.; Cha, K. C.; Tung, V. C.; Yang, Y.; Kaner, R. B., The effects of thionyl chloride on the properties of graphene and graphene–carbon nanotube composites. *J. Mater. Chem.* **2011,** 21, 3391-3396.

173. Xie, J.; Wang, H.; Bai, H.; Yang, P.; Shi, M.; Guo, P.; Wang, C.; Yang, W.; Song, H., Wormlike Micelle Assisted Rod Coating: A General Method for Facile Fabrication of Large-Area Conductive Nanomaterial Thin Layer onto Flexible Plastics. *ACS Appl. Mater. Interfaces* **2012,** 4, 2891-2896.

174. Kim, S. M.; Jo, Y. W.; Kim, K. K.; Duong, D. L.; Shin, H.-J.; Han, J. H.; Choi, J.-Y.; Kong, J.; Lee, Y. H., Transparent Organic P-Dopant in Carbon Nanotubes: Bis(trifluoromethanesulfonyl)imide. *ACS Nano* **2012,** 4, 6998-7004.

175. Hu, L.; Li, J.; Liu, J.; Grüner, G.; Marks, T., Flexible organic light-emitting diodes with transparent carbon nanotube electrodes: problems and solutions. *Nanotechnol.* **2010,** 21, 155202.

176. Jo, S.-H.; Lee, Y.-K.; Yang, J.-W.; Jung, W.-G.; Kim, J.-Y., Carbon nanotube-based flexible transparent electrode films hybridized with self-assembling PEDOT. *Synth. Met.* **2012,** 162, 1279-1284.

177. Lee, B. R.; Kim, J. S.; Nam, Y. S.; Jeong, H. J.; Jeong, S. Y.; Lee, G.-W.; Han, J. T.; Song, M. H., Highly efficient polymer light-emitting diodes using graphene oxide-modified flexible single-walled carbon nanotube electrodes. *J. Mater. Chem.* **2012,** 22, 21481 - 21486.

178. Shi, Z.; Chen, X.; Wang, X.; Zhang, T.; Jin, J., Fabrication of Superstrong Ultrathin Free-Standing Single-Walled Carbon Nanotube Films via a Wet Process. *Adv. Funct. Mater.* **2011,** 21, 4358 - 4363.

179. Tantang, H.; Xiao, J.; Wei, J.; C-Park, M. B. E.; Li, L.-J.; Zhang, Q., Low-Cost and Ultra-Strong p-Type Doping of Carbon Nanotube Films by a Piranha Mixture. *Eur. J. Inorg. Chem.* **2011,** 2011, (27), 4182–4186.

180. Yang, S. B.; Kong, B.-S.; Jung, H.-T., Multistep Deposition of Gold Nanoparticles on Single-Walled Carbon Nanotubes for High-Performance Transparent Conducting Films. *J. Phys. Chem. C* **2012,** 116, 15581 - 15587.

181. Chandra, B.; Afzali, A.; Khare, N.; El-Ashry, M. M.; Tulevski, G. S., Stable Charge-Transfer Doping of Transparent Single-Walled Carbon Nanotube Films. *Chem. Mater.* **2010,** 22, 5179 - 5183.

182. Dan, D.; Irvin, G. C.; Pasquali, M., Continuous and Scalable Fabrication of Transparent Conducting Carbon Nanotube Films. *ACS Nano* **2009,** 3, 835 – 843.

183. Geng, H.-Z.; Lee, D. S.; Kim, K. K.; Han, G. H.; Park, H. K.; Lee, Y. H., Absorption spectroscopy of surfactant-dispersed carbon nanotube film: Modulation of electronic structures. *Chem. Phys. Lett.* **2008,** 455, 275 - 278.

184. Geng, H.-Z.; Kim, K. K.; Song, C.; Xuyen, N. T.; Kim, S. M.; Park, K. A.; Lee, D. S.; An, K. H.; Lee, Y. S.; Chang, Y.; Lee, Y. J.; Choi, J. Y.; Benayad, A.; Lee, Y. H., Doping and de-doping of carbon nanotube transparent conducting films by dispersant and chemical treatment. *J. Mater. Chem.* **2008,** 18, 1261–1266.

185. Han, J. T.; Kim, J. S.; Jeong, H. D.; Jeong, H. J.; Jeong, S. Y.; Lee, G.-W., Modulating Conductivity, Environmental Stability of Transparent Conducting Nanotube Films on Flexible Substrates by Interfacial Engineering. *ACS Nano* **2010,** 4, 4551-4558.

186. Kim, K. K.; Yoon, S.-M.; Park, H. K.; Shin, H.-J.; Kim, S. M.; Bae, J. J.; Cui, Y.; Kim, J. M.; Choi, J.-Y.; Lee, Y. H., Doping strategy of carbon nanotubes with redox chemistry. *New J. Chem.* **2010,** 34, 2183-2188.

187. Shin, J. H.; Shin, D. W.; Patole, S. P.; Lee, J. H.; Park, S. M.; Yoo, J. B., Smooth, transparent, conducting and flexible SWCNT films by filtration–wet transfer processes. *J. Phys. D: Appl. Phys.* **2009,** 42, 045305.

188. Southard, A.; Sangwan, V.; Cheng, J.; Williams, E. D.; Fuhrer, M. S., Solution-processed single walled carbon nanotube electrodes for organic thin-film transistors. *Org. Electron.* **2009,** 10, 1556-1561.

189. Unalan, H. E.; Fanchini, G.; Kanwal, A.; Du Pasquier, A.; Chhowalla, M., Design Criteria for Transparent Single-Wall Carbon Nanotube Thin-Film Transistors. *Nano Lett.* **2006,** 6, 677-682.

190. Wang, Y.; Di, C.-a.; Liu, Y.; Kajiura, H.; Ye, S.; Cao, L.; Wei, D.; Zhang, H.; Li, Y.; Noda, K., Optimizing Single-Walled Carbon Nanotube Films for Applications in Electroluminescent Devices. *Adv. Mater.* **2008,** 20, 4442-4449.

191. Wang, Y.; Huang, L.; Liu, Y.; Weil, D.; Zhang, H.; Kajiura, H.; Li, Y., Minimizing Purifi cation-Induced Defects in Single-Walled Carbon Nanotubes Gives Films with Improved Conductivity. *Nano Res.* **2009,** 2, 865-871.

192. Zhang, J.; Gao, L.; Sun, J.; Liu, Y.; Wang, Y.; Wang, J.; Kajiura, H.; Li, Y.; Noda, K., Dispersion of Single-Walled Carbon Nanotubes by Nafion in Water/Ethanol for Preparing Transparent Conducting Films. *J. Phys. Chem. C* **2008,** 112, 16370-16376.

193. Chien, Y.-M.; Lefevre, F.; Shih, I.; Izquierdo, R., A solution processed top emission OLED with transparent carbon nanotube electrodes. *Nanotechnol.* **2010,** 21, 134020.

194. Doherty, E. M.; De, S.; Lyons, P. E.; Shmeliov, A.; Nirmalraj, P. N.; Scardaci, V.; Joimel, J.; Blau, W. J.; Boland, J. J.; Coleman, J. N., The spatial uniformity and electromechanical stability of transparent, conductive films of single walled nanotubes. *Carbon* **2009,** 47, 2466-2473.

195. Green, A. A.; Hersam, M. C., Colored Semitransparent Conductive Coatings Consisting of Monodisperse Metallic Single-Walled Carbon

Nanotubes. *Nano Lett.* **2008,** 8, 1417-1422.

196. Han, J. T.; Kim, J. S.; Jo, S. B.; Kim, S. H.; Kim, J. S.; Kang, B.; Jeong, H. J.; Jeong, S. Y.; Lee, G.-W.; Cho, K., Graphene oxide as a multi-functional p-dopant of transparent single-walled carbon nanotube films for optoelectronic devices. *Nanoscale* **2012,** 4, 7735–7742.

197. Hecht, D. S.; Heintz, A. M.; Lee, R.; Hu, L.; Moore, B.; Cucksey, C.; Risser, S., High conductivity transparent carbon nanotube films deposited from superacid. *Nanotechnol.* **2011,** 22, 075201.

198. Hu, L.; Gruner, G.; Gong, J.; Kim, C.-J.; Hornbostel, B., Electrowetting devices with transparent single-walled carbon nanotube electrodes. *Appl. Phys. Lett.* **2007,** 90, 093124.

199. Jo, J. W.; Jung, J. W.; Lee, J. U.; Jo, W. H., Fabrication of highly conductive and transparent thin films from single-walled carbon nanotubes using a new non-ionic surfactant via spin coating. *ACS Nano* **2010,** 4, 582-5388.

200. Park, Y. T.; Ham, A. Y.; Yang, Y.-H.; Grunlan, J. C., Fully organic ITO replacement through acid doping of double-walled carbon nanotube thin film assemblies. *RSC Adv.* **2011,** 1, 662-671.

201. Paul, S.; Kim, D.-W., Preparation and characterization of highly conductive transparent films with single-walled carbon nanotubes for flexible display applications. *Carbon* **2009,** 47, 2436-2441.

202. De, S.; Lyons, P. E.; Sorel, S.; Doherty, E. M.; King, P. J.; Blau, W. J.; Nirmalraj, P. N.; Boland, J. J.; Scardaci, V.; Joimel, J.; Coleman, J. N., Transparent, Flexible, and Highly Conductive Thin Films Based on Polymer Nanotube Composites. *ACS Nano* **2009,** 3, 714-720.

203. Woo, J. Y.; Kim, D.; Kim, J.; Park, J.; Han, C.-S., Fast and Efficient Purification for Highly Conductive Transparent Carbon Nanotube Films. *J. Phys. Chem. C* **2010,** 114, 19169-19174.

204. Kim, Y.; Chikamatsu, M.; Azumi, R.; Saito, T.; Minami, N., Industrially Feasible Approach to Transparent, Flexible, and Conductive Carbon Nanotube Films: Cellulose-Assisted Film Deposition Followed by Solution and Photonic Processing. *Appl. Phys. Exp.* **2013,** 6, 025101.

205.Chen, L.-T.; Geng, H.-Z.; Wang, W.-Y.; Gao, J.; Cui, L.-J.; Hu, L., Purification and Dispersion of Single-walled Carbon Nanotubes for Transparent Conducting Films. *Integrated Ferroelectrics* **2013,** 145, 80-87.

206.Gao, J.; Wang, W.-I.; Chen, L.-T.; Cui, L.-J.; Hu, X.-Y.; Geng, H.-Z., Optimizing processes of dispersant concentration and post-treatments for fabricating single-walled carbon nanotube transparent conducting films. *Appl. Surf. Sci.* **2013,** 277, 128-133.

207.Kim, S.; Yim, J.; Wang, X.; Bradley, D. D. C.; Lee, S.; deMello, J. C., Spin- and Spray-Deposited Single-Walled Carbon-Nanotube Electrodes for Organic Solar Cells. *Adv. Funct. Mater.* **2010,** 20, 2310-2316.

208.Kim, T. A.; Lee, S.-S.; Kim, H.; Park, M., Acid-treated SWCNT/polyurethane nanoweb as a stretchable and transparent Conductor. *RSC Adv.* **2012,** 2, 10717-10724.

209.Li, X.; Gittleson, F.; Carmo, M.; Sekol, R. C.; Taylor, A. D., Scalable Fabrication of Multifunctional Freestanding Carbon Nanotube/ Polymer Composite Thin Films for Energy Conversion. *ACS Nano* **2012,** 6, 1347 - 1356.

210.Mistry, K. S.; Larsen, B. A.; Bergeson, J. D.; Barnes, T. M.; Teeter, G.; Engtrakul, C.; Blackburn, J. L., n-Type Transparent Conducting Films of Small Molecule and Polymer Amine Doped Single-Walled Carbon Nanotubes. *ACS Nano* **2011,** 5, 3714 - 3723.

211.Sim, J.-B.; Yang, H.-H.; Lee, M.-J.; Yoon, J.-B.; Choi, S.-M., Transparent conducting hybrid thin films fabricated by layer-by-layer assembly of single-wall carbon nanotubes and conducting polymers. *Appl. Phys. A* **2012,** 108, 305 - 311.

212.Yamamoto, T.; Noda, S.; Kato, M., A simple and fast method to disperse long single-walled carbon nanotubes introducing few defects. *Carbon* **2011,** 49, 3179 - 3183.

213.Zheng, Q.; Zhang, B.; Lin, X.; Shen, X.; Yousefi, N.; Huang, Z.-D.; Li, Z.; Kim, J.-K., Highly transparent and conducting ultralarge graphene oxide/single-walled carbon nanotube hybrid films produced by Langmuir–Blodgett assembly. *J. Mater. Chem.* **2012,** 22, 25072 - 25082.

214.Huang, J.-H.; Fang, J.-H.; Liu, C.-C.; Chu, C.-W., Effective Work Function Modulation of Graphene/Carbon Nanotube Composite Films As Transparent Cathodes for Organic Optoelectronics. *ACS Nano* **2011,** 5, 6262 - 6271.

215.Hu, B.; Li, D.; Manandharm, P.; Fan, Q.; Kasilingam, D.; Calvert, P., CNT/conducting polymer composite conductors impart high flexibility to textile electroluminescent devices. *J. Mater. Chem.* **2012,** 22, 1598 - 1605.

216.Barnes, T. M.; Wu, X.; Zhou, J.; Duda, A.; van de Lagemaat, J.; Coutts, T. J.; Weeks, C. L.; Britz, D. A.; Glatkowski, P., Single-wall carbon nanotube networks as a transparent back contact in CdTe solar cells. *Appl. Phys. Lett.* **2007,** 90, 243503.

217.Chhowalla, M., Transparent and conducting SWNT thin films for flexible electronics. *J. SID* **2007,** 15/12, 1085 - 1088.

218. Lee, E. H.; Ryu, J. H.; Jang, J.; Park, K. C., Patterned Single-Wall Carbon Nanotube Transparent Conducting Films for Liquid Crystal Switching Electrodes. *Jap. J. Appl. Phys.* **2011,** 50, 03CA04.

219. Liu, W.-B.; Pei, S.; Du, J.; Liu, B.; Gao, L.; Su, Y.; Liu, C.; Cheng, H.-M., Additive-Free Dispersion of Single-Walled Carbon Nanotubes and Its Application for Transparent Conductive Films. *Adv. Funct. Mater.* **2011,** 21, 2330–2337.

220. Pei, S.; Du, J.; Zeng, Y.; Liu, C.; Cheng, H.-M., The fabrication of a carbon nanotube transparent conductive film by electrophoretic deposition and hot-pressing transfer. *Nanotechnol.* **2009,** 20, 235707.

221. Rowell, M. W.; Topinka, M. A.; McGehee, M. D.; Prall, H.-J.; Dennler, G.; Sariciftci, N. S.; Hu, L.; Gruner, G., Organic solar cells with carbon nanotube network electrodes. *Appl. Phys. Lett.* **2006,** 88, 233506.

222. Su, Y.; Du, J.; Pei, S.; Liu, C.; Cheng, H.-M., Contamination-free and damage-free patterning of single-walled carbon nanotube transparent conductive films on flexible substrates. *Nanoscale* **2011,** 3, 4571-4574.

223. Xiao, G.; Tao, Y.; Lu, J.; Zhang, Z., Highly conductive and transparent carbon nanotube composite thin films deposited on polyethylene terephthalate solution dipping. *Thin Solid Films* **2010,** 518, 2822-2824.

224. Hellstrom, S. L.; Lee, H. W.; Bao, Z., Polymer-Assisted Direct Deposition of Uniform Carbon Nanotube Bundle Networks for High Performance Transparent Electrodes. *ACS Nano* **2009,** 3, 1423–1430.

225. Huang, Y. Y.; Terentjev, E. M., Transparent Electrode with a Nanostructured Coating. *ACS Nano* **2011,** 5, 2082-2089.

226. Lee, S.-H.; Teng, C.-C.; Ma, C. C. M.; Wang, I., Highly transparent and conductive thin films fabricated with nano-silver/double-walled carbon nanotube composites. *J. Coll. Interf. Sci.* **2011,** 364, 1-9.

227. Park, Y. T.; Ham, A. Y.; Grunlan, J. C., Heating and acid doping thin film carbon nanotube assemblies for high transparency and low sheet resistance. *J. Mater. Chem.* **2011,** 21, 363-368.

228. Park, Y. T.; Ham, A. Y.; Grunlan, J. C., High Electrical Conductivity and Transparency in Deoxycholate-Stabilized Carbon Nanotube Thin Films. *J. Phys. Chem. C* **2010,** 114, 6325-6333.

229. Salvatierra, R. V.; Oliveira, M. M.; Zarbin, A. J. G., One-Pot Synthesis and Processing of Transparent, Conducting, and Freestanding Carbon Nanotubes/Polyaniline Composite Films. *Chem. Mater.* **2010,** 22, 5222-5234.

230. Salvatierra, R. V.; Cava, C. E.; Roman, L. S.; Zarbin, A. J. G., ITO-Free and Flexible Organic Photovoltaic Device Based on High Transparent and Conductive Polyaniline/Carbon Nanotube Thin Films. *Adv. Funct. Mater.* **2013,** 23, (1490-1499).

231. Tantang, H.; Ong, J. Y.; Loh, C. L.; Dong, X.; Chen, P.; Chen, Y.; Hua, X.; Tana, L.; Lia, L.-J., Using oxidation to increase the electrical conductivity of carbon nanotube electrodes. *Carbon* **2009,** 47, 1867-1870.

232. Tenent, R. C.; Barnes, T. M.; Bergeson, J. D.; Ferguson, A. J.; To, B.; Gedavilas, L. M.; Heben, M. J.; Blackburn, J. L., Ultrasmooth, large area, high uniformity, conductive, transparent single-walled carbon nanotube films for photovoltaics produces by ultrasonic spraying. *Adv. Mater.* **2009,** 21, 3210-3216.

233. Zhang, D.; Ryu, K.; Liu, X.; Polikarpov, E.; Ly, J.; Tompson, M. E.; Zhou, C., Transparent, Conductive, and Flexible Carbon Nanotube Films and Their Application in Organic Light-Emitting Diodes. *Nano Lett.* **2006,** 6, 1880-1886.

234. Ng, M. H. A.; Hartadi, L. T.; Tan, H.; Poa, C. H. P., Efficient coating of transparent and conductive carbon nanotube thin films on plastic substrates. *Nanotechnol.* **2008,** 19, 205703.

Results and Discussion

2. Controlled transformations in transparent conducting films fabricated from highly stable hydrophilic dispersions of SWNTs through surface charge manipulation and acid treatment conditions

Preface

This section of the thesis deals with the preparation and optimization of single wall carbon nanotube (SWNT) dispersions. SWNTs were treated at reflux temperatures with nitric acid and mixture of nitric acid - sulphuric acid for different treatment durations. The acid treatment is a purification process that is employed to remove the metal catalyst particles from the SWNTs. This process is expected to have an effect on the electrical and optical properties of transparent conducting films (TCFs) fabricated from the dispersions of purified SWNTs which contain poly(sodium 4-styrene sulfonic acid) as a stabilizer. We have studied and found that the SWNTs purified with nitric acid for four hours at reflux temperature provides the optimum electrical and optical properties for the TCFs. We have also studied the effect of the pH value of the dispersion of SWNTs on the electrical and optical properties of the TCFs. The sheet resistance and optical transmittance of TCFs fabricated from the dispersions with pH values ranging from ~3 to ~12 were analyzed. We found that the TCFs fabricated from dispersions of higher pH value have better electrical and optical properties.

This section will be submitted as an original research article. The authors are Bibin T. Anto, Stefanie Eiden, Hans-C. Schwarz, Andreas M. Schneider and Peter Behrens. Prof. P. Behrens and Dr. S. Eiden provided general advice on the direction of this work. Mr. H-C. Schwarz and Dr. A. M. Schneider actively participated in the discussions of progress of this work.

Controlled transformations in transparent conducting films fabricated from highly stable hydrophilic dispersions of SWNTs through surface charge manipulation and acid treatment conditions

Bibin T Anto[1,2], Stefanie Eiden[2], Hans-C. Schwarz[2], Andreas M. Schneider[1], Peter Behrens[1]

[1] Institut für Anorganische Chemie, Leibniz Universität Hannover, Callinstraße 9, 30167 Hannover, Germany

[2] Bayer Technology Services GmbH, Chempark, 51368 Leverkusen, Germany

Abstract

Single wall carbon nanotubes (SWNTs) are considered to be one of the potential candidates for the production of transparent conducting films (TCFs), which can be used in many applications, e.g. touch panels, displays, and polymer solar cells. SWNTs are flexible, which makes them superior over the commonly used Indium Tin Oxide (ITO), a brittle material. Therefore, SWNTs may be used in flexible electronic applications. The absorptive nature of carbon in SWNTs at all optical wavelengths, brings in better colour neutrality to SWNT based TCFs than ITO and conducting polymers. However, better understanding on processing and fabrication of thin films are essential to drive this technology to industrial scale. Our work described in here, focused on effect of purification conditions of SWNTs on the quality of TCFs and the effect of pH value on the stability of the dispersions and TCFs. Here, we reveal that the figure of merit $\frac{\sigma_{d.c.}}{\sigma_{o.c.}}$ for such films can be increased by the factor of 2, when the pH of the SWNT dispersion increases. We also report the surface charge manipulated transformations in transparent conducting films fabricated from SWNT dispersions of different pH values.

Keywords

Single wall carbon nanotubes – SWNTs – purification – pH – transparent conductors

Introduction

Transparent conducting films (TCFs) are integral part of various electronics applications, e.g. organic light emitting diodes, displays, photovoltaic cells and touch panels. Currently, indium tin oxide (ITO) is the commonly used material in such applications due to its excellent properties of

optical transparency and electrically conductivity. Flexible electronic devices[1, 2] are receiving growing attention as the next generation applications, but the use of ITO as a TCF in such applications is jeopardized due to its brittle nature.[3] Moreover, the lack of availability and the increasing price[4] of ITO is driving the materials research towards alternate TCFs, including conducting polymers,[5-8] composites of conducting polymers and carbon nanotube,[9-11] transparent conducting oxides (TCOs),[12] metal nanowires,[13] graphene,[14, 15] and single wall carbon nanotubes (SWNTs).[16-19] SWNTs are more attractive due to their availability in abundance. In addition, they can be processed in aqueous solutions at low temperature, which is a key requirement for the application for the fabrication of thin films on low cost plastic substrates. Moreover, the work function - the minimum amount of energy required to remove an electron from an atom at the surface of a solid state compound - of SWNTs (4.5 - 5.1 eV) is also in the comparable range with that of ITO (4.4 - 4.9 eV).[20] The work function is a key parameter in defining energy level alignment of multilayer electronic devices.

Though vacuum deposited ITO films on glass substrates exhibit low sheet resistance at high optical transmittance, the performance of wet coated ITO films on plastic substrates is similar or inferior compared to SWNT TCFs.[21, 22] SWNTs applied on flexible substrates retain their electrical conductivity after number of cycles in bending tests.[23] Therefore, they are more suitable for applications in flexible electronics. An additional advantage of SWNTs is their colour neutrality,[24] since they absorb light all visible wavelengths.

The fabrication of TCFs from SWNTs involves several processing steps starting with the synthesis of SWNTs, e.g. via chemical vapour deposition,[25] pulsed laser evaporation,[26] the HiPCO process,[27] electric arc-discharge method,[28] followed by purification of SWNTs with strong oxidizing inorganic acids (mainly to remove the metal catalyst). The purified SWNTs have to be dispersed in suitable dispersing media to be utilized in film deposition processes, e.g. doctor-blading, dip-coating, spray-coating and spin coating. The last step is, doping of TCFs by immersing in inorganic acids in order to increase the film performance.[18] Since this extensive procedure from the pristine SWNTs to the final TCF product exhibits a number of alternative routes, it is necessary to understand the complex mechanisms that influence the electrical and optical properties of the films. On industrial applications, the stable and reliable performance of TCFs fabricated from SWNTs is of great concern – especially to scale-up the processes. This is a major issue as described in the following example. Saran *et al.* reported TCFs with thickness of about 1μm fabricated from dispersions of SWNTs (synthesized by pulsed laser evaporation)

exhibits sheet resistance R_s ~ 1000 Ω/□ at an optical transmittance of ~ 85 %.[29] In contrast, Wu *et al.* reported TCFs with thickness 50 nm fabricated from dispersions of SWNTs (also synthesized by pulsed laser evaporation) exhibits R_s ~ 30 Ω/□ at an optical transmittance of ~ 70 %.[30] Values reported by Wu *et al* are consistent with subsequent literature on SWNT TCFs, considering variations in nanotube type and processing methodologies. However, insights on issues such as – important details of effect of purification conditions of SWNTs; influence of pH of SWNT dispersions – were not considered in the previous reports.

Here, we focus on the effect of purification conditions of SWNTs and the performance of TCFs fabricated from dispersions of purified SWNTs. We report in detail about the effect of surface charges on the performance of TCFs prepared from SWNT dispersions of different pH and discuss the underlying principles. The choice of pH value for the SWNT dispersion depends on mainly two issues: (1) any aggregation from the dispersions has to be prevented. This holds especially true with regard to time from the dispersion of SWNTs; (2) the films fabricated from such dispersions should have reproducibility of both, high optical transmittance and low sheet resistance. TCFs, reported in this paper are characterized by figure of merit $\frac{\sigma_{d.c.}}{\sigma_{o.c.}}$, where $\sigma_{d.c.}$ and $\sigma_{o.c.}$ are the electrical and optical conductivities of SWNT films, respectively, which can be obtained from the following equation: [31, 32]

$$T_{550} = \left(1 + \frac{1}{2R_s}\sqrt{\frac{\mu_0}{\varepsilon_0}}\frac{\sigma_{o.c.}}{\sigma_{d.c.}}\right)^{-2}$$

where,

T_{550} is the optical transmittance of TCFs at a wavelength of 550nm (we observed that the average value of the transmittance between 400 to 700 nm is same as the transmittance at 550nm). R_s is the sheet resistance of the film, μ_0 and ε_0 are the permittivity and permeability of free space, respectively. $\frac{\sigma_{d.c.}}{\sigma_{o.c.}}$ is the ratio of electrical-to-optical conductivity and can be obtained by curve fitting the experimental values of R_s vs. T_{550}. In general, the larger the value of $\frac{\sigma_{d.c.}}{\sigma_{o.c.}}$ the better will be the performance of the TCF. We, report the effect of purification conditions of SWNTs and influence of the *p*H of SWNT dispersion on the figure of merit $\frac{\sigma_{d.c.}}{\sigma_{o.c.}}$ of the corresponding SWNT TCFs.

Experimental

Purification of SWNTs and preparation of dispersion: SWNTs, produced by arc-discharge method, were purchased from Fraunhofer IWS, Dresden. 20 g of SWNTs were purified by refluxing in 200 mL HNO_3 (65%) for 2 hours, in a round bottom flask. The mixture was allowed to cool down to room temperature, and was washed with 2 L of deionized (DI) water. At pH > 1 a portion of SWNTs become dispersible (IEP ~ 1.0, see fig. 4). The residue was collected separately; supernatant was acidified to pH < 1.0 to precipitate the suspended SWNTs and combined with the residue obtained before. During the process, SWNTs were kept in wet conditions (with minimum amount of water) as the dry SWNTs tend to agglomerate and therefore difficult to redisperse in water. Afterwards, the acid treated SWNT mixture was dialyzed against DI water until the pH of DI water becomes 7.0 in order to remove all excess ions and impurities. Finally, the purified SWNT mixture was sonicated in DI water using Branson Sonifier 450 (80W, 30 min) to produce a better dispersion. The mixture was then centrifuged (3500 rpm/30 min) to remove undispersed materials. Then the supernatant – the SWNT dispersion – was collected and used for further characterization and film fabrication. Dispersions of SWNTs treated at different conditions (HNO_3:H_2SO_4::3:1 v/v for 4 hours, HNO_3 for 3 to 6 hours) were prepared in a similar way by treating SWNTs in respective acids for corresponding durations as summarized in Table 1. Typical concentration of dispersions used for testing and characterization were 0.2 to 0.3 wt% SWNT. The pH of the dispersions was modified by dialyzing against liquid ammonia and DI water, as needed; dispersions of pH > 8 were modified by adding few drops of liquid ammonia to the dialyzed SWNT dispersions.

Fabrication of transparent conductive films (TCFs): TCFs were fabricated on glass slides using the Meyer rod coating method (doctor blading). The films were annealed at 120 ± 10 °C for 1 min. Multilayered coatings were prepared to reach low sheet resistance values (< 500 $\Omega/\square$), typically 3 to 4 layers. All the data were repeated 2 to 3 times to confirm the reproducibility. Films were reproduced in large area (ISO A4 size) poly carbonate sheets, which were O_2 plasma treated prior to doctor blading.

Electrical and optical properties: Sheet resistance of TCFs was measured using 2 point probe method, across square area, i.e. 1 x 1 cm^2, with a probe dimension of 1 cm^2. The standard error, if any, involved in the measurement of sheet resistance is uniform throughout all the measurements. Typically, four to five measurements were taken for each data point and the average of the measurements was calculated. Standard deviation of the data points was

calculated to be ≤ 7%. Optical transmittance of the TCFs was recorded using Cary 50 UV-Vis spectrometer (Varian). Thicknesses of the films were measured using Dektek 150 profilometer (Veeco Instruments).

X-ray Photoelectron spectroscopy (XPS): Core-level and survey X-ray photoelectron spectra were acquired on a VersaProbe spectrometer (Physical Electronics) at a base pressure of less than 10^{-8} mbar using monochromatic Al Kα X-ray photons (1486.68 eV) irradiating at 45° relative to electron analyzer entrance. The photo-electrons were analyzed by a concentric hemispherical analyzer operated at constant pass energy of 29.35 eV for C1s & O1s core-level spectra, 117.4 eV for N1s & S2p core-level spectra, and 187.5 eV for survey spectra. The photoemission angle (θ) was set to 54.7°. The X-ray gun was operated at 50 W with a spot size of 200 µm scanning an area of 0.4 x 0.8 mm^2. Sample charging was avoided by using Indium substrate to provide a conductive ground; charge neutralization was not necessary. Core-level spectra were processed to give atomic stoichiometry values using Multipak 9.1 software that accounts empirical sensitivity factors taking into account photoionization cross sections, inelastic mean free paths, and the spectrometer intensity-energy response functions.

Raman spectroscopy: Raman spectra of SWNT films were recorded using Induram (Horiba Jobin-Yvon) spectrometer, coupled with confocal laser scanning microscope. Excitation wavelength used for the all the measurements is 488 nm. Films for the measurements were prepared by drop-casting corresponding SWNT dispersions on to a glass slide and annealed at 120°C/ 1min.

Zeta potential: Iso electric point (IEP) determination experiments on purified SWNTs were performed on Malvern Zetasizer 3000HSa. In order to have higher ionic strength, 0.2 g SWNT dispersion (0.3 wt%) was dispersed in 10 g of 1mM KCl. Measurements on similar concentration of SWNTs in DI water was also performed for comparison.

Results and discussion

Purification by refluxing in nitric acid was performed in order to remove the metal catalyst particles present in SWNTs. The purification procedure also oxidizes the SWNTs which introduces various functional moieties on the surface, e.g. –COOH, -OH, -C=O.[33, 34] After purification by refluxing in nitric acid (65%) for two to six hours, SWNTs were dispersed in water. The optimum reflux time was determined based on the performance analysis of TCFs with respect to acid treatment conditions of SWNTs with nitric acid. The optimum reflux duration was

determined by $\frac{\sigma_{d.c.}}{\sigma_{o.c.}}$ of TCFs, fabricated from the dispersions of SWNTs under different acid treatment conditions. The dispersions prepared from these purified SWNTs are used to fabricate transparent thin films by Mayer rod coating method.

Table 1: Summary of properties of SWNT dispersion and TCFs in this work.

S/No	Dispersion Notation [a]	Acid [b]	Reflux duration (hrs) [d]	pH of Dispersion [e]	$\frac{\sigma_{d.c.}}{\sigma_{o.c.}}$ [f]
1	SWNT(HNO$_3$/2hr)	HNO$_3$	2	3.23	3.1
2	SWNT(HNO$_3$/3hr)	HNO$_3$	3	3.1	3.5
3a	SWNT(HNO$_3$/4hr)	HNO$_3$	4	3.6	4
3b	SWNT(HNO$_3$/4hr)	HNO$_3$	4	6.28	4.5
3c	SWNT(HNO$_3$/4hr)	HNO$_3$	4	10.3	5.05
4	SWNT(HNO$_3$/5hr)	HNO$_3$	5	3.3	4.0
5	SWNT(HNO$_3$/6hr)	HNO$_3$	6	3.4	4.0
6a	SWNT(HNO$_3$/H$_2$SO$_4$)	HNO$_3$:H$_2$SO$_4$[c]	4	2.82	2.6
6b	SWNT(HNO$_3$/H$_2$SO$_4$)	HNO$_3$:H$_2$SO$_4$[c]	4	7.7	3.0
6c	SWNT(HNO$_3$/H$_2$SO$_4$)	HNO$_3$:H$_2$SO$_4$[c]	4	9.88	3.5
7a	SWCNT(HNO$_3$/4hr)[g]	HNO$_3$	4	3.6	4
7b	SWCNT(HNO$_3$/4hr)[g]	HNO$_3$	4	11.6	6

[a]   The subscript in the notation represents the acid, used for the purification and the amount of time for which the purification/reflux was performed with SWNTs

[b]   Acid used to reflux with SWNTs, during the process of purification. The temperature, during the reflux was maintained at 130 ± 5 °C.

[c]   The ratio of HNO$_3$-to-H$_2$SO$_4$ is kept at 3:1 v/v. Concentrations of HNO$_3$ and H$_2$SO$_4$ used in this work are 65% and 98%, respectively, unless otherwise stated.

[d]   The reflux temperature for the purification of SWNTs is kept at 130 ± 5 °C, throughout all the experiments listed above.

[e]   pH of the SWNT dispersions were modified (from acidic-to-basic) by dialyzing against 1mM NH$_4$OH and (or) DI water, as desired.

[f] $\frac{\sigma_{d.c.}}{\sigma_{o.c.}}$ of SWNT TCFs were calculated by curve fitting the experimental data for R_s vs. T_{550} of of various thin films fabricated from the dispersions listed above.

[g]   SWNT dispersions were prepared without any polymeric stabilizer such as PSSNa, which was used in all the dispersions except S/No. 7. Dispersions were stable for more than a year at ambient conditions.
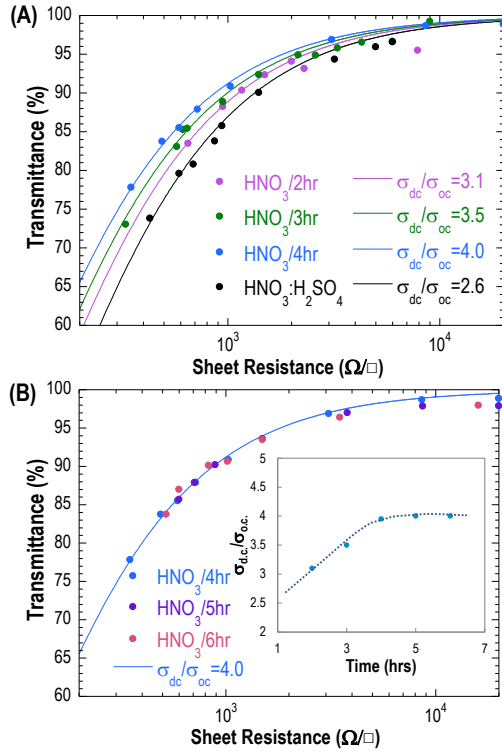
Figure 1: Electrical and optical properties of SWNT TCFs with respect to acid treatment conditions. (A) TCFs fabricated from 2 to 4 hour HNO_3 treated SWNT dispersion together with TCFs from HNO_3:H_2SO_4 [3:1 v/v] treated SWNT dispersions. (B) TCFs fabricated from 4 to 6 hours HNO_3 treated SWNT dispersions, plotted separately for better clarity. Inset shows the performance of TCFs of HNO_3 treated films from 2 to 6 hours.

First, the properties of TCFs fabricated from the acidic dispersions of SWNTs were examined. Substantial difference in $\frac{\sigma_{d.c.}}{\sigma_{o.c.}}$ of TCFs fabricated from the dispersions of SWNTs treated with nitric acid from two to six hours have been observed (Fig. 1A, Table 1 S/No. 1, 2 & 3a). $\frac{\sigma_{d.c.}}{\sigma_{o.c.}} =$ 3.1 is observed for the films prepared from SWNT(HNO_3/2hr) dispersions, and it has increased to 3.5 for SWNT(HNO_3/3hr) films. TCFs fabricated from SWNT(HNO_3/4hr) from acidic conditions showed the maximum $\frac{\sigma_{d.c.}}{\sigma_{o.c.}}$ of 4. Longer reflux durations of SWNTs did not improve the $\frac{\sigma_{d.c.}}{\sigma_{o.c.}}$ (Fig 1B, Table 1 S/No 3a, 4 & 5). The upward trend on the $\frac{\sigma_{d.c.}}{\sigma_{o.c.}}$ of SWNT TCFs can be attributed to the increase in doping level by nitric acid with respect to increase in reflux duration. It is known from the literature that the *SWNT films* post-treated with HNO_3 help to improve the

electrical conductivity through doping.[16, 35-39] Shin *et al* reported that the TCFs fabricated from dispersion of SWNTs in N-methylpyrrolidone solvent showed a significant decrease in R_s from ~1400 $\Omega/\square$ to ~ 100 $\Omega/\square$ at a given T_{550} of ~ 90%, after the TCFs were immersed in HNO$_3$ for 10 minutes.[40] Though the SWNT TCFs described in this report were not doped immersing the films in inorganic acids, analogous effect of doping is achieved through purifying the SWNTs in inorganic acids. X-ray photoelectron spectroscopic (XPS) investigation on our SWNTs is consistent with these findings as the stoichiometry changes from $C_{94.65}O_{4.99}$ for the original compound to $C_{94.65}O_{4.99}N_{0.36}$ for SWNT(HNO$_3$/2hr), $C_{94.72}O_{4.85}N_{0.40}$ for SWNT(HNO$_3$/3hr), $C_{94.84}O_{4.77}N_{0.44}$ for SWNT(HNO$_3$/4h r) and $C_{93.54}O_{5.91}N_{0.55}$ for SWNT(HNO$_3$/6hr).
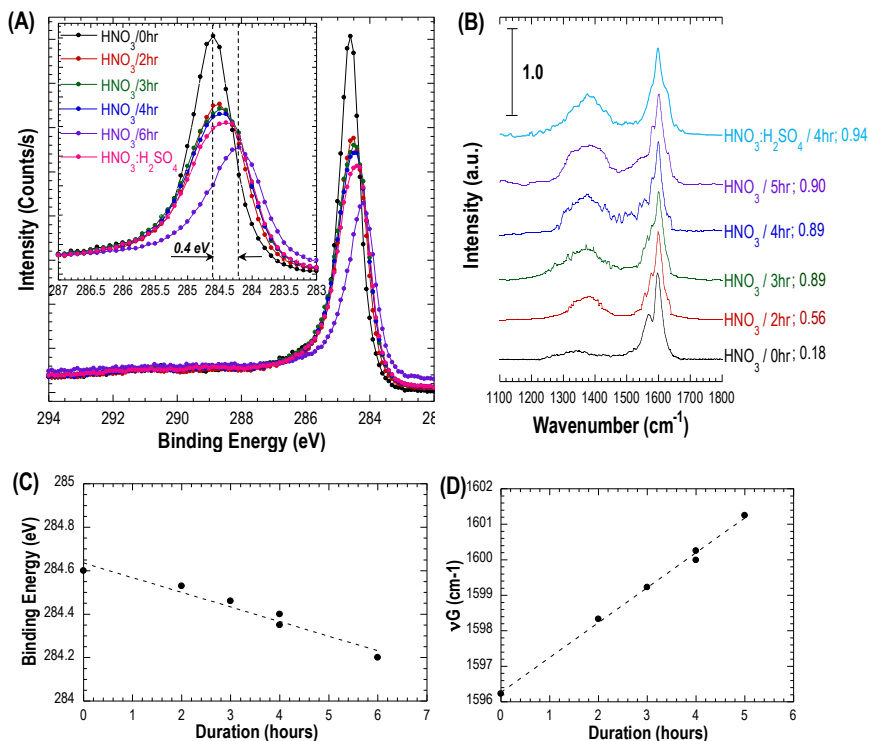
Figure 2: (A) C1s core-level x-ray photoelectron spectra of SWNT at different reflux durations. Inset shows the down-shift in C1s binding energy, attributed to oxidation & doping of SWNTs. (B) Raman spectra of SWNTs that underwent different acid treatment conditions. Excitation wavelength used for the measurement is 488 nm. The value after semi-column in legends are, disorder (D)-to-tangential (G) mode ratio. (C) C1s binding energy levels of SWNTs with respect to acid treatment durations. (D) Behavior of tangential mode with respect to acid treatment duration.

The binding energy of 284.6 eV for C1s core level spectra for SWNT(HNO$_3$/0hr) has been downshifted by 0.4 eV for SWNT(HNO$_3$/6hr) samples (Fig. 2A and C). The downshift in binding energy of C1s core-level spectra is possibly due to the the oxidation induced functional moieties and predominantly due to the doping effects from nitrogen containing molecules.[40, 41] The presence of nitrogen detected from N1s core level spectra has increased from 0.36-%, for SWNTs refluxed in nitric acid for 2 hours, to 0.44-% for SWNTs refluxed in HNO$_3$ for 4 hours (see Table 2). The increment in presence of nitrogen suggests that the doping level also increased with respect to time. This could be a possible reason for the increase in $\frac{\sigma_{d.c.}}{\sigma_{o.c.}}$ of TCFs prepared from dispersions of SWNTs refluxed in HNO$_3$ with increasing reflux time to 4h. Similar $\frac{\sigma_{d.c.}}{\sigma_{o.c.}}$ is observed for TCFs prepared from dispersions of SWNTs refluxed in HNO$_3$ for 5 and 6 hours (Table 1, S/No. 4 & 5). The XPS investigation on SWNT(HNO$_3$/6hr) shows the stoichiometry of $C_{93.54}O_{5.91}N_{0.55}$. Interestingly, the level of nitrogen in SWNT(HNO$_3$/6hr) samples have increased to 0.55-%, and the oxygen containing moieties to 5.91-%. Deconvolution of C1s core-level spectra shows that the total amount of sp^2 hybridized carbon (80.93-%) due to the longer oxidation time in HNO$_3$. Thus, the increased doping effect from the nitrogen containing molecules is counter-balanced by the reduction in sp^{2}hybridized carbon atoms that contributes to electrical conductivity. This could be the possible reason for no increase in $\frac{\sigma_{d.c.}}{\sigma_{o.c.}}$ beyond 4 hours of reflux duration of SWNTs with HNO$_3$. Improving $\frac{\sigma_{d.c.}}{\sigma_{o.c.}}$ of SWNT TCFs through post-treatment by HNO$_3$ will increase the process complexity with regard to scaling up to roll-to-roll fabrication methods.
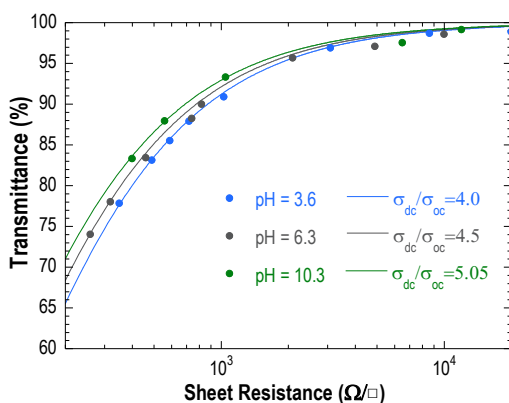

Figure 3: Electrical and optical properties of TCFs fabricated from same dispersion of SWNTs with PSSNa, underwent 4 hours of HNO3 treatment, at different pH conditions.

Table 2: Summary of x-ray photoelectron spectra of SWNTs described this work.

S/No	Notation	C1s[a]					O1s	N1s[b]			S2p
		C=C	C-C	O-C=O	π-π	∑C1s		NO	C=N	∑N1s	
1	SWNT(HNO3/0hr)	82.42	2,39	2,50	9,19	96,5	3,5	-	-	-	-
2	SWNT(HNO3/2hr)	83.50	3,81	2,68	4,66	94,65	4,99	0,22	0,14	0,36	-
3	SWNT(HNO3/3hr)	84.50	3,34	2,64	4,68	94,72	4,85	0,27	0,13	0,40	-
4	SWNT(HNO3/4hr)	85.71	1,72	2,64	4,78	94,84	4,77	0,25	0,19	0,44	-
5	SWNT(HNO3/6hr)	80.93	4.03	4.46	4.12	93.54	5.91	0,35	0.20	0.55	-
6	SWNT(NO3/H2SO4)	82.0	4,20	2,90	4,57	93,67	5,76	0,25	0,23	0,48	0,10

[a]   Deconvoluted values of C1s core-level spectra obtained using Multipak 4.1

[b]   Deconvoluted values of N1s core-level spectra obtained using Multipak 4.1

Raman spectroscopy also supports the possible oxidation and doping levels of SWNTs by HNO_3 treatment reached their maximum at 3 – 4 hours reflux duration (Fig. 2B). We noticed that the disorder (D)-to-tangential (G) mode ratio, calculated from integrated absorption cross-sections of Raman spectra of SWNTs reached its maximum of 0.89 in 3- 4 hours. The D-to-G ratio has slightly increased to 0.9 for SWNTs refluxed in HNO_3 for 5 hours. Evidence of p-type doping in SWNTs with respect to reflux duration is supported by the upshift in tangential mode (ν_G), which is due to the softening of lattice, due to the electron withdrawing nitrogen containing moieties sorbed onto the SWNTs (see fig 2D). Though the upshift in ν_G has increased linearly with respect to reflux duration of SWNTs in HNO_3, oxidation time longer than 4 hours could significantly reduce the amount of sp2 hybridized carbon atoms. The doping levels of SWNTs were tried to increase by employing a more strongly oxidizing acid H_2SO_4 (98%) in combination with HNO_3(65%);   the ratio of HNO_3 to H_2SO_4 is kept 3:1 v/v. The combination of 3:1 v/v corresponds to ~ 2.5:1 molar ratio of HNO_3-to-H_2SO_4, which is used to introduce nitro (-NO_2) groups on aromatic rings through electrophilic substitution reactions. We assumed that this mixture could increase the oxidation and doping on SWNTs through which the sheet resistance of TCFs can be brought down. After the treatment, the oxidation levels and presence of nitrogen in the SWNTs increased, but the $\frac{\sigma_{d.c.}}{\sigma_{o.c.}}$ of TCFs fabricated from these SWNT dispersions decreased. The $\frac{\sigma_{d.c.}}{\sigma_{o.c.}}$ of SWNT(HNO_3/H_2SO_4) films dropped to 2.6 compared to 4 for SWNT(HNO_3/4hr) films (Fig.1A, Table 1 S/No. 3a & 6a). XPS analysis suggests that the sp2 hybridization of carbon atoms in SWNT(HNO_3/H_2SO_4) have been damaged more as the combination of H_2SO_4 and HNO_3 is more strong (Table 2 S/No 4 & 6). This could be a possible reason for the reduction in $\frac{\sigma_{d.c.}}{\sigma_{o.c.}}$ for SWNT(HNO_3/H_2SO_4) compared to SWNT(HNO_3/4hr) films.

During the purification of SWNTs by refluxing with oxidizing acids some of the sp^2 carbon atoms are transformed to C=N structures (for e.g. pyridinic) that adds key features in enhancing the surface charge induced transformations in SWNT TCFs. The transformation of sp^2 carbon atoms to C=N structures are detected from the evolution of new peak centered around binding energy levels (~ 401 eV) of N1s core-level XPS spectra of SWNTs.[35] C=N signature has increased from 0.14 at.-% to 0.20 at.-% for SWNTs refluxed by nitric acid from 2 to 6 hours (Table 2 S/No 2-5). Addition of different functional groups, due to oxidation, add further possibilities to improve the $\frac{\sigma_{d.c.}}{\sigma_{o.c.}}$ of TCFs.
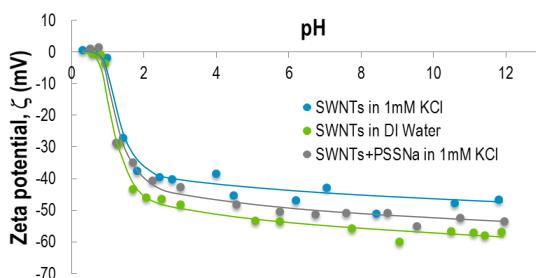
Figure 4: IEP measurement: Zeta potential of SWNTs that underwent 4 hours HNO$_3$ treatment.

In order to determine the effect of pH of SWNT dispersions on the performance of TCFs, the pH of SWNT(HNO$_3$/4hr) dispersions was adjusted by dialysis with DI water and liquid ammonia, as required. $\frac{\sigma_{d.c.}}{\sigma_{o.c.}}$ of TCFs can be increased by adjusting the pH value of the SWNT dispersions from acidic to basic. TCFs coated from the dispersion of SWNT(HNO$_3$/4hr) of pH 3.6 (acidic), show a $\frac{\sigma_{d.c.}}{\sigma_{o.c.}}$ of 4.0. $\frac{\sigma_{d.c.}}{\sigma_{o.c.}}$ of TCFs is increased to 4.5 for the films when the pH of the dispersion is adjusted to 6.28, and increased further to 5.05 when the pH of the SWNT(HNO$_3$/4hr) dispersion is elevated to 10.3 (Fig. 3, Table 1 S/no. 3).

Zeta potential (ζ, mV) of SWNTs(HNO$_3$/4hr) dispersions increases with respect to increase in pH. We notice that ζ has increased from ~ 40 mV for the pH between 2 and 4 to ~ 50 mV for the pH between 4 and 8 (Fig. 4). ζ for the SWNTs(HNO$_3$/4hr) dispersions of pH beyond 8 are centered at around 55 mV. These transformations in ζ might be as well interpreted as a result of the deprotonation of functional moieties, which increase the surface charge on the SWNTs. We

propose the following hypothesis for this effect: At different pH values the functional moieties present in SWNTs – e.g. carboxylic ($pK_a \sim 2$), pyridinic ($pK_a \sim 5$) and phenolic groups ($pK_a \sim 10$) are deprotonated.[42-47] This deprotonation results in increase of the electrostatic repulsion, leading to manipulation of the spatial increment between the adjacent SWNTs. It is known from literature that the force between equally charged cylindrical objects of equal radii is repulsive, and the volume between the two cylindrical objects will have the high concentration of ions of opposite charges. [48, 49] The high concentration of ions of opposite charges resulting in strong electrostatic repulsion leads to an increased distance between cylindrically shaped SWNTs. Larger spacing between SWNTs increases the transmission of photons through the TCFs. These effects would possibly causes an increase in light transmission at a given sheet resistance of TCFs and therefore to a higher $\frac{\sigma_{d.c.}}{\sigma_{o.c.}}$ values. In other words, due to the increased spacing between SWNTs, the optical transmittance of SWNT(HNO$_3$/4hr) films rose from 77.5% to 82% at a given sheet resistance of 350 Ω/□ (Fig. 3).

Table 3: Comparison of properties of TCFs fabricated from SWNT dispersions at different pH

Dispersion	pH[a]	R_s (Ω/□)[b]	T_{550} (%)[c]	t (nm)[d]	$\frac{\sigma_{d.c.}}{\sigma_{o.c.}}$ [e]	$\sigma_{d.c.}$ (Sm^{-1}) [f]	$\sigma_{o.c.}$ (Sm^{-1}) [g]
SWNT(HNO$_3$/4hr)	11.6	235±5	79	29.5±4	6	1.47 x 10^5	2.4 x 10^4
SWNT(HNO$_3$/4hr)	3.6	490±20	83	29±3	4	7 x 10^4	1.75 x 10^4

[a] pH of the SWNT dispersion used to fabricate the TCFs; SWNTs used here are SWNT(HNO$_3$/4hr).

[b] Sheet resistance of TCFs fabricated from SWNT(HNO$_3$/4hr) dispersion

[c] Optical transmittance of TCFs fabricated from SWNT(HNO$_3$/4hr) dispersion

[d] Thickness of TCFs measured using profilometry.

[e] Figure of merit of TCFs

[f] Electrical conductivity of TCFs, calculated from, reciprocal of product of sheet resistance and film thickness.

[g] Optical conductivity of TCFs, calculated by incorporating sheet resistance, transmittance and thickness values on the equation described in the paper.
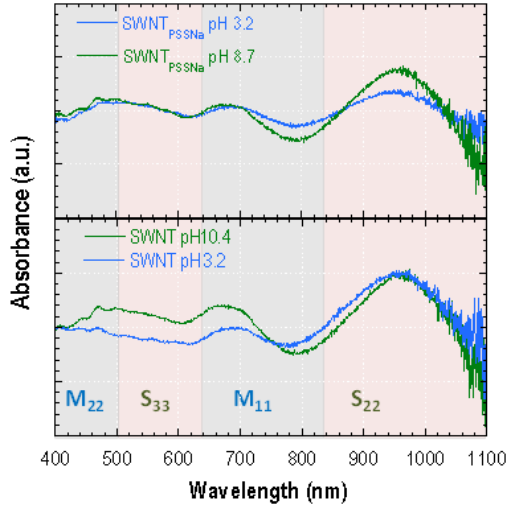
Figure 5: Optical absorbance spectra of SWNTs at different pH conditions.

The increase in spatial distance between the contact pairs of SWNTs with increase in pH is also supported by the optical absorbance spectra. Broadening of van-Hove Singularities (vHS) are observed when the pH of SWNT dispersions become acidic (pH = 3) (Fig. 5). The vHS of SWNTs sharpen at higher pH, which is due to the minimization of inter-tube coupling that can be attributed to the larger distance between adjacent contact-pairs of SWNTs (Fig. 5). Effects of inter-tube coupling between SWNTs and bundles and its implications on the inter-band transitions (vHS) are reported.[50-52] Effect of Broadening of vHS with respect to decrease in pH of SWNT dispersions is in accordance with the report by Zhao et al.[53] It is reported that the vHS of surface modified water soluble SWNTs broadens with respect to decrease in pH; intensity difference in vHS has been attributed to electrostatic doping, surface charge manipulation and intercalation & deintercalation of H+ ions in SWNT bundles.[53] Thus, increase in spatial arrangement with respect to increase in surface charge eventually results in relatively higher $\frac{\sigma_{d.c.}}{\sigma_{o.c.}}$ values of SWNT TCFs.
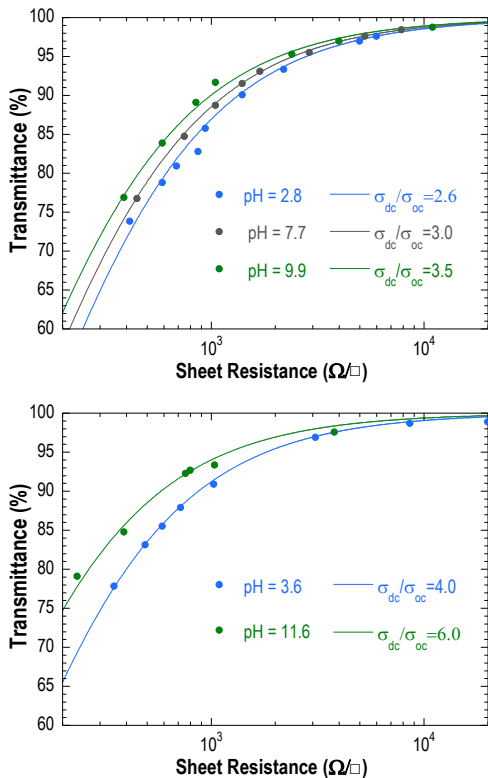
Figure 6: Electrical and optical properties of TCFs at different pH conditions. (A) TCFs fabricated from dispersion of SWNTs, underwent 4 hours $HNO_3:H_2SO_4[3:1]$ treatment. (B) TCFS fabricated from dispersion of SWNTs without PSSNa, underwent 4 hours HNO_3 treatment.

The mechanism of inter-tube coupling on the broadening of vHS is further evidenced and supported from the differential thickness of SWNT TCFs fabricated from the dispersion of different pH (Table 3). For example, films of thickness 29.5±4 nm, fabricated from SWNT(HNO_3/4hr) dispersions of pH 11.6 gives R_s = 235±5 $\Omega/\square$ at T_{550} = 79%, $\frac{\sigma_{d.c.}}{\sigma_{o.c.}} = 6$. A similar film of thickness 29±3 nm fabricated from SWNT(HNO_3/4hr) dispersions of pH 3.6 gives R_s = 490±20 $\Omega/\square$ at T_{550} = 83%, $\frac{\sigma_{d.c.}}{\sigma_{o.c.}} = 4$. Optical conductivity, $\sigma_{o.c.}$ of SWNT TCFs fabricated from the dispersion of pH 11.6 is calculated to be 2.4x10^4 Sm^{-1}, which is ~ 40 % higher than the $\sigma_{o.c.}$= 1.75x10^4 Sm^{-1} for SWNT TCFs fabricated from the dispersion of pH 3.6. Optical conductivity of SWNT TCFs fabricated from acidic dispersions are similar to the value

($\sigma_{o.c.}$= 1.7x10^4 Sm^{-1}) reported by Doherty et al for sodium dodecyl sulfate and sodium dodecyl benzene sulfonate stabilized SWNT TCFs.[54] Thus, by manipulating the spatial distance between the SWNTs and bundles by increasing the surface charge, increases the possibility of better statistical assembly of SWNTs that leads to the formation of thinner films with high percolation effects and hence better optical and electrical properties. To test the universality of the principle of surface of charge induced transformation in SWNT TCFs, we have conducted the similar experiments on SWNT(HNO$_3$/H$_2$SO$_4$) dispersion. Here we found that the $\frac{\sigma_{d.c.}}{\sigma_{o.c.}}$ is increased from 2.6 to 3.5, when the pH of the dispersions is modified from 2.8 to 9.9 (Fig. 6A, Table1 S/No. 6). Similarly for the SWNT(HNO$_3$/4hr) dispersions, without polymeric stabilizer (poly(4-styrenesulfonic acid, sodium salt)), $\frac{\sigma_{d.c.}}{\sigma_{o.c.}}$ was increased by factor of 2 when the pH of the dispersion is modified from 3.6 (acidic) to 11.6 (basic) (Fig. 6B, Table1 S/No. 7). These new insights on surface charge induced transformation in SWNT TCFs, opens up further possibilities on materials and technology development in flexible transparent electronics applications.

Conclusion

Effect of purification SWNTs with nitric acid at different reflux durations have been studied and analyzed. The optimum reflux duration for SWNTs is found to be 4 hours in nitric acid, based on the maximum possible $\frac{\sigma_{d.c.}}{\sigma_{o.c.}}$ of the TCFs prepared from dispersions of SWNTs purified between 2 to 6 hours. The principle behind the effect of purification conditions and the effect of doping were analyzed using x-ray photoelectron spectroscopy and Raman spectroscopy. We found that the maximum possible $\frac{\sigma_{d.c.}}{\sigma_{o.c.}}$ for TCFs under optimum purification condition to be 4. Effect of pH of the dispersion of SWNTs on the electrical and optical properties of TCFs was also studied in detail. The surface charge on the SWNTs can be controlled by adjusting the pH of the dispersion, by which the spacing between the SWNTs can be manipulated. The surface charge difference in SWNTs with respect to pH is analyzed by zeta potential and optical absorption spectroscopy. Maximum possible $\frac{\sigma_{d.c.}}{\sigma_{o.c.}}$ = 6.0 for SWNT TCFs can be obtained from the dispersions of SWNTs at higher pH, due to increased spacing between adjacent contact pairs of SWNTs.

Sicking and Wolfgang Weiner for their extensive support during XPS and Raman spectroscopic measurements, respectively.

References

[1]   A. Nathan, A. Ahnood, M. T. Cole, S. Lee, Y. Suzuki, P. Hiralal, F. Bonaccorso, T. Hasan, L. G-Gancedo, A. Dyadyusha, S. Haque, P. Andrew, S. Hofmann, J. Moultrie, D. Chu, A. J. Flewitt, A. C. Ferrari, M. J. Kelly, J. Robertson, G. A. J. Amaratunga, W. I. Milne, *Proc. of the IEEE* **2012**, *100*, 1486.

[2]   W. S. Wong, A. Salleo, in *Electronic Materials: Science & Technology* (Ed.: H. L. Tuller), Springer, New York, **2009**, p. 462.

[3]   Y. Chen, B. Cotterell, W. Wang, *Eng. Fract. Mech.* **2002**, *69*, 597.

[4]   A. Chipman, *Nature* **2007**, *449*, 131.

[5]   T. Aernouts, P. Vanlaeke, W. Geens, J. Poortmans, P. Heremans, S. Borghs, R. Mertens, R. Andriessen, L. Leenders, *Thin Solid Films* **2004**, *451-452*, 22.

[6]   G. Gustafsson, Y. Cao, G. M. Treacy, F. Klavetter, N. Colaneri, A. J. Heeger, *Nature* **1992**, *357*, 477.

[7]   J. Huang, X. Wang, A. J. deMello, J. C. deMello, D. D. C. Bradley, *J. Mater. Chem.* **2007**, *17*, 3551.

[8]   F. Jonas, A. Karbach, B. Muys, E. van Thillo, R. Wehrmann, A. Elschner, R. Dujadin, *Vol. EP0686662 A2* (Ed.: E. P. Office), Bayer A.G., Germany, **1995**, pp. 1.

[9]   N. F. Anglada, M. Kaempgen, V. Skákalová, U. D-Weglikowska, S. Roth, *Diamond Relat. Mater.* **2004**, *13*, 1256.

[10]   E. Kymakis, G. Klapsis, E. Koudoumas, E. Stratakis, N. Kornilios, N. Vidakis, Y. Franghiadakis, *EPJ Appl. Phys.* **2007**, *36*, 257.

[11]   J. B. Yoo, J. S. Moon, J. H. Park, T. Y. Lee, Y. W. Kim, C. Y. Park, J. M. Kim, K. W. Jin, *Diamond Relat. Mater.* **2005**, *14*, 1882–1887.

[12]   E. Fortunato, D. Ginley, H. Hosono, D. C. Paine, *MRS Bull.* **2009**, *32*, 242.

[13]   L. Hu, H. Wu, Y. Cui, *MRS Bull.* **2011**, *36*, 760.

[14]   J. K. Wassei, R. B. Kaner, *Mater. today* **2010**, *13*, 52.

[15]   J. Song, F.-Z. Kam, R.-Q. Png, J.-M. Zhou, G.-K. Lim, P. K. H. Ho, L.-L. Chua, *Nat. Nanotechnol.* **2013**, *8*, 356.

[16]   Q. Cao, J. A. Rogers, *Adv. Mater.* **2009**, *21*, 29.

[17]   G. Gruner, *J. Mater. Chem.* **2006**, *16*, 3533.

[18]   L. Hu, D. S. Hecht, G. Grüner, *Chem. Rev.* **2010**, *110*, 5790.

[19]   L. Hu, J. Li, J. Liu, G. Grüner, T. Marks, *Nanotechnol.* **2010**, *21*, 155202.

[20]   C. M. Aguirre, S. Auvray, S. Pigeon, R. Izquierdo, P. Desjardins, R. Martel, *Appl. Phys. Lett.* **2006**, *88*, 183104.

[21]   N. Al-Dahoudi, M. A. Aegerter, *J. Sol-Gel Sci. Tech.* **2003**, *26*, 693.

[22]   S. H. Lee, N. Y. Ha, *Optics Express* **2011**, *19*, 21803.

[23]   C. Weeks, J. Peltola, I. Levitskz, P. Gladkowski, J. van de Lagemaat, G. Rumbles, T. Barnes, T. Coutts, *Proc. of the IEEE* **2006**, *1*, 295.

[24]   C. M. Trottier, P. Glatkowski, P. Wallis, J. Luo, *J. Soc. Info. Disp.* **2005**, *13*, 759.

[25]   H. Dai, A. G. Rinzler, P. Nikolaev, A. Thess, D. T. Colbert, R. E. Smalley, *Chem. Phys. Lett.* **1996**, *260*, 471.

[26]   T. Guo, P. Nikolaev, A. Thess, D. T. Colbert, R. E. Smalley, *Chem. Phys. Lett.* **1995**, *243*, 49.

[27]   P. Nikolaev, M. J. Bronikowski, R. K. Bradley, F. Rohmund, D. T. Colbert, K. A. Smith, R. E. Smalley, *Chem. Phys. Lett.* **1999**, *313*, 91.

[28]   T. W. Ebbesen, P. M. Ajayan, *Nature* **1992**, *358*, 220.

[29]   N. Saran, K. Parikh, D.-S. Suh, M. Munoz, H. Kolla, S. K. Manohar, *J. Am. Chem. Soc.* **2004**, *126*, 4462.

[30]   Z. Wu, Z. Chen, X. Du, J. M. Logan, J. Sippel, M. Nikolou, K. Kamaras, J. R. Reynolds, D. B. Tanner, A. F. Hebard, A. G. Rinzler, *Science* **2004**, *305*, 1273.

[31]   M. Dressel, G. Grüner, *Electrodynamics of Solids: Optical Properties of Electrons in Matter*, Cambridge University Press, Cambridge, **2002**.

[32]   L. Hu, D. S. Hecht, G. Grüner, *Nano Lett.* **2004**, *4*, 2513–2517.

[33]   K. Flavin, I. Kopf, E. D. Canto, C. Navio, C. Bittencourt, S. Giordani, *J. Mater. Chem.* **2011**.

[34]   H. Kuzmany, A. Kukovecz, F. Simona, M. Holzweber, C. Kramberger, T. Pichler, *Synth. Met.* **2004**, *141*, 113.

[35]   H.-Z. Geng, K. K. Kim, K. P. So, Y. S. Lee, Y. Chang, Y. H. Lee, *J. Am. Chem. Soc.* **2007**, *129*, 7758.

[36]   J. W. Jo, J. W. Jung, J. U. Lee, W. H. Jo, *ACS Nano* **2010**, *4*, 582.

[37]   Q. Liu, T. Fujigaya, H.-M. Cheng, N. Nakashima, *J. Am. Chem. Soc.* **2010**, *132*, 16581.

[38]   Y. Maeda, K. Komoriya, K. Sode, J. Higo, T. Nakamura, M. Yamada, T. Hasegawa, T. Akasaka, T. Saito, J. Lu, S. Nagase, *Nanoscale* **2011**, *3*, 1904.

[39]   R. C. Tenent, T. M. Barnes, J. D. Bergeson, A. J. Ferguson, B. To, L. M. Gedavilas, M. J. Heben, J. L. Blackburn, *Adv. Mater.* **2009**, *21*, 3210.

[40]   D.-W. Shin, J. H. Lee, Y.-H. Kim, S. M. Yu, S.-Y. Park, J.-B. Yoo, *Nanotechnol.* **2009**, *20*, 475703.

[41]   U. D. Weglikowska, V. Skakalova, R. Graupner, S. H. Jhang, B. H. Kim, H. J. Lee, L. Ley, Y. W. Park, S. Berber, D. Tomanek, S. Roth, *J. Am. Chem. Soc.* **2005**, *127*, 5125.

[42]   A. Albert, E. P. Serjeant, *Ionisation constants of acids and bases*, John Wiley & Sons, New York, **1962**.

[43]   Braude, F. C. Nachod, *Determination of organic structures by physical methods*, Academic Press, New York, **1955**.

[44]   W. P. Jencks, J. Regenstein, *Ionisation constants of acids and bases*, CRC Press, Taylor & Francis, Boca Raton, **2010**.

[45]   G. Kortum, W. Vogel, K. Andrussow, *Dissociation constants of organic acids in aqueous solution*, Butterworths, London, **1961**.

[46]   E. P. Serjeant, B. Dempsey, *Ioinisation constants of organic acids in aqueous solution (IUPAC Chemical Data Series)*, Pergamon Press, **1979**.

[47]   Y. Yukawa, *Handbook of organic structural analysis*, W. A. Benjamin, New York, **1965**.

[48]   D. Harries, *Langmuir* **1998**, *14*, 3149.

[49]   F. Oosawa, *Biopolymers* **1968**, *6*, 1633.

[50]   Y.-K. Kwon, S. Saito, D. Tománek, *Phys. Rev. B* **1998**, *58*, R13314.

[51]   A. A. Maarouf, C. L. Kane, E. J. Mele, *Phys. Rev. B* **2000**, *61*, 11156.

[52]   H. Stahl, J. Appenzeller, R. Martel, P. Avouris, B. Lengeler, *Phys. Rev. Lett.* **2000**, *85*, 5186.

[53]   W. Zhao, C. Song, P. E. Pehrsson, *J. Am. Chem. Soc.* **2002**, *124*, 12418.

[54]   E. M. Doherty, S. De, P. E. Lyons, A. Shmeliov, P. N. Nirmalraj, V. Scardaci, J. Joimel, W. J. Blau, J. J. Boland, J. N. Coleman, *Carbon* **2009**, *47*, 2466.

3. Molecular scale engineering of transparent conducting films fabricated from hydrophilic single wall carbon nanotube dispersions containing mixed stabilizers

Preface

This section of the thesis deals with the effect of stabilizers used in the dispersion of single wall carbon nanotubes (SWNTs) on the electrical and optical properties of transparent conducting films (TCFs). We have used poly(sodium 4-styrene sulfonic acid) (PSS), poly(vinyl pyrrolidone) (PVP) and a mixture of both for this analysis. The sheet resistance and optical transmittance of the resulting TCFs were analyzed. We found that the TCFs prepared from dispersions containing a mixture of PSS and PVP provide comparatively better electrical and optical properties than TCFs prepared from dispersions containing a single stabilizer. This effect was studied further and supported with other stabilizers: lignosulfonic acid sodium salt (LSNa), poly(vinyl alcohol) (PVA), mixture of LSNa and PVA, and a mixture of LSNa and PVP. Again, we observed that dispersions containing mixtures of stabilizers lend better electrical and optical properties to the fabricated TCFs. We try to explain this effect through supramolecular forces between SWNTs and stabilizers and call this approach molecular scale engineering.

This section will be submitted as an original research article. The authors are Bibin T. Anto, Stefanie Eiden, Hans-C. Schwarz, Andreas M. Schneider and Peter Behrens. Prof. P. Behrens and Dr. S. Eiden supervised this work. Mr. H-C. Schwarz and Dr. A. M. Schneider actively participated in the discussions of progress of this work.

Molecular scale engineering of transparent conducting films fabricated from hydrophilic single wall carbon nanotube dispersions containing mixed stabilizers

Bibin T Anto[1,2], Stefanie Eiden[2], Hans-C. Schwarz[2], Andreas M. Schneider[1], Peter Behrens[1]

[1] Institut für Anorganische Chemie, Leibniz Universität Hannover, Callinstraße 9, 30167 Hannover, Germany

[2] Bayer Technology Services GmbH, Chempark, 51368 Leverkusen, Germany

Abstract

Transparent conducting films prepared from single wall carbon nanotubes are considered to be potential candidates for flexible electronics applications. The absorptive nature of carbon in SWNTs at all optical wavelengths, brings in better colour neutrality to SWNT based TCFs than ITO and conducting polymers base films. Employing large amount of molecular stabilizers and washing away with highly concentrated inorganic acids, are common practice in literatures, to enhance the overall performance of transparent conducting films. Our work described in here, reports that employing appropriate combination of molecular stabilizers in appropriate ratio can enhance the overall performance $\frac{\sigma_{d.c.}}{\sigma_{o.c.}}$ of TCFs. $\frac{\sigma_{d.c.}}{\sigma_{o.c.}}$ of SWNT TCFs can be enhanced by more than 70% by employing mixture of polystyrene sulphonic acid (PSS) and polyvinyl pyrrolidone (PVP) as stabilizers, when compared to the SWNT TCFs comprising single molecular stabilizers. We also report the possible underlying principle behind the performance of SWNT TCFs with different combinations of molecular stabilizers.

Keywords: Single wall carbon nanotubes – SWNTs – Surfactant effects – Stabilizer effects – transparent conductors

Introduction

Flexible transparent electronics[1,2] is a developing field that promises many advantages over the conventional processing techniques, which require ultra-high vacuum, high energy, and high cost. On this note it is essential to develop transparent conducting films (TCFs), which complies

with flexible back-planes (polymeric substrates, for e.g. polycarbonate, polyethylene terephthalate, polyethylene naphthalate) used in flexible electronic devices. Widely used transparent conductor, Indium Tin Oxide (ITO) is not suitable for flexible electronics applications, due to its brittle nature.[3] In addition, the availability of ITO is deteriorating in the recent years.[4] Other materials under research for the development of TCFs are transparent conducting oxides (TCOs),[5] metal nanowires,[6] conducting polymers,[7-10] conducting polymer-carbon nanotube composites,[11-13] graphene[14, 15] and single wall carbon nanotubes.[16-18] TCOs are as similar as ITO – brittle in nature, and require ultra-high vacuum for film deposition. Metal nanowires are solution processable, but very expensive compared to their counterparts. Graphene is a rather new material, and lot of research is still going on to make it robust and improve its availability. Poly(3,4-ethylenedioxy thiophene):Poly(4-styrenesulfonic acid) (PEDT:PSS) showed great potential when it was reported for the first time. However, the sheet resistance of the transparent film made out of this material drifts due to the moisture absorption nature of the sulfonic acid groups. ITO and PEDT:PSS are not colour neutral,[19] which is one of the key requirement for transparent conducting films. Single walled carbon nanotubes (SWNTs) are considered to be more suitable candidates, as they show better flexibility than ITO,[20] and better colour neutrality than both ITO and PEDT:PSS films.[19] SWNTs have further advantages such as good availability and solution processability. Its adaptability of film fabrication at room temperatures makes it more attractive as well.

Fabrication of TCFs from SWNTs involved several steps, starting from material synthesis to the final deposition of film. The key step is to produce dispersions of SWNTs with appropriate solvent and stabilizer molecules. The addition of molecular stabilizers is inevitable in the production of SWNT dispersions, as the stabilizers are needed to increase the dispersibility of SWNTs in a solvent through interfacial interactions. Many stabilizers used for the fabrication of TCFs are small molecules that are easy to remove by washing after film fabrication. Supra-molecular forces like hydrogen bonding, ionic interaction, van der Waals forces, π–π interactions are the common interactions between SWNTs and stabilizers that facilitates the dispersibility of SWNTs. The chain length of small molecules is shorter, and the amount of stabilizers required to produce SWNT dispersions is large. Polymers have longer chains which possibly entangle with SWNTs, additional to possible supra-molecular interactions, to facilitate the dispersion of SWNTs. Therefore, the amount of polymers required to disperse the SWNTs is

lower compared to small molecules. Most of the stabilizer molecules are insulative in nature that deteriorates the electrical conductivity of SWNT film. A sheet resistance of 400 $\Omega/\square$ at 79 % optical transmittance was achieved for TCFs - containing sodium dodecyl sulphate (SDS) - fabricated without any post treatment of washing or doping.[21] Better electrical and optical properties are reported for SWNT TCFs that are either fabricated from dispersions containing no stabilizers in organic solvents (e.g. 1,2-dichlorobenzene,[22] dichloroethane,[23] and chlorosulphonic acid,[24]), in combinations of inorganic acids[25], and by dry transfer technique,[26] which involve no solvent medium at all. The organic solvents are not as environmentally friendly as water. Many reports[27-32] employ the method of fabricating TCFs with large amount of stabilizers and then wash away these insulating moieties with water and inorganic acids to enhance the electrical conductivity. Washing with inorganic acids such as HNO_3, H_2SO_4, $SOCl_2$, etc. not only remove the stabilizers, but also dope the TCFs that enhance the electrical conductivity.[33] However, handling of highly corrosive chemicals on the large scale roll-to-roll coating machineries is an unsafe practice for both machinery as well as employees. Therefore, the amount of surfactant should be kept to a minimum that is required for a good thin film formation. Treating SWNTs in different oxidising acids (e.g. HNO_3, H_2SO_4, etc.) helps to improve the dispersibility of nanotubes due to the interaction between the oxidation induced hydroxyl, carboxyl, and carbonyl moieties and SWNTs.[34] Hence, the requirement of stabilizers as dispersant can be reduced to a greater extent. The treatment with oxidising acids also helps to remove metal catalysts that are used to prepare the SWNTs. There is very little literature on SWNT dispersions without the use of stabilizing agents. However, appropriate stabilizers improve the stability of dispersions and enhance the functional properties of the SWNT dispersions.

Mostly polymers and small molecules are used as stabilizers while making SWNT dispersions. Commonly used stabilizers for the fabrication of TCFs are sodium dodecyl sulphate (SDS),[35] sodium dodecyl benzene sulphonate (SDBS),[36] sodium cholate (SC),[37] triton TX-100.[38] In rare cases polystyrene sulfonic acid-sodium salt (PSS),[39] polyvinyl pyrrolidone (PVP),[40] nafion,[29] carboxymethyl cellulose (CMC),[41] polyethyleneglycol (PEG),[42] etc are mentioned. In this report, we reveal that by choosing a suitable combination of stabilizers at appropriate ratio, the electrical and optical properties of TCFs can be enhanced. We also report in detail about the possible underlying principle behind the performance of TCFs fabricated with different stabilizer molecules.

The TCFs reported in this paper, are characterized by the commonly used figure of merit $\frac{\sigma_{d.c.}}{\sigma_{o.c.}}$, which indicates the ratio of electrical $\sigma_{d.c.}$ and optical conductivities $\sigma_{o.c.}$ of the SWNT film. In general, the larger the value of $\frac{\sigma_{d.c.}}{\sigma_{o.c.}}$ the better will be the performance of TCF. $\frac{\sigma_{d.c.}}{\sigma_{o.c.}}$ can be obtained from the following equation: [43,44]

$$T_{550} = \left(1 + \frac{1}{2R_s}\sqrt{\frac{\mu_0}{\varepsilon_0}}\frac{\sigma_{o.c.}}{\sigma_{d.c.}}\right)^{-2}$$

where,

R_s is the sheet resistance of the film, μ_0 and ε_0 are the permittivity and permeability of free space respectively. T_{550} is the optical transmittance of TCFs at a wavelength of 550nm (we observed that the average value of the transmittance between 400 to 700 nm is same as the transmittance at 550nm). $\frac{\sigma_{d.c.}}{\sigma_{o.c.}}$ is the ratio of electrical-to-optical conductivity and can be obtained by curve fitting the experimental values of R_s vs. T_{550}.

Experimental

Purification of SWNTs and preparation of dispersion: poly(sodium 4-styrene sulfonate) (PSS, M_w ~ 70000), polyvinylpyrrolidone (PVP,K30, M_w ~ 52000), Lignosulfonic acid sodium salt (LSNa, M_w ~ 52000) and poly(vinyl alcohol) (PVA, M_w ~ 13000-23000) are purchased from sigma-aldrich. SWNTs, produced by arc-discharge method, were purchased from Fraunhofer IWS, Dresden. 20g of SWNTs were purified by refluxing in 200 mL HNO_3 (65%) for 2 hours, in a round bottom flask. The mixture was allowed to cool down to room temperature, and was washed with 2L of deionized (DI) water. At pH > 1 a portion of SWNTs become dispersible (IEP = 1.0, reported elsewhere[45]). The residue was collected separately; supernatant was acidified to pH < 1.0 to precipitate the suspended SWNTs and combined with the residue obtained before. During the process, SWNTs were kept in wet conditions (with minimum amount of water) as the dry SWNTs tend to agglomerate and therefore difficult to redisperse in water. Afterwards, the acid treated SWNT mixture was dialyzed against DI water until the pH of DI water becomes 7.0 in order to remove all excess ions and impurities. Finally, the purified SWNT mixture was sonicated in DI water together with stabilizers using Branson Sonifier 450 (80W, 30 min) to produce a better dispersion. The mixture was then centrifuged (3500 rpm/30 min) to

remove undispersed materials. Then the supernatant – the SWNT dispersion – was collected and used for further characterization and film fabrication. Details of optimum purification conditions reported elsewhere[45]). Different combinations of stabilizers (poly(4-styrene sulfonicacid sodium salt) (PSS), polyvinylpyrrolidone (PVP), Lignosulfonicacid sodium salt (LSNa), poly(vinyl alcohol) (PVA) were used to make a better dispersion. Purification conditions and combinations of stabilizers are given in Table 1. Typical concentration of dispersions used for testing and characterization were 0.2 to 0.3 wt% SWNT. The pH of the dispersions was kept between 3 - 3.5, in order to avoid overlapping of pH induced transformations in SWNT TCFs.[45]

Fabrication of transparent conductive films (TCFs): TCFs were fabricated on glass slides using the Meyer rod coating method (doctor blading). The films were annealed at 120 ± 10 °C for 1 min. Multilayered coatings were prepared to reach low sheet resistance values (< 500 $\Omega/\square$), typically 3 to 4 layers. All the data were repeated 2 to 3 times to confirm the reproducibility. Films were reproduced in large area (ISO A4 size) poly carbonate sheets, which were O_2 plasma treated prior to doctor blading.

Electrical and optical properties: Sheet resistance of TCFs was measured using 2 point probe method, across square area, i.e. 1 x 1 cm^2, with a probe dimension of 1cm^2. The standard error, if any, involved in the measurement of sheet resistance is uniform throughout all the measurements.

Typically, four to five measurements were taken for each data point and the average of the measurements was calculated. Standard deviation of the data points was calculated to be ≤ 7%. Optical transmittance of the TCFs was recorded using Cary 50 UV-Vis spectrometer (Varian). Thicknesses of the films were measured using Dektek 150 profilometer (Veeco Instruments). The surface morphology of transparent thin films were captured using FEI Sirion 100T scanning electron microscopy.

X-ray Photoelectron spectroscopy (XPS): Core-level and survey X-ray photoelectron spectra were acquired on a VersaProbe spectrometer (Physical Electronics) at a base pressure of less than 10^{-8} mbar using monochromatic Al Kα X-ray photons (1486.68 eV) irradiating at 45° relative to electron analyzer entrance. The photo-electrons were analyzed by a concentric hemispherical analyzer operated at constant pass energy of 29.35 eV for C1s & O1s core-level

spectra, 117.4 eV for N1s & S2p core-level spectra, and 187.5 eV for survey spectra. The photoemission angle (θ) was set at 54.7°. The X-ray gun was operated at 4.5 W with a minimum possible spot size of 20 µm. Measurement was perfomed at two different points within the scanning an area of 0.25 x 0.25 mm^2. Sample charging was avoided by using Indium substrate to provide a conductive ground; charge neutralization was not necessary. Core-level spectra were processed to give atomic stoichiometry values using Multipak 9.1 software that accounts empirical sensitivity factors taking into account photoionization cross sections, inelastic mean free paths, and the spectrometer intensity-energy response functions.

Raman spectroscopy: Raman spectra of SWNT films were recorded using Induram (Horiba Jobin-Yvon) spectrometer, coupled with confocal laser scanning microscope. Excitation wavelength used for the all the measurements is 488 nm. Films for the measurements were prepared by drop-casting corresponding SWNT dispersions on to a glass slide and annealed at 120°C/ 1min.

Results and Discussion:

SWNTs were purified by refluxing in different combinations of acids for different durations, in order to find the optimum conditions for dispersibility and performance of TCFs. Detailed information on purification is reported elsewhere.[45] Stability of SWNT dispersion can be enhanced by adding appropriate amount of stabilizer molecules during preparation. As the stabilizer molecules are insulative by nature, the amount of stabilizer should be as minimum as possible to improve the film formation. Polymeric PSS and PVP molecules are longer than usual stabilizer molecules, and has the ability to disperse carbon nanotubes at very high concentrations in water and other polar solvents.[46] PVP enhances the adhesion between the carbon nanotube films and polycarbonate or other polymeric substrates. In addition, the highest possible electrical conductivity for carbon nanotube films are also obtained with PSS as a stabilizer.[46] However, neither PSS nor PVP are widely used for the fabrication of TCFs . Here, we present the first investigations on the effect of dispersions containing PSS and PVP.

SWNTs used here are purified by refluxing in mixture of HNO_3:H_2SO_4 (3:1 v/v) for four hours. Different ratios of SWNT-to-stabilizers, 1:10 to 10:1, were tested and the optimum ratio is found to be 10:1 wt/wt with regard to the figure of merit $\frac{\sigma_{d.c.}}{\sigma_{o.c.}}$ of TCFs. This is also the lowest amount of

stabilizer necessary for the dispersion of the purified and functionalized SWNTs in water. Significant difference between TCFs prepared with PSS (SWNT$_{PSS}$) and PVP (SWNT$_{PVP}$) is observed. SWNT$_{PSS}$ films fabricated from dispersions containing SWNT and PSS show a larger $\frac{\sigma_{d.c.}}{\sigma_{o.c.}} = 2.6$ compared to $\frac{\sigma_{d.c.}}{\sigma_{o.c.}} = 1.2$ for SWNT$_{PVP}$ films (Fig 1, Table 1: S/No. 1a-b). The better performance of SWNT$_{PSS}$ TCFs can be explained by the presence of π electrons in PSS that facilitate more effective charge transfer between SWNTs. Moreover, the presence of sulphonic acid group (SO_3) in PSS, which is an electron withdrawing group, may lead to p-doping of the SWNTs. This assumption is evidenced by an upshift of 2 cm^{-1} in the tangential mode in Raman spectra. This shift can be ascribed to the depletion in the conduction band due to p-type doping (Fig 2B, $\mathcal{V}_G$ =1595 cm^{-1} for SWNT$_{PVP}$; $\mathcal{V}_G$ =1597 cm^{-1} for SWNT$_{PSS}$).[47]
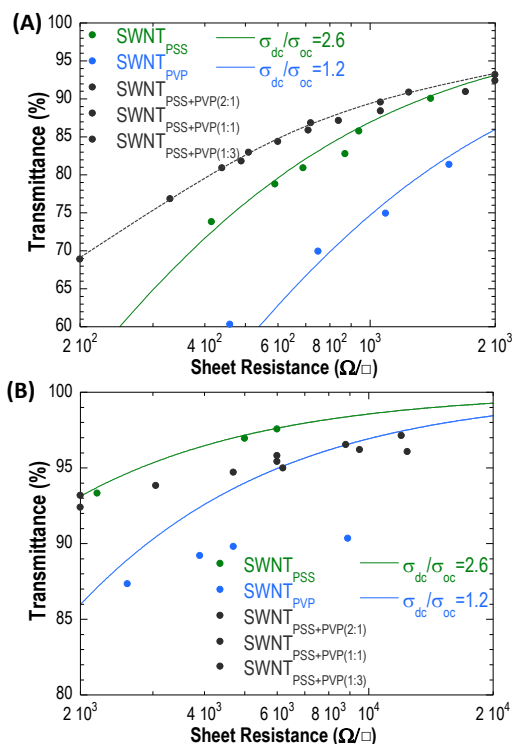
Figure 1: Electrical and optical properties of SWNT TCFs fabricated from different dispersions containing, PSS, PVP and mixture of PSS+PVP molecular stabilizers. SWNTs used here are purified by refluxing in HNO$_3$:H$_2$SO$_4$ (3:1 v/v). Data were plotted separately for clarity; (A) Shows the data for films of sheet resistances in the range of 200 to 2000Ω/□ and (B) shows the data for the films of sheet resistances in the range of 2 to 20 k Ω/□.

Table 1: Summary of properties of SWNT TCFs described in this report

S/No	Purification Conditions		Notation	Stabilizer	Ratio (wt/wt)	R_s[c] ($\Omega/\square$)	T_{550}[d] (%)	$\frac{\sigma_{d.c.}}{\sigma_{o.c.}}$
	Acid [a]	t [b]						
1a	$HNO_3:H_2SO_4$ [f]	4	$SWNT_{PSS}$	PSS	10	415	73.8	2.6
1b	$HNO_3:H_2SO_4$ [f]	4	$SWNT_{PVP}$	PVP	10	460	60.3	1.2
1c	$HNO_3:H_2SO_4$ [f]	4	$SWNT_{PSS+PVP}$ [g]	PSS PVP	10	200	68.9	4.6
2a	HNO_3	4	$SWNT_{LSNa}$	LSNa	10	260	74	4.5
2b	HNO_3	4	$SWNT_{PVA}$	PVA	10	420	81.3	4.5
2c	HNO_3	4	$SWNT_{LSNa+PVA}$ [h]	LSNa PVA	10	240	71.4	4.5
3a	HNO_3	4	$SWNT_{(PSS)}$	PSS	10	350	77.8	4.0
3b	HNO_3	4	$SWNT_{(PVP)}$	PVP	10	430	73.5	2.7
3c	HNO_3	4	$SWNT_{(PSS+PVP)}$ [i]	PSS PVP	10	215	78.2	6.7
4	HNO_3	4	$SWNT_{(LSNa+PVP)}$ [j]	LSNa PVP	10	230	79.6	6.8

[a] Acid used to reflux with SWNTs, during the process of purification. The temperature, during the reflux was maintained at 130 ± 5 °C.

[b] The duration at which, the SWNTs were refluxed at different combinations of acid listed above.

[c] Sheet resistance of transparent conducting films fabricated from respective dispersions.

[d] Optical transmittance of transparent conducting films fabricated from respective dispersions.

[e] Figure of merit of transparent TCFs calculated by incorporating the R_s and T_{550} values in the expressions described in the text.

[f] The ratio of HNO_3-to-H_2SO_4 is kept at 3:1 v/v. Concentrations of HNO_3 and H_2SO_4 used in this work are 65% and 98%, respectively, unless otherwise stated.

[g] The ratio of PSS to PVP was varied from 2:1, 1:1 and 1:3 wt/wt, while maintaining the SWNT to stabilizer ratio at 10.

[h] Ratio of LSNa to PVA was kept at 2:1 wt/wt.

[i] Ratio of PSS to PVP was kept at 2:1 wt/wt.

[j] Ratio of LSNa to PVP was kept at 2:1 wt/wt.

The performance of SWNT films can be improved by using dispersions containing mixture of PSS and PVP. Different combinations were tested with a ratio of PSS to PVP of 2:1, 1:1 and 1:3 wt/wt. TCFs prepared with these combinations of PSS & PVP led to similar results (Fig 1). The experimental data of SWNT$_{PSS+PVP}$ TCFs could not be fitted using the theoretical expression used for other TCFs with single stabilizers. Therefore, for comparison, $\frac{\sigma_{d.c.}}{\sigma_{o.c.}}$ = 4.6, is calculated from the lowest possible R_s = 200 Ω/□ and T_{550} = 69% (Table 1: S/No. 1c). Performances of SWNT$_{PSS+PVP}$ films are better by 77% better compared to the $\frac{\sigma_{d.c.}}{\sigma_{o.c.}}$ of SWNT$_{PSS}$ and SWNT$_{PVP}$ films. To understand the underlying mechanism, we first examined the optical absorption spectra of all three films. Interestingly, the van Hove singularities (vHS) become broader in the sequence SWNT$_{PVP}$ – SWNT$_{PSS}$ – SWNT$_{PSS+PVP}$ (Fig 2). Broadening and intensity difference in van Hove singularities occur due to the types of tubes,[48] effect of chirality[49] and diameter of SWNTs,[50] molecular environments, and charge screening effects. Effects of intertube coupling between SWNTs and bundles and its implications on the inter-band transitions (vHS) are also reported.[51] We attribute the broadening of vHS to molecular environments, where the inter-tube interaction between SWNTs are dominated by the spatial arrangement that arises from the molecular stabilizers. We propose that the spacing between adjacent contact-pairs of SWNT has been altered by the different stabilizers and due to their different ways of interactions with SWNTs. The van Hove singularities (S_{22} and M_{11}, second order and first order inter-band transitions in semiconducting and metallic SWNTs, respectively) for SWNT$_{PSS}$ films are broader than that of SWNT$_{PVP}$ films.
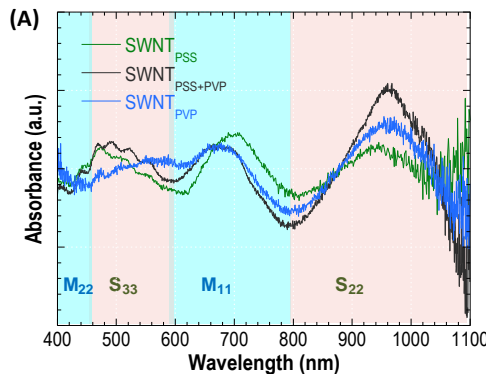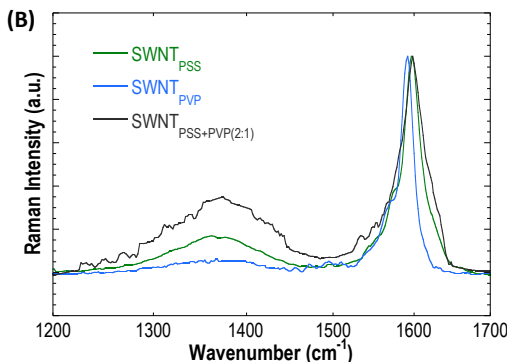
Figure 2: (A) Optical absorption spectra of SWNT TCFs fabricated from different dispersions containing different composition of stabilizers. (B) Raman spectra of SWNTs TCFs containing different compositions of stabilizers. Excitation wavelength used for the measurement is 488 nm.

The possible interactions for PSS with SWNTs are through hydrogen bonding, van der Waals forces, ionic interactions and – most importantly – from π-π interactions. In contrast, PVP can only interact with SWNTs through hydrogen bonding and van der Waals forces. Hydrogen bonding and ionic interactions arise from the functional moieties present in functionalized SWNTs and functional moieties present in molecular stabilizers. Thus, PSS has the advantage of interacting more with SWNTs through π electrons. Therefore, PVP is expected to wrap around[51] the SWNTs resulting in more isolated particles compared to the scenario, where PSS orients along[52] SWNTs and bundles (Fig 3A). This was evidenced by the scanning electron micrographs, where we observe the relatively oriented spaghetti-like morphology in SWNT$_{PSS}$ TCFs, whereas a more spaghetti-like morphology for SWNT$_{PVP}$ TCFs (Fig 3B). Inter-tube interactions are minimized when PVP is wrapped around the SWNTs, compared to SWNTs with PSS as stabilizer. Hence a relative broadening of van Hove singularities is observed in SWNT$_{PSS}$ TCFs. In comparison, TCFs fabricated from dispersions containing mixture of PSS and PVP shows narrow van Hove singularities (S_{22} and M_{11}). A possible explanation is that, due to strong interaction between PSS and SWNTs than PVP, PSS assembles next to SWNTs and the PVP act as spacer between SWNT-PSS stack arrangements (see Fig. 3 and schematic diagram in Fig 4). As a result of increases in spacing between adjacent SWNTs, the inter-tube interactions are further minimized. Hence the coupling between adjacent tubes becomes weaker, and the van Hove singularities become narrower as observed in the case of

SWNT$_{PSS+PVP}$ TCFs. Increased spacing between adjacent SWNTs and bundle is also supported by scanning electron micrograph of SWNT$_{PSS+PVP}$ TCFs, where a relatively larger gap is observed compared to SWNT$_{PSS}$ and SWNT$_{PVP}$ films (Fig3C). As the spacing between adjacent contact-pairs of SWNTs increased by employing appropriate mixtures of stabilizers, the amount of photons transmitted through the TCF also increases for a given sheet resistance. That could be a possible reason for better performance of SWNT$_{PSS+PVP}$ TCFs compared to the other films.
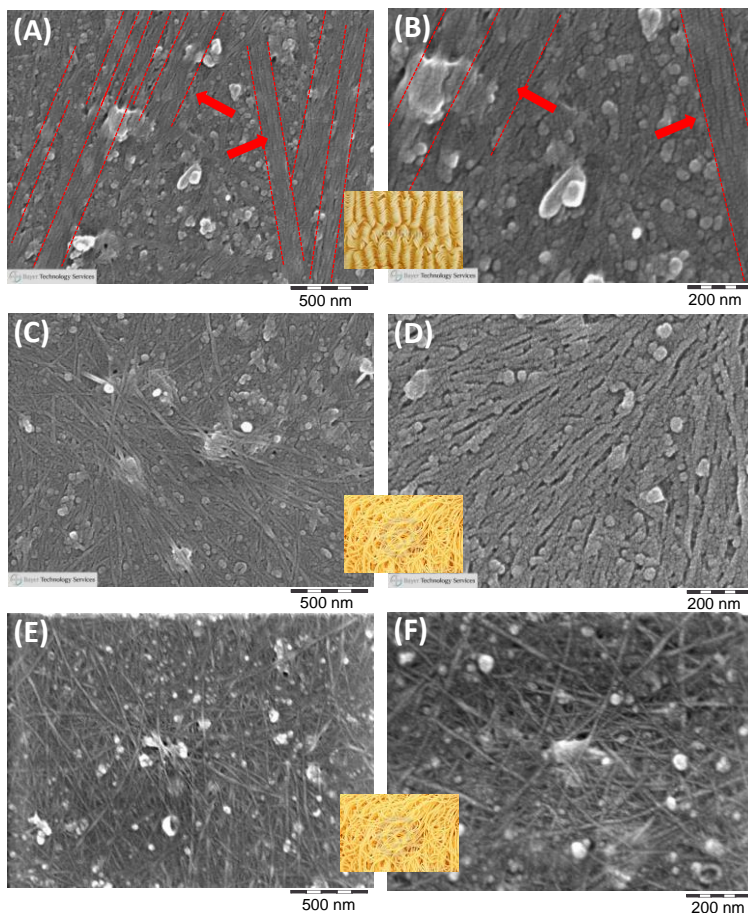
Figure 3: Scanning electron micrographs of SWNT TCFs fabricated from dispersion containing different compositions of molecular stabilizer. (A - B) TCF with PSS as stabilizer (C-D) TCF with PVP as stabilizer; red arrow mark in indicated the stacking orientation of SWNTs & bundles. (E-F) TCF with combination of PSS and PVP as stabilizer; ratio of PSS to PVP is 2:1 wt/wt. Inset images shows the comparative representation of spatial arrangements in spaghetti noodles.

Core-level x-ray photoelectron spectra (XPS) further supports the assumption that PVP acts as a spacer between the SWNT-PSS stack arrangements. The stoichiometry composition was detected and analyzed region-specifically at two different points on the TCF films. A minimum possible x-ray spot size of 20µm was used, and scanned across an area of 250 µm², in order to avoid overlapping of compositions of two different points of analysis in the films.
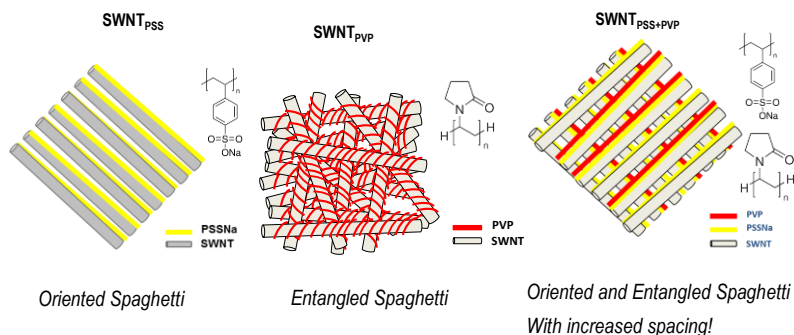

Figure 4: Schematic representation of hypothesis of molecular scale spatial orientation in SWNT transparent conducting films.

Table 2: Stoichiometric compositions obtained from x-ray photoelectron spectra of SWNT TCFs

S/No	Points	C1s	N1s	O1s	S2p	Na1s	Remarks
SWNT$_{PSS}$ films [a]							
1a	1	71.8	3.15	19.5	0.7	4.9	Uniform Distribution
1b	2	72	3.4	19.2	0.7	4.7	Uniform Distribution
SWNT$_{PVP}$ films [a]							
2a	1	68.7	2.7	22.12	-	6.5	Uniform Distribution
2b	2	67.9	2.4	23.4	-	6.3	Uniform Distribution
SWNT$_{PSS+PVP}$ films [a]							
3a	1	71.1	4.95	15.9	0	8.13	PVP rich
3b	2	68.4	3	20.7	0.4	7.6	PSS rich

[a]. SWNTs used here, were purified by refluxing it in mixture of HNO$_3$:H$_2$SO$_4$ (3:1 v/v) for 4 hours.
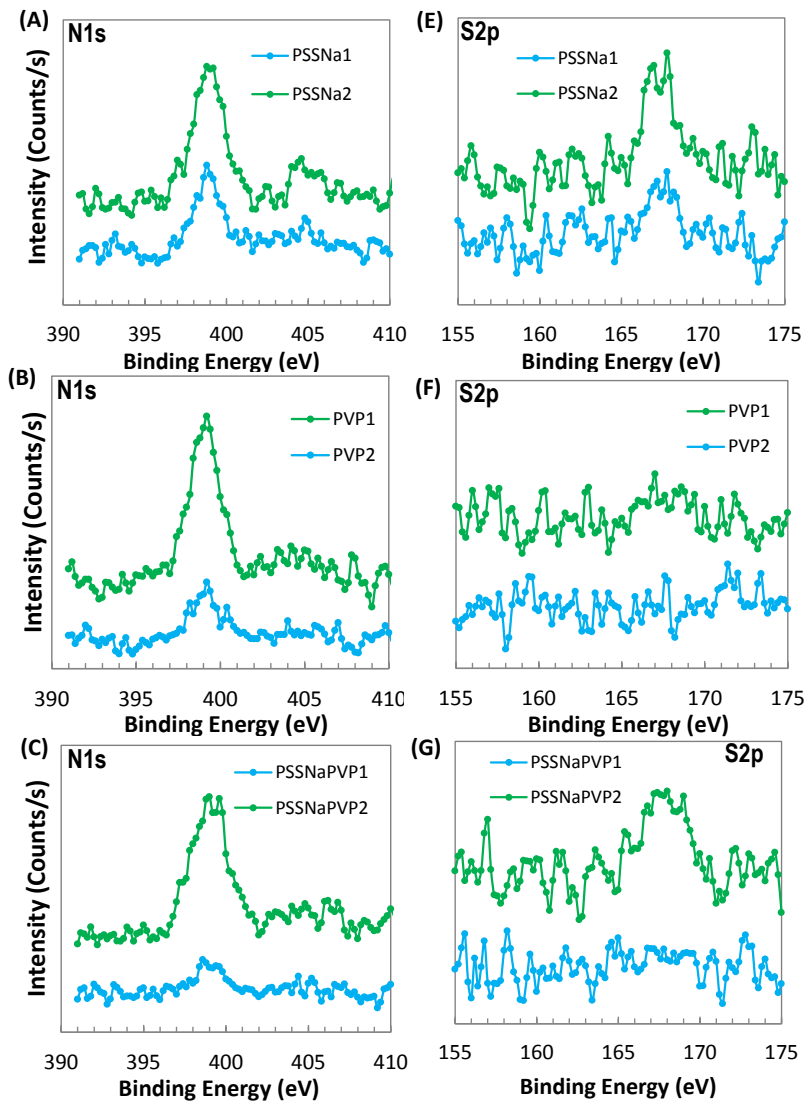
Figure 5: Core-level x-ray photoelectron spectra of SWNT TCFs containing different compositions of molecular stabilizers. (A – C) Core-level N1s spectra of SWNT$_{PSS}$, SWNT$_{PVP}$ and SWNT$_{PSS+PVP}$ films, respectively. (D – F) Core-level S2p spectra of SWNT$_{PSS}$, SWNT $_{PVP}$ and SWNT$_{PSS+PVP}$ films, respectively.

Stoichiometry compositions at two different points on a SWNT$_{PSS+PVP}$ TCF are measured and analyzed. (Fig 5C, F; Table 2, S/No. 3). According to the S2p core-level spectra, the absence of sulphur in region 1 suggests that the sulphur containing PSS polymer chains does not exists in this region (Fig 5F). According to the N1s core-level spectra, the amount of nitrogen in region 2 is relatively less compared to region 1, also suggests that the region 2 is PSS rich (Fig 5C). Moreover the amount of oxygen detected from O1s core-level spectra in PVP-rich region 1 (15.9 at-%) is relatively less compared to 20.7 at-% detected in PSS-rich region 2. The higher amount of oxygen could be attributed to the SO$_3^-$ groups in PSS polymer chains (Table 2, S/No. 3). Therefore, the stoichiometry of two different points observed in SWNT$_{PSS+PVP}$ films suggests that there are separate regions that are either rich in PSS or rich in PVP. No significant difference in the amount of oxygen has been detected from different regions of SWNT$_{PSS}$ and SWNT$_{PVP}$ TCFs. Stoichiometry compositions of two different points of analysis of SWNT$_{PSS}$ and SWNT$_{PVP}$ films are similar (Fig 5A, B, D and E; Table 2 S/No 1-2). Since there is no significant difference on the compositions of the two analyzed points, we assume that the SWNTs as well as the stabilizing agents PSS and PVP are uniformly distributed across the analyzed section of the SWNT$_{PSS}$ and SWNT$_{PVP}$ films, respectively. Though, the relatively larger x-ray spot size (20 μm) is limited to determine the sub-μm spatial arrangements between SWNTs, PSS and PVP polymer chains, the regio-specific difference in stoichiometry in SWNT$_{PSS+PVP}$ TCFs can be correlated to the molecular-scale spatial non-uniformity. Thus, the XPS results are used as a support to our hypothesis that PVP acts as a spacer between SWNT-PSS stack orientation, which was drawn from optical absorption spectroscopy and scanning electron microscopy.
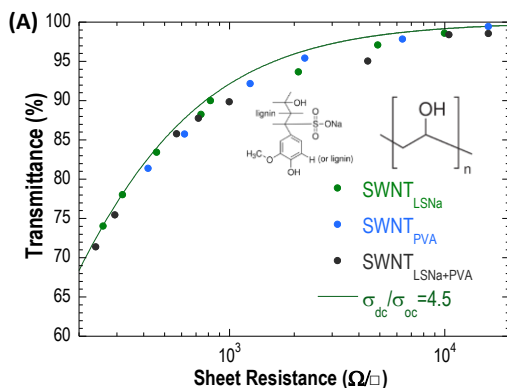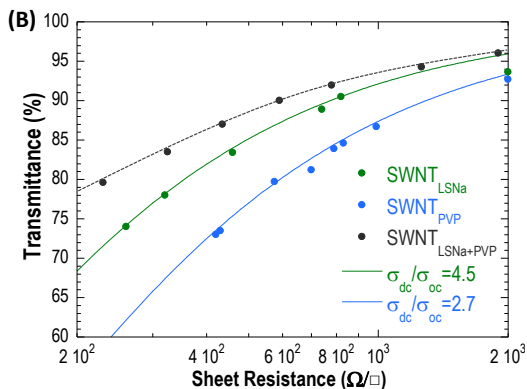
Figure 6: Electrical and optical properties of SWNT TCFs containing different combinations of molecular stabilizers. SWNTs used here are purified by refluxing in HNO$_3$. (A) Sheet resistance vs. optical transmittance of SWNT$_{(LSNa)}$, SWNT$_{(PVA)}$ and SWNT$_{(LSNa+PVA)}$ films. (B) Sheet resistance vs. optical transmittance of SWNT$_{(LSNa)}$, SWNT$_{(PVP)}$ and SWNT$_{(LSNa+PVP)}$ films.

To investigate the feasibility of using other stabilizing agents, lignosulphonic acid sodium salt (LSNa) was used in combination with polyvinyl alcohol (PVA). The SWNTs used were purified by refluxing in nitric acid for four hours. The ratio between LSNa and PVA is kept at 2:1 wt/wt. The $\frac{\sigma_{d.c.}}{\sigma_{o.c.}}$ of SWNT$_{LSNa}$, SWNT$_{PVA}$ and SWNT$_{LSNa+PVA}$ remain unaltered at 4.5. Here again, LSNa interacts with SWNTs through hydrogen bonding, van der Waals forces, ionic interactions and most importantly through $\pi-\pi$ interactions. PVA interacts in a similar way as that of PVP with SWNTs, i.e. through hydrogen bonding and van der Waals forces. Therefore, it is assumed that the PVA polymer chains wrap around the SWNTs and the LSNa polymer chains orient along the SWNTs. LSNa monomers are bulkier than PSS and PVA monomers are less bulky than PVP, hence the relatively less bulky PVA is squeezed in between SWNT-LSNa stack arrangement. PVA is not bulky enough to increase the spacing beyond the limit of LSNa, therefore the spatial manipulation does not occur here. Therefore, The performance of TCFs fabricated from dispersions containing both LSNa and PVA is not different from TCFs fabricated from separate SWNT dispersions with LSNa and PVP individually (Fig 6A). Relatively higher $\frac{\sigma_{d.c.}}{\sigma_{o.c.}}$ for TCFs fabricated from dispersions of SWNTs purified by HNO$_3$ for four hours, compared to HNO$_3$:H$_2$SO$_4$ (3:1 v/v) for four hours are attributed to oxidation and effect of p-doping, which is described elsewhere. LSNa and PVP were used in combination to see the effect of molecular-scale spatial manipulation; the ratio between LSNa and PVP was kept at 2:1. The SWNTs used were purified by refluxing in nitric acid for four hours.
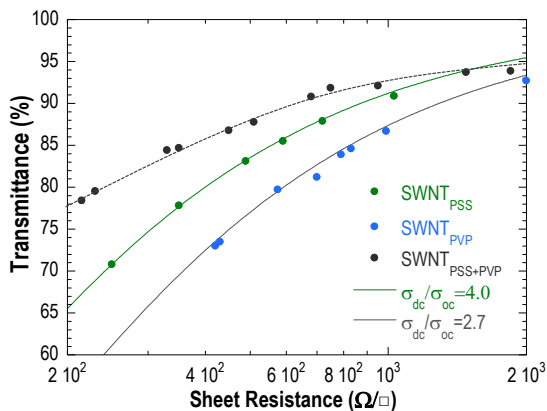
Figure 7: Sheet resistance vs. optical transmittance of SWNT$_{(PSS)}$, SWNT$_{(PVP)}$ and SWNT$_{(PSS+PVP)}$ TCFs. SWNT used here are purified by refluxing in HNO$_3$.

The SWNT$_{(LSNa+PVP)}$ TCFs does not follow the theoretical expression that was used to fit the experimental data of SWNT$_{(LSNa)}$ and SWNT$_{(PVP)}$ TCFs (Fig 6B). The SWNT$_{(LSNa+PVP)}$ film has better performance compared to SWNT$_{(LSNa)}$ and SWNT$_{(PVP)}$ films(Fig 6B; Table 1, S/No. 2a, 3b & 4). The maximum $\frac{\sigma_{d.c.}}{\sigma_{o.c.}}$ of 6.8 obtained for SWNT$_{(LSNa+PVP)}$TCFs is relatively higher than the $\frac{\sigma_{d.c.}}{\sigma_{o.c.}}$ of SWNT$_{(LSNa)}$ and SWNT$_{(PVP)}$ TCFs, 4.5 and 2.7 respectively. The results of combination of LSNa and PVP as stabilizer in SWNT TCFs, reiterates the hypothesis of molecular scale spatial manipulation effect. Thus, choosing right combinations of stabilizers at appropriate ratio could help to improve the performance of TCFs. To test the repeatability of the principle, we have conducted the experiment with PSS and PVP on SWNTs purified by refluxing in nitric acid for four hours. Similar trend that of SWNT$_{PSS + PVP}$ films, were observed for SWNT$_{(PSS+PVP)}$ films (Fig 7). The maximum $\frac{\sigma_{d.c.}}{\sigma_{o.c.}}$ of 6.7 was observed for SWNT$_{(PSS+PVP)}$ films compared to 4 and 2.7 for SWNT$_{(PSS)}$ and SWNT$_{(PVP)}$ films respectively (Table1, S/No. 3). Additional advantage of using the combinations of PSS and PVP in SWNT dispersions helps to improve the wettability on polycarbonate sheets. The results of SWNT$_{PSS+PVP}$ films were reproduced on PC substrate without any surface modification, which was not possible for SWNT$_{PSS}$ and SWNT$_{PVP}$ films without additional surface treatments.

Conclusion

We have demonstrated that by templating the appropriate combination of stabilizers at appropriate ratio will increase the overall performance of transparent conducting films fabricated from SWNT dispersions. The SWNT TCFs prepared using combination of PSS and PVP exhibits better electrical and optical properties compared to TCFs prepared either with PSS or PVP. The underlying principle behind the effect of combination of stabilizers on the performance of the TCFs is analyzed. Manipulation of spatial increment between the adjacent contact-pairs of SWNTs is the possible mechanism. This occurs when a stabilizer with less affinity towards SWNTs acts as a spacer between SWNT and other stabilizer. Therefore the increment in spacing between the SWNTs eventually increases the transmission of photons. The effect is further tested with other stabilizers LSNa and PVA to check the universality of principle. These new insights open up further possibilities enhancing the performance of transparent conducting films and technological developments.

References

[1]   D. S. Hecht, L. Hu, G. Irvin, *Adv. Mater.* **2011**, *23*, 1482–1513.

[2]   W. S. Wong, A. Salleo, in *Electronic Materials: Science & Technology* (Ed.: H. L. Tuller), Springer, New York, **2009**, p. 462.

[3]   Y. Chen, B. Cotterell, W. Wang, *Eng. Fract. Mech.* **2002**, *69*, 597.

[4]   A. Chipman, *Nature* **2007**, *449*, 131.

[5]   E. Fortunato, D. Ginley, H. Hosono, D. C. Paine, *MRS Bull.* **2009**, *32*, 242.

[6]   L. Hu, H. Wu, Y. Cui, *MRS Bull.* **2011**, *36*, 760.

[7]   T. Aernouts, P. Vanlaeke, W. Geens, J. Poortmans, P. Heremans, S. Borghs, R. Mertens, R. Andriessen, L. Leenders, *Thin Solid Films* **2004**, *451-452*, 22.

[8]   G. Gustafsson, Y. Cao, G. M. Treacy, F. Klavetter, N. Colaneri, A. J. Heeger, *Nature* **1992**, *357*, 477.

[9]   J. Huang, X. Wang, A. J. deMello, J. C. deMello, D. D. C. Bradley, *J. Mater. Chem.* **2007**, *17*, 3551.

[10]   F. Jonas, A. Karbach, B. Muys, E. van Thillo, R. Wehrmann, A. Elschner, R. Dujadin, *Vol. EP0686662 A2* (Ed.: E. P. Office), Bayer A.G., Germany, **1995**, pp. 1.

[11]   N. F. Anglada, M. Kaempgen, V. Skákalová, U. D-Weglikowska, S. Roth, *Diamond Relat. Mater.* **2004**, *13*, 1256.

[12]   E. Kymakis, G. Klapsis, E. Koudoumas, E. Stratakis, N. Kornilios, N. Vidakis, Y. Franghiadakis, *EPJ Appl. Phys.* **2007**, *36*, 257.

[13]   J. B. Yoo, J. S. Moon, J. H. Park, T. Y. Lee, Y. W. Kim, C. Y. Park, J. M. Kim, K. W. Jin, *Diamond Relat. Mater.* **2005**, *14*, 1882–1887.

[14]   J. Song, F.-Z. Kam, R.-Q. Png, J.-M. Zhou, G.-K. Lim, P. K. H. Ho, L.-L. Chua, *Nat. Nanotechnol.* **2013**, *8*, 356.

[15]   J. K. Wassei, R. B. Kaner, *Mater. today* **2010**, *13*, 52.

[16]   Q. Cao, J. A. Rogers, *Adv. Mater.* **2009**, *21*, 29.

[17]   G. Gruner, *J. Mater. Chem.* **2006**, *16*, 3533.

[18]   L. Hu, D. S. Hecht, G. Grüner, *Chem. Rev.* **2010**, *110*, 5790.

[19]   C. M. Trottier, P. Glatkowski, P. Wallis, J. Luo, *J. Soc. Info. Disp.* **2005**, *13*, 759.

[20]   N. Saran, K. Parikh, D.-S. Suh, M. Munoz, H. Kolla, S. K. Manohar, *J. Am. Chem. Soc.* **2004**, *126*, 4462.

[21]   S. Sorel, U. Khan, J. N. Coleman, *Appl. Phys. Lett.* **2012**, *101*, 103106.

[22]   N. Kishi, I. Miwa, T. Okazaki, T. Saito, T. Mizutani, H. Tsuchiya, T. Soga, T. Jimbo, *Appl. Phys. Lett.* **2012**, *100*, 063121.

[23]   Y. I. Song, C. M. Yang, D. Y. Kim, H. Kanoh, K. Kaneko, *J. Coll. Interf. Sci.* **2008**, *318*, 365.

[24]   A. Saha, S. Ghosh, R. B. Weisman, A. A. Marti, *ACS Nano* **2012**, *6*, 5727.

[25]   V. C. Tung, L.-M. Chen, M. J. Allen, J. K. Wassei, K. Nelson, R. B. Kaner, Y. Yang, *Nano Lett.* **2009**, *9*, 1949.

[26]   W. Ma, L. Song, R. Yang, T. Zhang, Y. Zhao, L. Sun, Y. Ren, D. Liu, L. Liu, J. Shen, Z. Zhang, Y. Xiang, W. Zhou, S. Xie, *Nano Lett.* **2007**, *7*, 2307.

[27]   D. Dan, G. C. Irvin, M. Pasquali, *ACS Nano* **2009**, *3*, 835 – 843.

[28]   H.-Z. Geng, K. K. Kim, K. P. So, Y. S. Lee, Y. Chang, Y. H. Lee, *J. Am. Chem. Soc.* **2007**, *129*, 7758.

[29]   H.-Z. Geng, K. K. Kim, C. Song, N. T. Xuyen, S. M. Kim, K. A. Park, D. S. Lee, K. H. An, Y. S. Lee, Y. Chang, Y. J. Lee, J. Y. Choi, A. Benayad, Y. H. Lee, *J. Mater. Chem.* **2008**, *18*, 1261–1266.

[30]   J. T. Han, J. S. Kim, H. D. Jeong, H. J. Jeong, S. Y. Jeong, G.-W. Lee, *ACS Nano* **2010**, *4*, 4551.

[31]   R. Jackson, B. Domercq, R. Jain, B. Kippelen, S. Graham, *Adv. Funct. Mater.* **2008**, *18*, 2548.

[32]   K. K. Kim, S.-M. Yoon, H. K. Park, H.-J. Shin, S. M. Kim, J. J. Bae, Y. Cui, J. M. Kim, J.-Y. Choi, Y. H. Lee, *New J. Chem.* **2010**, *34*, 2183.

[33]   D.-W. Shin, J. H. Lee, Y.-H. Kim, S. M. Yu, S.-Y. Park, J.-B. Yoo, *Nanotechnol.* **2009**, *20*, 475703.

[34]   H. Kuzmany, A. Kukovecz, F. Simona, M. Holzweber, C. Kramberger, T. Pichler, *Synth. Met.* **2004**, *141*, 113.

[35]   T. M. Barnes, X. Wu, J. Zhou, A. Duda, J. van de Lagemaat, T. J. Coutts, C. L. Weeks, D. A. Britz, P. Glatkowski, *Appl. Phys. Lett.* **2007**, *90*, 243503.

[36]   H. Tantang, J. Y. Ong, C. L. Loh, X. Dong, P. Chen, Y. Chen, X. Hua, L. Tana, L.-J. Lia, *Carbon* **2009**, *47*, 1867.

[37]   Y. T. Park, A. Y. Ham, J. C. Grunlan, *J. Mater. Chem.* **2011**, *21*, 363.

[38]   M. H. A. Ng, L. T. Hartadi, H. Tan, C. H. P. Poa, *Nanotechnol.* **2008**, *19*, 205703.

[39]   J.-B. Sim, H.-H. Yang, M.-J. Lee, J.-B. Yoon, S.-M. Choi, *Appl. Phys. A* **2012**, *108*, 305.

[40]   S.-H. Jo, Y.-K. Lee, J.-W. Yang, W.-G. Jung, J.-Y. Kim, *Synth. Met.* **2012**, *162*, 1279.

[41]   K. S. Mistry, B. A. Larsen, J. D. Bergeson, T. M. Barnes, G. Teeter, C. Engtrakul, J. L. Blackburn, *ACS Nano* **2011**, *5*, 3714.

[42]   J. W. Jo, J. W. Jung, J. U. Lee, W. H. Jo, *ACS Nano* **2010**, *4*, 582.

[43]   M. Dressel, G. Grüner, *Electrodynamics of Solids: Optical Properties of Electrons in Matter*, Cambridge University Press, Cambridge, **2002**.

[44]   L. Hu, D. S. Hecht, G. Grüner, *Nano Lett.* **2004**, *4*, 2513–2517.

[45]   B. T. Anto, S. Eiden, H.-C. Schwarz, A. M. Schneider, P. Behrens, *Manuscript in prep.* **2013**.

[46]   S. Eiden, D. Duff, S. Stein, N. Wetzold, *Chemie Ing. Technik* **2012**, *84*, 252.

[47]   M. S. Dresselhaus, G. Dresselhaus, R. Saito, A. Jorio, *Physics Reports* **2005**, *409*, 47.

[48]   M. E. Itkis, S. Niyogi, M. E. Meng, M. A. Hamon, H. Hu, R. C. Haddon, *Nano Lett.* **2002**, *2*, 155.

[49]   S. Ohmori, T. Saito, M. Tange, B. Shukla, T. Okazaki, M. Yumura, S. Iijima, *J. Phys. Chem. C* **2010**, *114*, 10077.

[50]   A. A. Green, M. C. Hersam, *Nano Lett.* **2008**, *8*, 1417.

[51]   V. V. Didenko, V. C. Moore, D. S. Baskin, R. E. Smalley, *Nano Lett.* **2005**, *5*, 1563.

[52]   G. Guan, Z. Yang, L. Qiu, X. Sun, Z. Zhang, J. Rena, H. Peng, *J. Mater. Chem. A* **2013**, *1*, 13268.

4. Effect of moisture and moisture absorption induced de-doping of transparent conductive single wall carbon nanotube films

Preface

This section of the thesis deals with the effect of doping of transparent conducting films (TCFs) prepared from single wall carbon nanotube (SWNT) dispersions. From the previous two sections, we have understood that the intrinsic electrical properties of SWNTs are not sufficient for commercial applications. Therefore, it is essential to use external dopants to enhance the electrical properties of SWNT TCFs in order to use these films in applications such as light emitting displays, solar panels and touch panels. Following a suggestion from the literature, we have used graphene oxide as the dopant to analyze the effect of doping. The sheet resistance of SWNT TCFs coated with graphene oxide was improved, which is attributed to *p*-doping. We have also analyzed the stability of the doping effect at ambient conditions, under elevated temperatures, as well as under inert gas conditions. We have found that the doped SWNT TCFs are stable at inert conditions, which suggests that these materials can be used in commercial applications with proper encapsulation.

This section will be submitted as an original research article. The authors are Bibin T. Anto, Hans-C. Schwarz, Stefanie Eiden, Andreas M. Schneider and Peter Behrens. Prof. P. Behrens and Dr. S. Eiden provided the general advice on the direction of this work. Mr. H-C. Schwarz forwarded the idea to apply graphene oxide doping for the improvement of the electrical conductivity. He developed the method to apply the graphene oxide coating and he prepared the graphene oxide dispersions used in this work. Dr. A. M. Schneider actively participated in the discussions of the progress of this work.

Effect of moisture and moisture absorption induced dedoping of transparent conductive single wall carbon nanotube films

Bibin T Anto[1,2][#], Hans-C. Schwarz[2][#], Stefanie Eiden[1], Andreas M. Schneider[1], Peter Behrens[1]

[1] Institut für Anorganische Chemie, Leibniz Universität Hannover, Callinstraße 9, 30167 Hannover, Germany

[2] Bayer Technology Services GmbH, Chempark, 51368 Leverkusen, Germany

[#] These two authors equally contributed to this work.

Abstract

Transparent conducting films (TCFs) prepared from single wall carbon nanotubes (SWNTs) are considered to be potential candidates for next generation flexible electronics applications. The absorptive nature of carbon at all optical wavelengths provides better colour neutrality to SWNT based TCFs compared to indium tin oxide (ITO) and conducting polymers based films. Chemical doping of SWNT transparent conducting films is necessary as the pristine films have below par electrical and optical properties with regards to several applications. We report here that employing graphene oxide as a chemical dopant improves the electrical and optical properties of TCFs; overall 60 % increase in performance of TCFs compared to un-doped TCFs. We also report in detail about the stability of SWNT TCFs under ambient, inert and at elevated temperature. The stability of TCFs can only be maintained if proper encapsulation is provided. The possible underlying mechanism on "moisture" and "moisture induced de-doping" of TCFs has been reported in detail.

Keywords: Single wall carbon nanotubes – transparent conductors – doping – graphene oxide – stability

Introduction

Transparent conducting films are the integral part of electronic displays, touch panels and devices. Indium tin oxide (ITO) is the commonly used material as transparent conducting electrodes in the commercially available devices today. However, the brittle nature of ITO disembarked its possibility of usage in flexible electronic devices.[1] The scarcity of Indium in the recent years lead materials research towards the alternate TCFs.[2] Other materials under research for the development of TCFs are: transparent conducting oxides (TCOs),[3] metal

nanowires,[4] conducting polymers,[5-8] conducting polymer-carbon nanotube composites,[9-11] graphene[12, 13] and single wall carbon nanotubes.[14-16] TCOs are also brittle in nature similar to ITO, which requires ultra-high vacuum for film deposition. Though, metal nanowires are solution , the expensive nature of this material its possibility in flexible TCFs applications. Single walled carbon nanotubes (SWNTs) are considered to be more suitable candidates [17, 18] due to their higher degree of flexibility compared to ITO,[19] better colour neutrality compared to both ITO and (poly(3,4-ethylenedioxythiophene):poly(4-styrenesulphonic acid))PEDT:PSS films.[20] ITO films show a tolerable yellow haze whereas the PEDT:PSS films come with blue tint. SWNTs have other advantages such as availability in abundance, good refractive index match, solution processability, printability that avoids etching with corrosive chemicals, and processability at low temperatures that are compatible with polymer substrates. The minimum possible sheet resistance at a given optical transmittance of un-doped SWNT TCFs is below the functional requirement for flexible electronics applications.[21] Therefore a post-treatment process of chemical doping on these films is necessary to enhance the electrical properties. Several inorganic materials such as HCl,[22] HNO_3,[23] H_2SO_4,[24] several mixtures $HNO_3:H_2SO_4$,[24] $SOCl_2$,[25] Oleum,[26] HNO_3 vapour,[27] $SOCl_2$ vapour,[28] NO_2 gas,[29] camphorsulfonic acid,[30, 31] are used as chemical dopants to enhance the electrical properties of SWNT TCFs. Kim et al reported a sheet resistance of 170 $\Omega/\square$ at an optical transmittance of 93.5% for SWNT wet coated films doped with HNO_3 for 30 minutes.[23] Nasibulin et al reported a sheet resistance of 84 $\Omega/\square$ at an optical transmittance of 90% for SWNT TCFs prepared by dry transfer technique and then doped by NO_2 gas.[29] Most of the dopants reported in the literature are electron withdrawing by nature, employing p-type doping through depletion of conduction band.[32] n-type doping is also possible on SWNT transparent conducting films. Mistry et al reported a sheet resistance of 70 $\Omega/\square$ at an optical transmittance of 75% for SWNT TCFs doped with n-type dopant, hydrazine (N_2H_2).[33] The sheet resistance of inorganic acid doped SWNT TCFs are not stable at ambient conditions, other dopants such as conducting polymers,[34, 35] ultraviolet radiation – ozone (UV-O_3)[36] graphene oxide (GO),[32, 37] triethyloxonium hexachloroantimonate,[38] hydrogentetrachloroaurate-trihydrate,[39] tetrafluorotetracyano-p-quinodimethane (F4TCNQ),[40] bis(tetrafluoromethanesulfonyl)imide (TFSI),[37] m-cresol,[30, 31] tetraethyl orthosilicate (TEOS)[41] and potassium (K) or bromine (Br) or Iodine (I)[42, 43] have been investigated. Most of the doping materials used are labile and ionic in nature, which could cause the problem of electromigration[44] and also affect other active layers in a device. Kim et al reported a sheet resistance of 40 $\Omega/\square$ at a transmittance of 84% for SWNT TCFs doped with

TFSI, which involves several post-fabrication processing steps including repeated cycles of washing and drying for hours before doping.[37]

The TCFs reported in this paper are characterized by a figure of merit $\frac{\sigma_{d.c.}}{\sigma_{o.c.}}$, where $\sigma_{d.c.}$ and $\sigma_{o.c.}$ are the electrical and optical conductivities of SWNT films, respectively, which can be obtained from the following equation: [45, 46]

$$T_{550} = \left(1 + \frac{1}{2R_s} \sqrt{\frac{\mu_0}{\varepsilon_0}} \frac{\sigma_{o.c.}}{\sigma_{d.c.}} \right)^{-2}$$

where,

T_{550} is the optical transmittance of TCFs at a wavelength of 550 nm (we observed that the average value of the transmittance between 400 to 700 nm is same as the transmittance at 550 nm), R_s is the sheet resistance of the film, μ_0 and ε_0 are the permittivity and permeability of free space, respectively. $\frac{\sigma_{d.c.}}{\sigma_{o.c.}}$ is the ratio of electrical-to-optical conductivity and can be obtained by curve fitting the experimental values of R_s vs. T_{550}. In general, the larger the value of $\frac{\sigma_{d.c.}}{\sigma_{o.c.}}$ the better will be the performance of the TCF.

$\frac{\sigma_{d.c.}}{\sigma_{o.c.}}$ is found to be in a wider range, starting from close to zero up to values larger than 50, as reported in literature for SWNT TCFs. The differences are attributed to various parameters of SWNTs, e.g. chirality and the electronic properties (semiconducting or metallic tubes, or the mixture of both) and variations in purification and processing methods applied in the fabrication of TCFs. Han et al reported a $\frac{\sigma_{d.c.}}{\sigma_{o.c.}}$ of 20.5 for SWNT TCFs doped with graphene oxide (GO); the SWNT films were prepared from dispersion containing copious amount of surfactant (1% sodium dodecyl benzene sulphonate, SDBS), and were repeatedly washed to remove the surfactants.[32] Graphene oxide is a p-type dopant, electron withdrawing in nature due to the presence of oxygen containing moieties. It also has an additional advantage, that the ability to support charge transport through the available sp2 hybridized carbon atoms. Moreover, handling

of GO is much simpler than handling highly corrosive inorganic materials that are detrimental to environment and machinery equipment.

In order to use SWNT TCFs in flexible electronics applications they are expected to have a stable sheet resistance and optical transmittance. Few reports highlight the stability of SWNT TCFs chemically doped by HNO_3,[47, 48] $SOCl_2$,[48] N_2H_2[33] and Triethyloxonium hexachloroantimonate[38]. These doped SWNT TCFs are not stable under the circumstances reported therein, e.g. N_2H_2 doped films are not stable under inert conditions.[33] Here, we reveal that the stability of GO doped SWNT TCFs can be maintained under inert conditions. We also report in detail about the possible doping and "moisture induced de-doping" mechanism of doped SWNT TCFs. The "moisture induced de-doping" refers to the increase in sheet resistance of films due to the absorption of moisture through functional moieties, which suppress the effect of doping.

Experimental

Purification of SWNTs and preparation of dispersion: poly(sodium 4-styrene sulfonate) (PSS, $M_w \approx 70000$), is purchased from sigma-aldrich. SWNTs, produced by arc-discharge method, are purchased from Fraunhofer IWS, Dresden. 20g of SWNTs were purified by refluxing in 200 mL HNO_3 (65%) for 2 hours, in a round bottom flask. The mixture was allowed to cool down to room temperature, and was washed with 2 L of deionized (DI) water. At pH > 1 a portion of SWNTs become dispersible (IEP = 1.0)[49]. The residue was collected separately. The supernatant was acidified to pH < 1.0 to precipitate the suspended SWNTs and combined with the residue obtained before. During the process, SWNTs were kept in wet conditions (with minimum amount of water) as the dry SWNTs tend to agglomerate and therefore are difficult to redisperse in water. Afterwards, the acid treated SWNT mixture was dialyzed against DI water until the pH of DI water becomes 7.0 in order to remove all excess ions and impurities. Finally, the purified SWNT mixture was sonicated in DI water together with stabilizers using a Branson Sonifier 450 (80W, 30 min) to produce a better dispersion. The mixture was then centrifuged (3500 rpm/30 min) to remove undispersed materials. Then the supernatant – the SWNT dispersion – was collected and used for further characterization and film fabrication. Details of optimum purification conditions reported elsewhere.[49] Typical concentration of dispersions used for testing and characterization were 0.2 to 0.3 wt% SWNT. The pH of the dispersions was kept between 3 - 3.5, in order to avoid overlapping of pH induced transformations in SWNT TCFs.

Preparation of GO dispersion: Preparation procedures of graphene oxide dispersions are adapted from literature.[32, 50] Graphene oxide powder is obtained from Leibniz University of Hannover, which is prepared as follows: 15 g of $KMnO_4$ was added slowly to a stirring mixture of 2.5 g of graphite and 330 mL of H_2SO_4:H_3PO_4 (9:1 v/v) in a round bottom flask. The mixture is stirred continuously for 12 hours at 50 °C after the addition of $KMnO_4$. Later, 300 mL of DI water-ice mixture is added and stirred for 10 minutes in an ice-bath. Then 3 mL of H_2O_2 (30%) solution and 500 mL of DI water is added and stirred further for 2 hours at room temperature. The precipitate from the mixture was centrifuged (at 18000 g) and washed with DI water repeatedly. Then the mixture was washed with 150 mL of ethanol to obtain graphene oxide. Finally, the graphene oxide mixture was added with 300 mL of DI water and freeze-dried under vacuum to obtain the graphene oxide powder (designated as GO1).

Alternatively, 15 g of $KMnO_4$ is added slowly to a stirring mixture of 5 g of graphite and 115 mL of H_2SO_4 in a round bottom flask. The mixture is stirred continuously for 2 hours in an ice-bath after the addition of $KMnO_4$. Afterwards, the mixture is stirred continuously for 4 days at room temperature. Then, 230 mL of DI water is added and stirred for 10 minutes in an ice-bath. 13 mL of H_2O_2 (30%) solution is added and stirred further for 2 hours at room temperature. The precipitate from the mixture was centrifuged and washed with DI water and finally freeze-dried under vacuum to obtain the GO powder (designated as GO2).

In another method, 15g of $KMnO_4$ is added to slowly to a stirring mixture of 5g of graphite and 115 mL of H_2SO_4. The mixture is stirred further for one hour. Then, 13 mL of H_2O_2 is added and stirred continuously. The resulting precipitate is centrifuged, washed and freeze-dried under vacuum to obtain GO powder (designated as GO3).

Dispersions of GO are prepared by sonicating 40 mg of GO powder (Branson 450; 120W, 1 hr)in 100 mL of DI water. Then the mixture was centrifuged at 18000g for 1 hour and the supernatant is collected to have GO sheets of size < 500nm. These dispersions are bar coated onto the SWNT TCFs, for chemical doping.

Fabrication of transparent conductive films (TCFs): TCFs were fabricated on glass slides using the Meyer rod coating method (doctor blading). The films were annealed at 120 ± 10 °C for 1 min. Multilayered coatings were prepared to reach low sheet resistance values (< 500 $\Omega/\square$), typically 3 to 4 layers. All the data were repeated 2 to 3 times to confirm the reproducibility.

Electrical and optical properties: Sheet resistance of TCFs was measured using 2 point probe method, across square area, i.e. 1 x 1 cm^2, with a probe dimension of 1 cm^2. The standard error, if any, involved in the measurement of sheet resistance is uniform throughout all the measurements.

Typically, four to five measurements were taken for each data point and the average of the measurements was calculated. Standard deviation of the data points was calculated to be ≤ 7%. Optical transmittance of the TCFs was recorded using Cary 50 UV-Vis spectrometer (Varian).

Raman spectroscopy: Raman spectra of SWNT films were recorded using Induram (Horiba Jobin-Yvon) spectrometer, coupled with confocal laser scanning microscope. Excitation wavelength used for the all the measurements is 488 nm. Films for the measurements were prepared by drop-casting corresponding SWNT dispersions on to a glass slide and annealed at 120°C for 1min.

Thermo Gravimetric Analysis (TGA): TGA of SWNT and GO samples were performed using Metler Toledo - TGA/SDTA851e analyzer, under 20% O_2 in Ar (flow rate: 80 mL-min^{-1}). Temperature profile for the samples are kept between 27 °C and 500 °C, at a ramp rate of 5 °C/min. 175 μL of SWNT dispersions (0.3 wt-%)and 26 mg of GO powder was used for measurements. As a standardization procedure, all the samples were kept at 27 °C for 30 minutes, before starting the measurement.

Results and Discussion:

We first investigate the effect of chemical doping of SWNT TCFs by GO dispersions. Films were fabricated by coating a GO layer on top of every SWNT layer in a film in order to maximize the possibility of doping the SWNTs that are within the film. Synergistic effect is observed for the SWNT TCFs after doped with different GOs. Summary of the results are given in Table1. The figure of merit is improved up to 60%: $\frac{\sigma_{d.c.}}{\sigma_{o.c.}} = 6.5$ is observed for SWNT TCFs doped by GO1 (SWNT/GO1) compared to $\frac{\sigma_{d.c.}}{\sigma_{o.c.}} = 4.1$ for SWNT TCFs without GO doping (Fig 1A, Table 1). $\frac{\sigma_{d.c.}}{\sigma_{o.c.}} = 5.6$ is observed for SWNT/GO2 TCFs, which is 36.5% higher than the pristine SWNT TCFs; $\frac{\sigma_{d.c.}}{\sigma_{o.c.}} = 5.4$ is observed for SWNT/GO3 TCFs, which is 31.7.% higher than the pristine SWNT TCFs. An increment of 58.5% in $\frac{\sigma_{d.c.}}{\sigma_{o.c.}}$ for SWNT/GO1 films is higher than SWNT TCFs doped with other GO dispersions described here. We attribute this effect to *p*-doping of SWNTs by graphene oxide. *p*-type doping is supported by Raman spectroscopy, where an upshift in

tangential mode can be observed for doped SWNT TCFs compared to pristine SWNT films. The upshift in tangential mode is due to the electron withdrawing GO species that lead to the softening of SWNT lattice.[51] From the Raman spectra, the tangential mode signature is centered at $\mathcal{V}_G$ = 1601.2 cm^{-1} for SWNT/GO1, $\mathcal{V}_G$ = 1600 cm^{-1} for SWNT/GO2 and $\mathcal{V}_G$ = 1599.6 cm^{-1} for SWNT/GO3 films = 1601.2 cm^{-1} compared to the $\mathcal{V}_G$ = 1594.6 cm^{-1} for un-doped SWNT films (Fig 1B; Table 2, S/No 1 & 2). We see that the overall upshift in tangential mode is $\Delta\mathcal{V}_G \geq 5$ cm^{-1} for p-doped SWNT TCFs. The effect of p-doping from GO layers is further supported by optical absorption spectroscopy, where the disappearance of semiconducting inter-band transition (S_{33}) in SWNT/GO2 films are observed, compared to SWNT films (Fig. 3A and B). Intra band transition arises from the p-doping effect of depletion of the conduction band due to the electron withdrawing groups in GO layers, will have transition energy range in infra-red regions.[52]

Table1: Summary of figure of merit of doped SWNT TCFs

S/No.	TCFs	$\dfrac{\sigma_{d.c.}}{\sigma_{o.c.}}$	$\Delta\dfrac{\sigma_{d.c.}}{\sigma_{o.c.}}$	% Increase[a]
1	SWNT	4.1	-	-
2	SWNT/GO1	6.5	2.4	58.5
3	SWNT/GO2	5.6	1.5	36.5
4	SWNT/GO3	5.4	1.3	31.7

[a] % Increase for doped films is calculated with respect to SWNT TCFs

The observed difference in $\frac{\sigma_{d.c.}}{\sigma_{o.c.}}$ of SWNT/GO1, SWNT/GO2 and SWNT/GO3 TCFs are explained as follows. The SWNT/GO1 TCFs have the larger $\Delta\frac{\sigma_{d.c.}}{\sigma_{o.c.}}$ = 2.4 compared to SWNT/GO2 and SWNT/GO3 TCFs. Raman spectra of SWNT/GO1 TCFs shows a larger upshift of 6.6 cm^{-1} compared to the other two GO doped films. $\Delta\mathcal{V}_G$ = 5.4 cm^{-1} for SWNT/GO2 and 5 cm^{-1} for SWNT/GO3 films are observed from the Raman spectra (Fig 1B; Table 2). This indirectly suggests that the effect of p-doping achieved through GO1 dispersions is greater than the p-doping achieved by GO2 and GO3 dispersions. Therefore, SWNT/GO1 TCFs has higher $\frac{\sigma_{d.c.}}{\sigma_{o.c.}}$ compared to other GO doped TCFs.
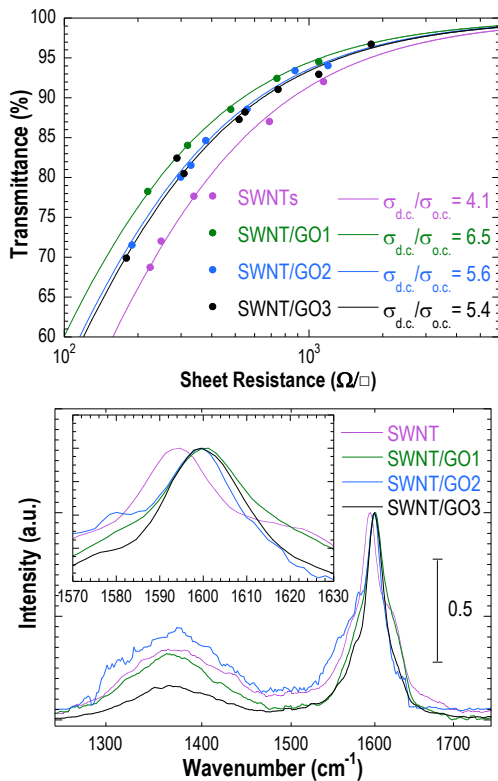
Figure 1: (A) Electrical and optical properties of as prepared and different GO doped SWNT TCFs; (B) Raman spectra of as prepared and different GO doped SWNTs TCFs. Excitation wavelength used for the measurement is 488 nm.

Table 2: Summary of vibrational properties of SWNT/GO films

S/No.	Notation	$\mathcal{V}_G$ (cm^{-1})[a]	$\Delta\mathcal{V}_G$ (cm^{-1})	$\mathcal{V}_D$ (cm^{-1}) [b]
1	SWNT	1594.6	-	1371
2	SWNT/GO1	1601.2	6.6	1369.3
3	SWNT/GO2	1600	5.4	1373.1
4	SWNT/GO3	1599.6	5	1364.2

[a]. Signature of tangential mode vibrations in single wall carbon nanotubes[51]

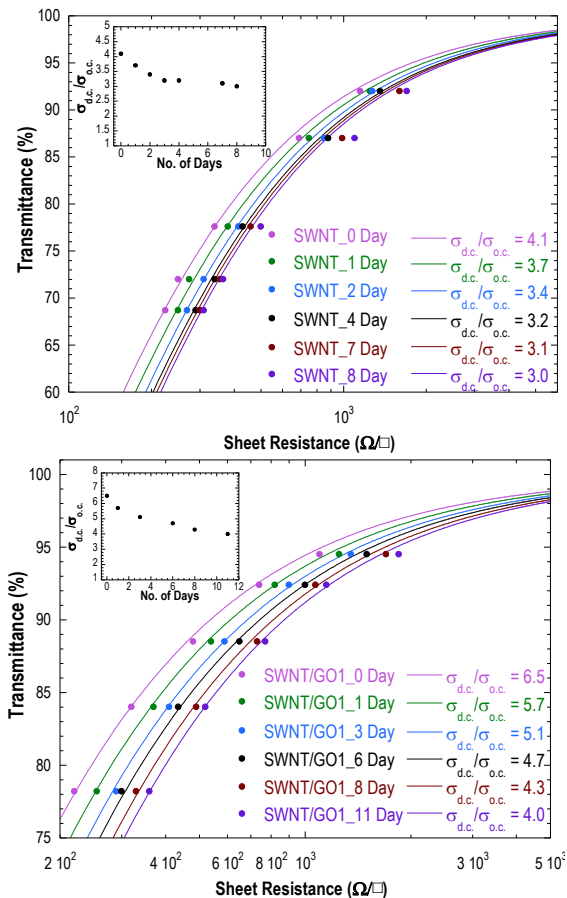[b]. Signature of disordered band vibrations in single wall carbon nanotubes[51]

Figure 2: Stability of single wall carbon nanotube transparent conducting films under ambient conditions: (A) Electrical and optical properties of as prepared SWNT TCFs, with respect to time. (B) Electrical and optical properties of GO doped films, SWNT/GO1, with respect to time. Inset in (A) and (B) shows the regression of figure of merit with respect to time for SWNT TCFs.

The difference in *p*-doping achieved on the SWNT TCFs is further supported by the core-level x-ray photoelectron spectroscopy. We found the following stoichiometry for the treated films: $C_{64.7}O_{32.8}S_{1.3}N_{1.2}$ for GO1, $C_{68.1}O_{30.5}S_{0.7}N_{0.6}Na_{0.2}$ for GO2 and $C_{63.7}O_{31.6}S_{1.4}N_{1.6}Na_{1.7}$ for GO3. As it is difficult to fully dehydrate the GO samples, the oxidation rate deduced from stoichiometry may contain errors. From the O1s core level spectra, we detected that the GO1 samples have higher oxygen content (32.8 at-%) compared to the GO2 and GO3 samples that have 30.5 at-% and 31.6 at-% respectively. These results imply that comparatively more oxygen containing

functional moieties (e.g. carboxylate, hydroxyl, and carbonyl) are introduced into the GO1 samples through the oxidation process than the GO2 and GO3 samples. Our observations are consistent with Marcano et al, who have reported a strongly oxidized GO synthesized using the mixture of $H_2SO_4:H_3PO_4$ (9:1 v/v).[50] The p-doping occurs due to the oxygen containing moieties that are electron withdrawing by nature. Therefore the effect of p-doping by GO1 samples is larger than the other two GOs. The contributions from N1s and Na1s on the stoichiometry are possibly due to the presence of impurities in graphite powder, which is used as a precursor.

Both GO2 and GO3 samples are prepared by oxidizing the graphite powder in H_2SO_4 for 96 hours and 1 hour, respectively. A slight difference is observed on the $\frac{\sigma_{d.c.}}{\sigma_{o.c.}}$ of SWNT TCFs doped with GO2 & GO3 (5.6 and 5.4 respectively). This result is in accordance with the Raman spectra where the upshift in tangential mode signatures of SWNT/GO2 and SWNT/GO3 TCFs are also slightly different. The tangential mode difference, $\Delta\mathcal{V}_G$ = 0.4 cm^{-1} between the SWNT/GO2 and SWNT/GO3 films are observed. These results indirectly suggest that the longer oxidation duration of graphite in H_2SO_4 did not introduce significantly enough electron withdrawing functional moieties compared to the shorter oxidation time.

Table 3: Summary of stoichiometry of GOs from x-ray photoelectron spectra

S/No.	Notation	Conditions	Duration (hrs)	XPS Stoichiometric ratio				
				C1s	N1s	O1s	S2P	Na1s
1	GO1	$H_2SO_4:H_3PO_4$	12	64.7	1.2	32.8	1.3	-
2	GO2	H_2SO_4	96	68.1	0.6	30.5	0.7	0.2
3	GO3	H_2SO_4	1	63.7	1.6	31.6	1.4	1.7

Our results on SWNT TCFs doped with graphene oxide to enhance the performance of TCFs is consistent with other literature results where an increase in $\frac{\sigma_{d.c.}}{\sigma_{o.c.}}$ of TCFs attributed to p-doping arises from the electron withdrawing groups in graphene oxide layers.[32, 53-55] The maximum increment in $\frac{\sigma_{d.c.}}{\sigma_{o.c.}}$ of 58.5% on our GO doped SWNT TCFs is in the same regime as the increase in $\frac{\sigma_{d.c.}}{\sigma_{o.c.}}$ of 63% reported on GO doped films by Han et al[32].
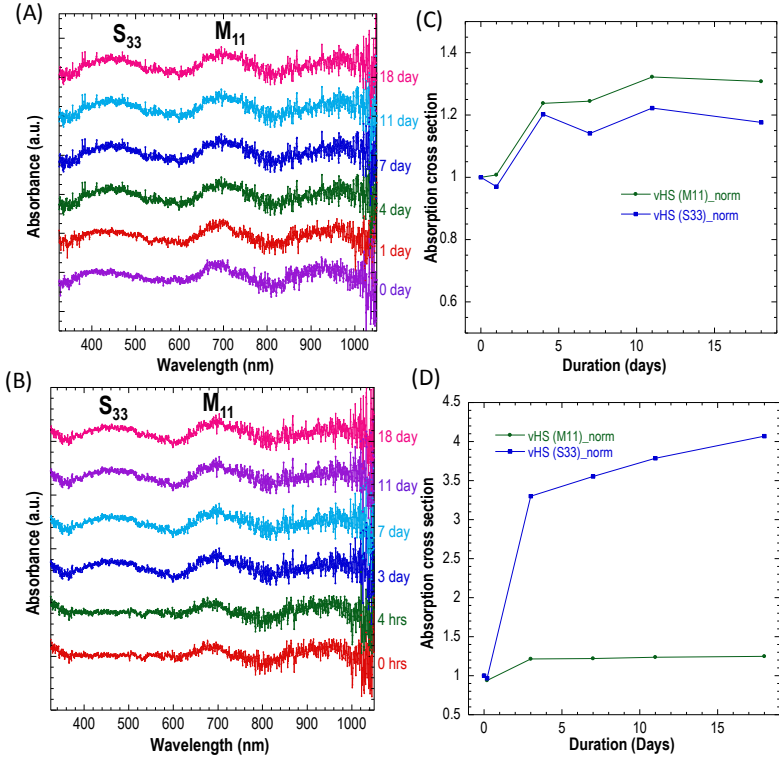
Figure 3: Optical transition transformation spectroscopy: Optical absorption spectra of (A) SWNT TCF at different time (R_s = 220Ω/□; T_{550} = 69%) and (B) SWNT/GO1 TCFs (R_s = 200Ω/□; T_{550} = 73%). (C) and (D) Evolution of semiconducting (S_{33}) and metallic (M_{11}) inter-band transitions of SWNT and SWNT/GO2 TCFs, respectively.

In addition, the stability of SWNT TCFs under ambient conditions was investigated. SWNT TCFs and GO doped TCFs are not stable under ambient conditions as described further. The $\frac{\sigma_{d.c.}}{\sigma_{o.c.}}$ of both undoped and GO doped SWNT TCFs are decreasing with respect to time under ambient conditions. Sheet resistance R_s of the TCFs increases with respect to time exhibiting a drastic increase in R_s within the first 3 – 4 days from the date of fabrication (Fig 2A and B). The increase in R_s with respect to time is consistent with other reports, where SWNT films were doped with HNO$_3$,[47, 48, 56] SOCl$_2$,[48] HNO$_3$ & SOCl$_2$,[48] hydrazine[33] and Triethyloxonium hexachloroantimonate.[38] The effect of storing the materials under ambient conditions on the stability of TCFs is monitored by optical absorption spectroscopy. We observed a drastic restoration of semiconducting inter-band transition (S_{33}) after 3 days in ambient conditions,

which possibly arises due to the de-doping of TCFs, after 3-4 days for both SWNT and SWNT/GO1 TCFs. Only a marginal increase in integrated absorption cross-section of S_{33} bands is noticed beyond 4 days for both un-doped and GO doped SWNT TCFs (Fig 3). Minor change in metallic inter-band transition (M_{11}) is observed, as p-doping does not influence the metallic transitions.[52] These absorption spectroscopic results are consistent with the stability of $\frac{\sigma_{d.c.}}{\sigma_{o.c.}}$ of TCFs under ambient conditions. Therefore, the drastic increase within the R_s on the first 3 – 4 days is possibly due to the moisture absorption by the hygroscopic oxygen containing moieties on SWNTs. The effect of p-doping on SWNTs by the electron withdrawing groups is possibly suppressed by the water molecules absorbed the functional moieties. After 3 – 4 days, the rate of moisture absorption by the functional moieties might have decreased. Thus, the increase in R_s has slowed down after 3 – 4 days

In contrast, it was found that both undoped and GO doped SWNT TCFs are stable under inert conditions as described further. The SWNT TCFs and SWNT/GO3 samples are stored in a glove bag, which is continuously purged with nitrogen gas. The TCFs are found to be stable with respect to time, and no changes in $\frac{\sigma_{d.c.}}{\sigma_{o.c.}}$ for both undoped and GO doped SWNT TCFs (Fig 4) are detected. The stability of the TCFs is again monitored by optical absorption spectroscopy. The integrated absorption cross-sections of semiconducting inter-band transitions (S_{33}), of both undoped and GO doped TCFs remain unchanged over a period of 10 days in inert conditions (Fig 5).

In a subsequent experiment, after storing the TCFs under inert conditions for ten days, they were exposed overnight to ambient conditions and then restored under inert conditions. A drastic decrease in $\frac{\sigma_{d.c.}}{\sigma_{o.c.}}$ of the TCFs is observed after the exposure to ambient conditions. The $\frac{\sigma_{d.c.}}{\sigma_{o.c.}}$ of both undoped and GO doped SWNT TCFs decreased by 20% and 25%, respectively (Fig. 4). Optical absorption spectra of the TCFs show that the semiconducting inter-band transition (S_{33}) of both undoped and GO doped TCFs evolved significantly after the exposure to ambient conditions (Fig. 5). We ascribe these results of decrease in $\frac{\sigma_{d.c.}}{\sigma_{o.c.}}$ and evolution of S_{33} bands are due to the moisture absorption induced de-doping that arise from the hydrophilic electron withdrawing moieties present in TCFs. The absorbed moisture by these functional moieties further suppresses the effect of doping. This could be a possible reason for the

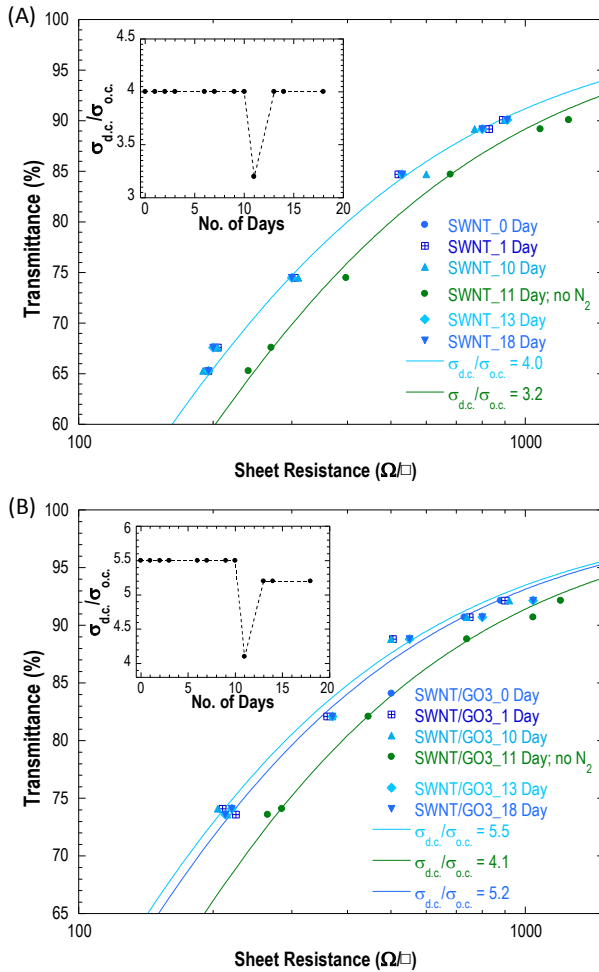evolution of S_{33} bands, which disappeared due to the depletion of conduction band through the doping process.

Figure 4: (A) Stability of single wall carbon nanotube transparent conducting films under nitrogen environment. (A) Electrical and optical properties of as prepared SWNT TCFs, with respect to time. (B) Electrical and optical properties of GO doped films, SWNT/GO3, with respect to time. Inset in (A) and (B) shows figure of merit with respect to time for SWNT and SWNT/GO3 TCFs, respectively.
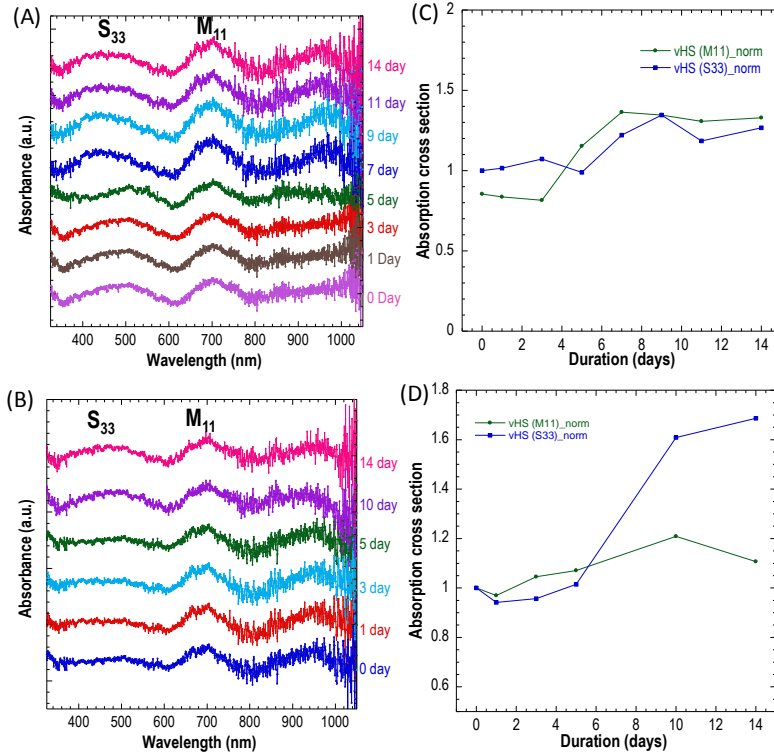
Figure 5: Optical transition transformation spectroscopy: Optical absorption spectra of (A) SWNT TCF at different time (R_s = 200Ω/□; T_{550} = 67%) and (B) SWNT/GO2 TCFs (R_s = 200Ω/□; T_{550} = 74%). (C) and (D) Evolution of semiconducting (S_{33}) and metallic (M_{11}) inter-band transitions of SWNT and SWNT/GO2 TCFs, respectively.

An Increment in $\frac{\sigma_{d.c.}}{\sigma_{o.c.}}$ is observed when the TCFs are restored to inert conditions. The samples were continuously purged with nitrogen under inert conditions. The $\frac{\sigma_{d.c.}}{\sigma_{o.c.}}$ of undoped SWNT TCFs is fully recovered to its initial value of 4. However the $\frac{\sigma_{d.c.}}{\sigma_{o.c.}}$ GO doped TCFs did not recovered fully to its initial value of 5.5; the maximum $\frac{\sigma_{d.c.}}{\sigma_{o.c.}}$ = 5.2 is observed for the GO doped TCFs after exposed to inert conditions for two or more days (Fig 4). The optical absorption spectra of undoped SWNT TCFs show that the S_{33} band is slightly suppressed, after restored to inert conditions. On the other hand, the S_{33} band of GO doped TCFS did not suppress after restored to inert conditions (Fig 5). The increment in $\frac{\sigma_{d.c.}}{\sigma_{o.c.}}$ of both undoped and GO doped TCFs

can be attributed to the removal of loosely bound water molecules by continuous purging of nitrogen. The highly hygroscopic GO probably have strongly bound water molecules on the films, which are difficult to remove by continuous purging of nitrogen. These observations on stability of both un-doped and GO doped SWNT TCFs under inert conditions gives the new insights that the instability is possibly triggered by the moisture absorption and moisture absorption induced de-doping. Therefore, doped SWNT TCFs can be used for commercial applications, if a proper encapsulation is provided.
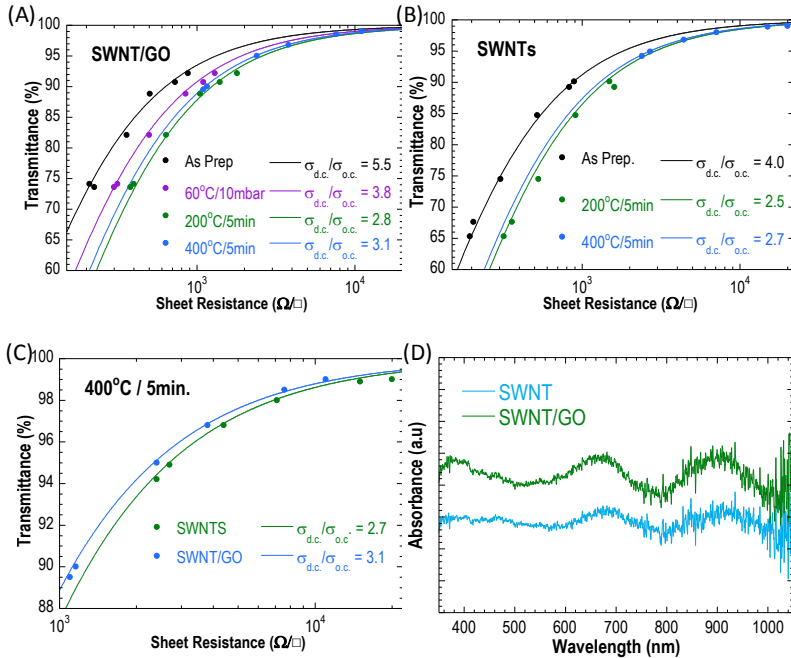

Figure 6: Stability of TCFs at elevated conditions: Deterioration of TCFs at different elevated pressure and temperatures, (A) SWNT/GO3 TCFs, (B) SWNT TCFs. (C) Electrical and optical properties of SWNT and SWNT/GO TCFs annealed at 400 °C / 4 hours, replotted for clarity. (D) Optical absorption spectra of SWNT and SWNT/GO (R_s = 205 and 225 $\Omega/\square$, respectively) TCFs, annealed at 400 °C/4 hours.

The stability of SWNT TCFs under vacuum and at elevated temperatures was investigated. The motivation is to remove the strongly absorbed water molecules from the TCFs. SWNT/GO3 TCFs are kept at 60 °C under vacuum ($\approx$10 mbar for 6 hours), in order to completely remove the sorbed moisture to restore the $\frac{\sigma_{d.c.}}{\sigma_{o.c.}}$ = 5.2 to its initial value of 5.5. But the $\frac{\sigma_{d.c.}}{\sigma_{o.c.}}$ of the TCFs

after vacuum exposure further deteriorated to 3.8 (Fig. 6A). This could be possibly due to the decomposition of graphene oxide. It is known form the literature that the decomposition of GO starts at temperature as low as 70 °C.[57, 58] During the decomposition process of GO, the electron withdrawing functional moieties decomposes. This will affect the effect of *p*-doping that results in decrement of $\frac{\sigma_{d.c.}}{\sigma_{o.c.}}$. Hence, the complete removal of sorbed water molecules can occur only at the expense of doping effects. The SWNT/GO3 samples were then annealed at 200 °C for 5 minutes at ambient conditions; $\frac{\sigma_{d.c.}}{\sigma_{o.c.}}$ of SWNT/GO3 TCFs is further reduced to 2.8. For comparison, un-doped SWNT TCFs are also annealed at 200 °C for 5 minutes at ambient conditions; the $\frac{\sigma_{d.c.}}{\sigma_{o.c.}}$ decreased from 2.5 from its initial value of 4 (Fig. 6A & B). These results are supported by the thermogravimetric analysis of GO and SWNTs. The thermogravimetric analysis of GO shows a gradual decomposition of GO, about 29.5% weight loss, at temperature below 170 °C is observed. Then a drastic weight loss (65.2 %) is observed at a temperature between 170 and 180 °C (Figure 7A). For SWNTs, a gradual weight loss occurred between 100 to 200 °C, approximately about 25% (i.e. from 0.4 wt% to 0.3 wt%). The weight loss of more than 99% in SWNT profile is observed due to the presence excess amount of water; the samples used for measurement is a SWNT dispersion with a concentration of 0.3 wt% (Figure 7B). These effects are consistent with those mentioned in the literature; desorption products such as H_2O, CO and CO_2 from decomposition of GO are observed between a temperature range from 70 to 300 °C.[57, 58] We attribute these results to the decomposition of functional moieties in GO and in SWNTs that occurs at wide range of temperatures 70 – 200 °C.
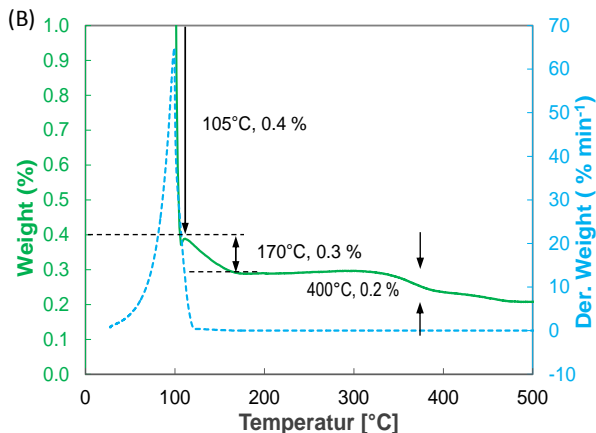

(A)
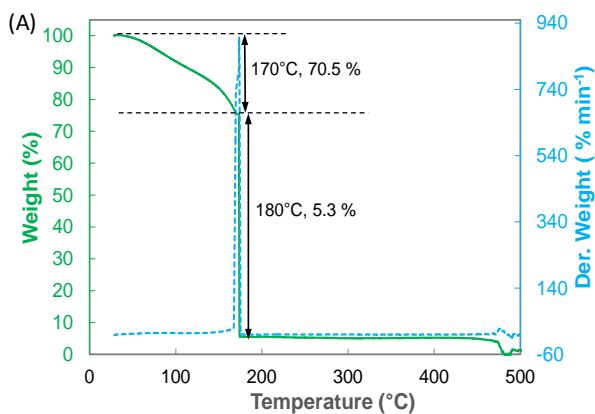
Figure 7: Thermo Gravimetric Analysis: (A) Weight loss profile of graphene oxide between 27 to 500 °C (B) Weight loss profile of SWNT dispersions (0.3 wt%) between 27 to 500 °C. Temperature ramp rate for the measurements are 5 °C/min.

Interestingly $\frac{\sigma_{d.c.}}{\sigma_{o.c.}}$ of SWNT and SWNT/GO3 TCFs increased by ≈10 %, when annealed further at 400 °C for 4 hours. The optical transmittances of the films are larger than 90 % and the sheet resistance increased by app. one order of magnitude order (Fig. 6 A, B and C). The effect of doping is expected to be completely removed after annealing at 400 °C, as all the electron withdrawing functional moieties desorb at this temperature.[59] The effect of complete removal of doping is further supported by optical absorption spectroscopy, where the salient features of inter-band transitions (M_{11} and S_{22}) reappeared strongly compared to doped SWNT and SWNT/GO3 TCFs (Fig. 5D). We observe a weight loss in SWNT films from the TGA, where a weight loss of about 33 % (0.3 wt% to 0.2 wt% between 200 and 400 °C) is observed (Figure 7B). We attribute this effect to the loss of traces of functional moieties along with amorphous carbon and polymer surfactants present in it TCFs undergo thermal decomposition processes at ≈ 400 °C that involve loss of carbon along with functional moieties,[57, 59] and loss of surfactant (PSS) that contributes to ≈ 12 vol-%. Loss of materials from the matrix leads to a film contraction, which results in thinner film with high optical transmittance. The increment in sheet resistance could possibly due to the cracks developed during the annealing process at 400°C, which affects the percolation network. From the optical absorption spectra, blue-shift of 17 nm in M_{11} band for SWNT/GO3 TCFs (667 nm) compared to SWNT TCFs (684 nm) and blue-shift

of 6 nm in S_{22} band for SWNT/GO3 TCFs (906 nm) compared to SWNT TCFs (912 nm) are observed (Fig. 6D). These effects can be attributed to the interaction between GO and SWNTs. The increment in $\frac{\sigma_{d.c.}}{\sigma_{o.c.}}$ of both TCFs after annealing at elevated temperature is possibly due to the removal of insulative species like residual amorphous carbon and polymer surfactants. Relatively higher $\frac{\sigma_{d.c.}}{\sigma_{o.c.}}$ for SWNT/GO3 films compared to the SWNT TCFs ($\Delta\frac{\sigma_{d.c.}}{\sigma_{o.c.}}$ = 0.4) could be attributed to the presence of sp2 hybridized carbon atoms from the graphene oxide layers in the film. These graphite / graphene layers facilitate charge transfer between SWNTs, which suggests that GO improves the performance of TCFs not only through p-doping, but also through effective charge transfer through conjugated π electron system.

Conclusion

We have demonstrated that graphene oxide can be used as a p-dopant for SWNT TCFs to enhance the overall performance, which is in agreement with other literatures. The maximum increment of ≈60% on the $\frac{\sigma_{d.c.}}{\sigma_{o.c.}}$ for graphene oxide doped SWNT TCFs is achieved. The effect of doping on the SWNTs is analyzed and studied using Raman spectroscopy and optical absorption spectroscopy. The stability of both un-doped and GO doped SWNT TCFs is under ambient and inert conditions are studied in detail. The effect of moisture and moisture induced de-doping of TCFs are also probed. The stability of TCFs at elevated temperatures and the effect of doping under elevated conditions are also probed. The TCFs are observed to be stable under inert conditions, which suggest that these materials can be used in commercial applications if proper encapsulation is provided. These new insights can open up further possibilities for research and technological developments.

References

[1]   Y. Chen, B. Cotterell, W. Wang, *Eng. Fract. Mech.* **2002**, *69*, 597.

[2]   A. Chipman, *Nature* **2007**, *449*, 131.

[3]   E. Fortunato, D. Ginley, H. Hosono, D. C. Paine, *MRS Bull.* **2009**, *32*, 242.

[4]   L. Hu, H. Wu, Y. Cui, *MRS Bull.* **2011**, *36*, 760.

[5]   T. Aernouts, P. Vanlaeke, W. Geens, J. Poortmans, P. Heremans, S. Borghs, R. Mertens, R. Andriessen, L. Leenders, *Thin Solid Films* **2004**, *451-452*, 22.

[6]   G. Gustafsson, Y. Cao, G. M. Treacy, F. Klavetter, N. Colaneri, A. J. Heeger, *Nature* **1992**, *357*, 477.

[7]   J. Huang, X. Wang, A. J. deMello, J. C. deMello, D. D. C. Bradley, *J. Mater. Chem.* **2007**, *17*, 3551.

[8]   F. Jonas, A. Karbach, B. Muys, E. van Thillo, R. Wehrmann, A. Elschner, R. Dujadin*, Vol. EP0686662 A2* (Ed.: E. P. Office), Bayer A.G., Germany, **1995**, pp. 1.

[9]   N. F. Anglada, M. Kaempgen, V. Skákalová, U. D-Weglikowska, S. Roth, *Diamond Relat. Mater.* **2004**, *13*, 1256.

[10]   E. Kymakis, G. Klapsis, E. Koudoumas, E. Stratakis, N. Kornilios, N. Vidakis, Y. Franghiadakis, *EPJ Appl. Phys.* **2007**, *36*, 257.

[11]   J. B. Yoo, J. S. Moon, J. H. Park, T. Y. Lee, Y. W. Kim, C. Y. Park, J. M. Kim, K. W. Jin, *Diamond Relat. Mater.* **2005**, *14*, 1882–1887.

[12]   J. Song, F.-Z. Kam, R.-Q. Png, J.-M. Zhou, G.-K. Lim, P. K. H. Ho, L.-L. Chua, *Nat. Nanotechnol.* **2013**, *8*, 356.

[13]   J. K. Wassei, R. B. Kaner, *Mater. today* **2010**, *13*, 52.

[14]   Q. Cao, J. A. Rogers, *Adv. Mater.* **2009**, *21*, 29.

[15]   G. Gruner, *J. Mater. Chem.* **2006**, *16*, 3533.

[16]   L. Hu, D. S. Hecht, G. Grüner, *Chem. Rev.* **2010**, *110*, 5790.

[17]   D. S. Hecht, L. Hu, G. Irvin, *Adv. Mater.* **2011**, *23*, 1482–1513.

[18]   W. S. Wong, A. Salleo, in *Electronic Materials: Science & Technology* (Ed.: H. L. Tuller), Springer, New York, **2009**, p. 462.

[19]   N. Saran, K. Parikh, D.-S. Suh, M. Munoz, H. Kolla, S. K. Manohar, *J. Am. Chem. Soc.* **2004**, *126*, 4462.

[20]   C. M. Trottier, P. Glatkowski, P. Wallis, J. Luo, *J. Soc. Info. Disp.* **2005**, *13*, 759.

[21]   B. Mackey, *SID Digest. Tech. Papers* **2011**, *42*, 617.

[22]   W.-B. Liu, S. Pei, J. Du, B. Liu, L. Gao, Y. Su, C. Liu, H.-M. Cheng, *Adv. Funct. Mater.* **2011**, *21*, 2330–2337.

[23] Y. Kim, M. Chikamatsu, R. Azumi, T. Saito, N. Minami, *Appl. Phys. Exp.* **2013**, *6*, 025101.

[24] H. Tantang, J. Xiao, J. Wei, M. B. E. C-Park, L.-J. Li, Q. Zhang, *Eur. J. Inorg. Chem.* **2011**, *2011*, 4182–4186.

[25] J. Gao, W.-I. Wang, L.-T. Chen, L.-J. Cui, X.-Y. Hu, H.-Z. Geng, *Appl. Surf. Sci.* **2013**, *277*, 128.

[26] D. Dan, G. C. Irvin, M. Pasquali, *ACS Nano* **2009**, *3*, 835 – 843.

[27] Y. T. Park, A. Y. Ham, Y.-H. Yang, J. C. Grunlan, *RSC Adv.* **2011**, *1*, 662.

[28] J. K. Wassei, K. C. Cha, V. C. Tung, Y. Yang, R. B. Kaner, *J. Mater. Chem.* **2011**, *21*, 3391.

[29] A. G. Nasibulin, A. Kaskela, K. Mustonen, A. S. Anisimov, V. Ruiz, S. Kivistö, S. Rackauskas, M. Y. Timmermans, M. Pudas, B. Aitchison, M. Kauppinen, D. P. Brown, O. G. Okhotnikov, E. I. Kauppinen, *ACS Nano* **2011**, *5*, 3214.

[30] R. V. Salvatierra, C. E. Cava, L. S. Roman, A. J. G. Zarbin, *Adv. Funct. Mater.* **2013**, *23*.

[31] R. V. Salvatierra, M. M. Oliveira, A. J. G. Zarbin, *Chem. Mater.* **2010**, *22*, 5222.

[32] J. T. Han, J. S. Kim, S. B. Jo, S. H. Kim, J. S. Kim, B. Kang, H. J. Jeong, S. Y. Jeong, G.-W. Lee, K. Cho, *Nanoscale* **2012**, *4*, 7735–7742.

[33] K. S. Mistry, B. A. Larsen, J. D. Bergeson, T. M. Barnes, G. Teeter, C. Engtrakul, J. L. Blackburn, *ACS Nano* **2011**, *5*, 3714.

[34] T. M. Barnes, X. Wu, J. Zhou, A. Duda, J. van de Lagemaat, T. J. Coutts, C. L. Weeks, D. A. Britz, P. Glatkowski, *Appl. Phys. Lett.* **2007**, *90*, 243503.

[35] M. W. Rowell, M. A. Topinka, M. D. McGehee, H.-J. Prall, G. Dennler, N. S. Sariciftci, L. Hu, G. Gruner, *Appl. Phys. Lett.* **2006**, *88*, 233506.

[36] E. H. Lee, J. H. Ryu, J. Jang, K. C. Park, *Jap. J. Appl. Phys.* **2011**, *50*, 03CA04.

[37] S. M. Kim, Y. W. Jo, K. K. Kim, D. L. Duong, H.-J. Shin, J. H. Han, J.-Y. Choi, J. Kong, Y. H. Lee, *ACS Nano* **2012**, *4*, 6998.

[38] B. Chandra, A. Afzali, N. Khare, M. M. El-Ashry, G. S. Tulevski, *Chem. Mater.* **2010**, *22*, 5179.

[39] S. B. Yang, B.-S. Kong, D.-W. Kim, Y.-K. Baek, H.-T. Jung, *J. Phys. Chem. C* **2010**, *114*, 9296.

[40] N. Kishi, I. Miwa, T. Okazaki, T. Saito, T. Mizutani, H. Tsuchiya, T. Soga, T. Jimbo, *Appl. Phys. Lett.* **2012**, *100*, 063121.

[41] J. T. Han, J. S. Kim, H. D. Jeong, H. J. Jeong, S. Y. Jeong, G.-W. Lee, *ACS Nano* **2010**, *4*, 4551.

[42] R. S. Lee, H. J. Kim, J. E. Fischer, A. Thess, R. E. Smalley, *Nature* **1997**, *388*, 255.

[43] A. M. Rao, P. C. Eklund, S. Bandow, A. Thess, R. E. Smalley, *Nature* **1997**, *388*, 257.

[44]   R.-Q. Png, P.-J. Chia, S. Sivaramakrishnan, L.-Y. Wong, Z. Zhou, L.-L. Chua, P. K.-H. Ho, *Appl. Phys. Lett.* **2007**, *91*, 013511.

[45]   M. Dressel, G. Grüner, *Electrodynamics of Solids: Optical Properties of Electrons in Matter*, Cambridge University Press, Cambridge, **2002**.

[46]   L. Hu, D. S. Hecht, G. Grüner, *Nano Lett.* **2004**, *4*, 2513–2517.

[47]   H.-Z. Geng, K. K. Kim, K. P. So, Y. S. Lee, Y. Chang, Y. H. Lee, *J. Am. Chem. Soc.* **2007**, *129*, 7758.

[48]   R. Jackson, B. Domercq, R. Jain, B. Kippelen, S. Graham, *Adv. Funct. Mater.* **2008**, *18*, 2548.

[49]   B. T. Anto, S. Eiden, H.-C. Schwarz, A. M. Schneider, P. Behrens, *Manuscript in prep.* **2013**.

[50]   D. C. Marcano, D. V. Kosynkin, J. M. Berlin, A. Sinitskii, Z. Sun, A. Slesarev, L. B. Alemany, W. Lu, J. M. Tour, *ACS Nano* **2010**, *4*, 4806–4814.

[51]   M. S. Dresselhaus, G. Dresselhaus, R. Saito, A. Jorio, *Physics Reports* **2005**, *409*, 47.

[52]   R. K. Jackson, A. Munro, K. Nebesny, N. Armstrong, S. Graham, *ACS Nano* **2010**, *4*, 1377.

[53]   J.-H. Huang, J.-H. Fang, C.-C. Liu, C.-W. Chu, *ACS Nano* **2011**, *5*, 6262.

[54]   B. R. Lee, J. S. Kim, Y. S. Nam, H. J. Jeong, S. Y. Jeong, G.-W. Lee, J. T. Han, M. H. Song, *J. Mater. Chem.* **2012**, *22*, 21481.

[55]   Q. Zheng, B. Zhang, X. Lin, X. Shen, N. Yousefi, Z.-D. Huang, Z. Li, J.-K. Kim, *J. Mater. Chem.* **2012**, *22*, 250.

[56]   D.-W. Shin, J. H. Lee, Y.-H. Kim, S. M. Yu, S.-Y. Park, J.-B. Yoo, *Nanotechnol.* **2009**, *20*, 475703.

[57]   I. Jung, D. A. Field, N. J. Clark, Y. Zhu, D. Yang, R. D. Piner, S. Stankovich, D. A. Dikin, H. Geisler, C. A. Ventrice, R. S. Ruoff, *J. Phys. Chem. C* **2009**, *113*, 18480.

[58]   W. Scholtz, H.-P. Boehm, *Naturwissenschaften* **1963**, *51*, 160.

[59]   Z.-l. Wang, D. Xu, Y. Huang, Z. Wu, L.-m. Wanga, X.-b. Zhang, *Chem. Commun.* **2012**, *48*, 976.

5. Summary and outlook

The work in this thesis focusses more on the scientific insights on the development of stable transparent conductive films (TCFs) using single wall carbon nanotubes. We have demonstrated that the figure of merit $\frac{\sigma_{d.c.}}{\sigma_{o.c.}}$ of TCFs can be controlled by treating them with an acid treatment (HNO$_3$) procedure for a desired duration. This effect of acid treatment on SWNTs addresses that the pre-treatment of tubes are essential step to the production process of TCFs in order to remove the metal impurities. We have also learned that the dispersibility of tubes, which is good for solution processable techniques, has improved through the oxidation induced functional moieties on the SWNTs. We have shown that the $\frac{\sigma_{d.c.}}{\sigma_{o.c.}}$ of TCFs can be fine-tuned to their maximum by increasing the pH of the dispersions of SWNTs, from which the films are fabricated. This enables us to address the fundamental understanding on the surface charge mediated spatial distribution of SWNTs on the nanoscale network formation in TCFs. The better spatial distribution without affecting the percolation paths SWNTs on a nanoscale network film results in better transmission of photons at a given sheet resistance.

Secondly, our work shows that the $\frac{\sigma_{d.c.}}{\sigma_{o.c.}}$ of SWNT TCFs can be improved by employing a proper mixture of stabilizers. We have demonstrated that the TCFs fabricated with mixture of poly(4-styrene sulphonic acid) (PSS) and poly(vinyl pyrrolidone) (PVP) as stabilizers have shown better $\frac{\sigma_{d.c.}}{\sigma_{o.c.}}$ compared to the TCFs fabricated with single stabilizers (e.g. PSS or PVP). The universality of this effect was confirmed from further investigations with a mixture of Ligno(4-sodium sulphonic acid) (LSS) + poly(vinyl alcohol) (PVA) and a mixture of LSS + PVP. We have tried to propose a hypothesis behind these effects on molecular scale engineering of SWNTs through supramolecular forces (e.g. van der Waals forces, hydrogen bonding, ionic bonding and π-π

interactions). The stabilizers that have more affinity towards the SWNTs orients closer to the tubes and the other stabilizers orient as a spacer molecules. In this way a better spatial distribution can be achieved on nanotube films. As we have drawn conclusions from the spectroscopic and scanning electron microscopic evidences, further scope of work lies with high resolution microscopic investigation on these films or TCFs.

Thirdly, we have demonstrated that the stability of doped films can be improved by employing a proper encapsulation. The graphene oxide doped SWNT TCFs have shown better $\frac{\sigma_{d.c.}}{\sigma_{o.c.}}$ compared to the as prepared SWNT TCFs. The electrical conductivity of these films deteriorates at the ambient conditions, probably due to the absorption of moisture, which was evidenced from the spectroscopic data. However, when the films are kept under inert (nitrogen) conditions, the stability in electrical properties was observed.

Further scope of work on the SWNT TCFs lies on improving the electrical properties, which can be useful in display applications (e.g. LEDs, solar cells, flat panel displays). The lowest sheet resistance observed for SWNT TCFs from this work is ~ 200 $\Omega/\square$ at an optical transmittance of ~ 80%. However, the functional requirement of sheet resistance for the display applications is < 100 $\Omega/\square$ at an optical transmittance of >90%.[1] The SWNT TCFs fabricated in this work are via bar-coating; typically 3 to 4 layers are deposited from a SWNT dispersion concentration of 0.2 – 0.3 wt% and each layer is annealed before the deposition of next layer. It would be interesting to see the effect of doping by 6 - 12M HNO_3 on each layers. The required duration of doping process by immersion in HNO_3 need to be obtained experimentally. Most of the literatures employ the doping process on the final SWNT TCFs,

1.   Mackey, B., Invited Paper: Trends and Materials in Touch Sensing. *SID Digest*. *Tech. Papers* **2011,** 42, 617-620

by immersing it in HNO_3 or other dopants.[2,3] By doping the each layer one after the other, we are expected to achieve the maximum possible doping on the whole SWNT TCF comprising multiple layers. In this way the effect of doping can be improved, so as the electrical conductivity of the film.

In this thesis work, the doping experiments were performed on the TCFs fabricatted from SWNT dispersions of low pH values (~3). In this way, the effect of doping and the effect of pH of the dispersions was clearly distinguished. Further scope of work on this area lies on bringing these two effects of doping and pH of SWNT dispersions together to see if there is any synergystic end results.

2.   Grüner, G., Carbon nanotube films for transparent and plastic electronics. *J. Mater. Chem.* **2006,** 16, 3533-3539.
3.   Hu, L.; Hecht, D. S.; Grüner, G., Carbon nanotube thin films: Fabrication, properties, and applications. *Chem. Rev.* **2010,** 110, 5790-5844.

6. List of publications

Journal articles

H-C Schwarz, A.M. Schneider, S. Klimke, <u>B.T. Anto</u>, S. Eiden, P. Behrens, Transparent conductive three-layered composite films based carbon nanotubes with improved mechanical stability, **MRS Proc.** 1659, 213-218 (2014)

<u>B.T. Anto</u>, S. Sivaramakrishnan, L.L. Chua and P.K.H. Ho, Hydrophilic Sparse Ionic Monolayer-Protected Metal Nanoparticles: Highly Concentrated Nano-Au and Nano-Ag Inks that can be Sintered to Near-Bulk Conductivity at 150 °C, **Adv. Funct. Mater**. 20, 296 (2010)

S. Sivaramakrishnan, <u>B.T. Anto</u> and P.K.H. Ho, Optical modeling of the plasmon band of monolayer-protected nanometal clusters in pure and in polymer matrix thin films as a function of heat treatment, **Appl. Phys. Lett**. 94, 091909 (2009)

Book Chapter

<u>B.T. Anto</u>, L.L. Chua, S. Sivaramakrishnan, L.Y. Wong, R.Q. Png and P.K.H. Ho, Printable Metal Nanoparticle Inks for Thin-Film Metallization: Physicochemical Aspects, Chapter 2, Handbook of Nanophysics, Ed: Klaus D. Sattler, Taylor & Francis (CRC Press), 2010. (*invited book chapter*)

Patents

D. Rudhardt, <u>B.T. Anto</u>, C.D. Theivanayagam, F.C. Kartawidjaja, S. Bahnmüller, "Method for producing a metal nanoparticle dispersion, metal nanoparticle dispersion and use of said metal nanoparticle dispersion" **WO2013064502** & **DE102011085642.**

P.K.H. Ho, L.L. Chua, R.H. Friend, <u>B.T. Anto</u>, L.Y. Wong and R.Q. Png, "Metal nanoparticle inks", **WO2011071452**.

P.K.H. Ho, L.L. Chua, R.H. Friend, J.C. Tang, <u>B.T. Anto</u>, R.Q. Png and P.J. Chia, "Cross-linking Moiety", **WO2011068482, US 20120244294 & EP2507309A1**.

Conference presentations

B.T. Anto, S. Eiden, P. Behrens, Enhancing optical and electrical properties of transparent conducting single-walled carbon nanotube films, through manipulation of molecular environment, Ninth International conference on organic electronics, **ICOE 2013**, Grenoble, France

B.T. Anto, S. Eiden, P. Behrens, Unusual behaviour of transparent conducting films fabricated from hydrophilic dispersions of single wall carbon nanotubes stabilized with mixture of surfactants, **EMRS Spring Meeting 2013**, Strasbourg, France.

H-C. Schwarz, A.M. Schneider, B.T. Anto, S. Eiden, P. Behrens, Transparent conductive three-layered composite films based on carbon nanotubes with improved mechanical stability, **MRS Fall Meeting 2013**, Boston, USA.

B.T. Anto, S. Eiden, P. Behrens, Transparent conducting films from highly stable hydrophilic SWNT dispersions, Sixth Internatinoal conference on molecular electronics, **ElecMol 2012**, Grenoble, France.

B.T. Anto, S. Sivaramakrishnan, L.L. Chua and P.K.H. Ho, Sparse monolayer protected metal nanoparticles: a general route to high water dispersibility and low solid-sate coalescence temperature, **ICMAT 2009**, Singapore

7. Curriculum Vitae

Bibin Thomas Anto

Date of birth	30 July 1981
Place of birth	Kanyakumari, India
Family status	Married
Nationality	Indian

Education

Since October 2011	**Doctoral student** at the Institute für Anorganische Chemie of the Leibniz Universität Hannover in the group of Prof. Dr. Peter Behrens Final Grade: 1.0 (Sehr Gut)
August 2007 – Jan 2010	**Master of Science** *(by Research)* at the Organic Nano Device laboratory of the National University of Singapore in the group of Prof. Dr. Peter Ho Final Grade: A Thesis: Nanometal inks for plastic electronics applications
July 2001 – April 2004	**Bachelor of Technology** (Study of **polymer science and technology**) at the Madras Institute of Technology, Anna University, India Final Grade: First Class Thesis: Blends of Neoprene and acrylate rubbers
July 1998 – April 2001	Bachelor of Science (**Study of Physics**) at St. Jude's College, M.S. University, India Final Grade: First Class
June 1996 – April 1998	**School Education** at the St. Aloysius Higher Secondary School, India
June 1992 – April 1996	**School Education** at the St. Aloysius High School, India
June 1986 – April 1992	**School Education** at the St. Aloysius Primary School, India

Work Experience

August 2004 – July 2007	**Senior Engineer** - Product Development and Technical services,
	Supreme Petrochem Pvt. Ltd.
	Chennai, India.
June 2010 – December 2013	**Technical manager**
	Bayer (South East Asia) Pte. Ltd.
	Singapore
June 2011 – December 2013	**Marie Curie Research Fellow**
	Bayer Technology Services GmbH
	Leverkusen, Germany.